Metal-Ligand Cooperation of Cobalt(I) Complexes Bearing a Phenanthroline-Based Tetradentate PNNP Ligand and Its Application to Catalytic Hydrodehalogenation of Aryl Halides

Jheng, Nai-Yuan

February 2022

Metal-Ligand Cooperation of Cobalt(I) Complexes Bearing a Phenanthroline-Based Tetradentate PNNP Ligand and Its Application to Catalytic Hydrodehalogenation of Aryl Halides

Jheng, Nai-Yuan

Doctoral Program in Chemistry

Submitted to the Graduate School of

Pure and Applied Sciences

in Partial Fulfillment of the Requirements

for the Degree of Doctor of Philosophy in

Science

at the

University of Tsukuba

Index

List of publication

Acknowledgements

Chapter 1 General Introduction

1-1. Cobalt complexes

Research on catalysts has intensely sprouted in recent years due to reconsideration for over-exhausted resources such as their precious counterparts,[1] e.g. complexes of ruthenium, rhodium, and platinum. Therefore, the demand for more sustainable and cheaper surrogates encourages more scientists to develop new catalysts. With similar electronic configurations in valence shells to those of noble metal atoms, 3d metal complexes are considered as candidates to replace those precious metal catalysts. In addition, 3d metal complexes are usually inexpensive, more earth-abundant, and less toxic. Thus, there are recently more and more research focusing on the development of new 3d metal catalysts.

In the study of these new 3d metal catalysts, cobalt complexes are regarded as one of the most promising systems due to their involvement in various biochemical and catalytic reactions.[2] In industries, for example, both Fischer–Tropsch[3] and hydroformylation processes[4] are well-known cobalt-catalyzed processes. The former often makes use of a metallic cobalt usually supported on ruthenium, alumina, etc. to transform carbon monoxide (CO) and hydrogen (H_2) into hydrocarbons. The latter historically applies cobalt tetracarbonyl hydride, [$HCo(CO)_4$], as a catalyst to achieve aldehydes formation from alkenes, CO, and H_2. Interestingly, this reaction was discovered by Roelen while he studied the Fisher-Tropsch process in 1938 (Scheme 1).[5]

Fischer-Tropsch process

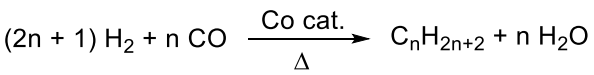

Hydroformylation (oxo process)

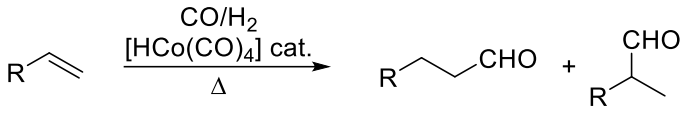

Scheme 1. The cobalt-catalyzed Fisher-Tropsch process and hydroformylation.

The cobalt complex, [$HCo(CO)_4$], is a well-defined cobalt catalyst, and the widely-accepted mechanism was proposed by Heck and Breslow in 1960.[6] It is also widely known that the phosphine-supported Rh(I) complex, [$HRh(CO)_2(PPh_3)_2$],[7] was developed by Wilkinson *et al.* and revealed to exhibit much higher catalytic performance for the hydroformylation reaction. However, it is worth mentioning that **a** recent study on cobalt catalyst systems revealed that a cationic cobalt(II) carbonyl hydrido complex bearing two phosphine ligands can approach the

performance of the Rh catalyst.[8]

Cobalamins (vitamin B_{12}) as an enzyme having a cobalt ion at the active center, which belong to one of B vitamins and cofactors involved in DNA syntheses, nervous systems, and other biological reactions,[9] are known to facilitate the generation of alkyl radicals, such as deoxyadenosyl radical via homolysis of a weak Co–C bond (ca. 20 ~ 30 kcal/mol) (Scheme 2).[10]

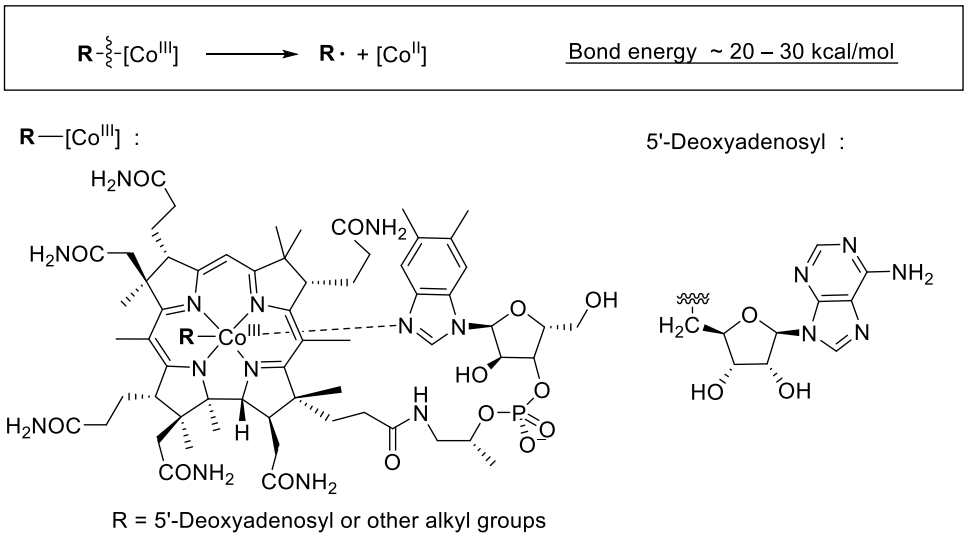

Scheme 2. Facile Co–C bond cleavage of cobalamins (vitamin B_{12}).

Such mechanisms of radical generation by cobalamins and related compounds were applied to reduction of aryl halides, establishing processes for syntheses (i.e. deprotection of halide in aromatic systems)[11] and degradation of organic halides, which are common chemical wastes and sources of pollution.[12] For example, pentachlorophenol (PCP) can be mainly converted to isomers of tetrachlorophenol by vitamin B_{12} and titanium(III) citrate at room temperature after 24 hours (Scheme 3).[13]

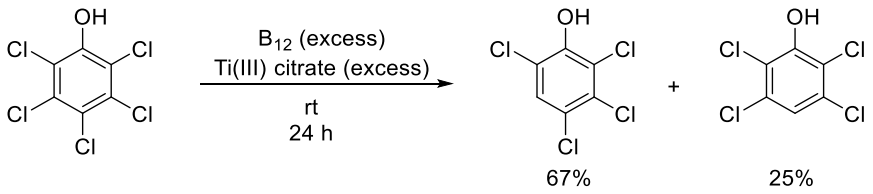

Scheme 3. Hydrodehalogenation of pentachlorophenol (PCP).

Although there are some practical reactions catalyzed by cobalt complexes, and they are highly expected as candidates of precious metal catalyst surrogates, most of the cobalt complexes

still cannot be compatible with other noble metal complexes. Therefore, to overcome the inferiority, suitable ligand designs are desired to further expand the reaction chemistry of cobalt complexes.

1-2. Consideration of ligand design

Recently, research on metal-ligand cooperation (MLC) has expanded the central idea of the design for new metal complexes.[14] Traditionally, reactions were considered to be conducted on a metal center in a complex; however, further research suggested that redox behaviors of ligands can also affect reactions. In 1966, Jørgensen suggested that ligands could be classified into two categories, "innocent" and "suspect".[15] The term "suspect" was then described as "noninnocent" by other chemists.[16] The "innocent" ligands, such as H_2O and halides, remain unchanged in the course of reactions. On the other hand, ligands sometimes undergo dissociation from the metal center and/or undergo chemical conversion. On this event, an oxidation state of the ligand changes, and thus it become difficult to define the total electronic structure of the ligand. In this case, Jørgensen coined the word "suspect" ("noninnocent").

The simplest form of noninnocent ligands are redox-active ligands. A classical example of such the ligands is NO, which can be in three different coordination modes, nitrosyl cation (NO^+), nitric oxide radical ($NO^{\cdot}$), and nitroxide anion (NO^-) (Figure 1a).[15,16a] It is known that ligands with a π-conjugated moiety can also demonstrate the noninnocence owing to capability to accept electrons in π^* orbitals.[16c] A simple example is pyrazine-type ligands which can reversibly accept an electron in the aromatic π system (Figure 1b).[16a, 17] Recent research indicates that noninnocent ligands also cover ligands without any π system such as a trifluoromethyl group ($-CF_3$). There are three coordination modes of CF_3 as a ligand, CF_3^+, CF_3, and CF_3^- (Figure 1c).[16b,18] Hoffmann *et al.* suggested that these systems can be termed as *σ*-noninnocence.

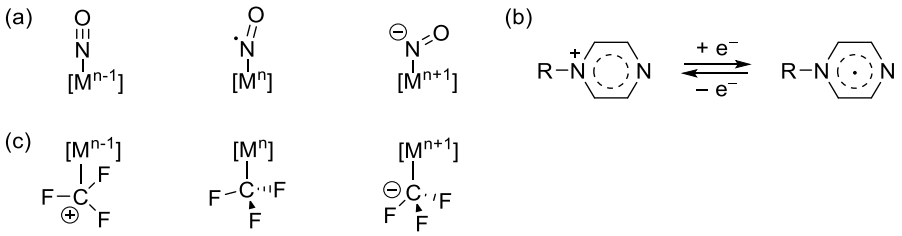

Figure 1. (a) Noninnocence of NO as a ligand: three modes of NO coordinating to a metal. (b) redox structures of pyrazine ligands. (c) Three modes of CF_3 ligand.

So far, with the concept of "noninnocent" combined with rigid chelating ability, various application has been established. Thus, the research shifted to ligands, which can fulfil the two factors of a π conjugate structure and a chelating ability. For example, a redox system of

catecholate/*o*-quinone and its derivatives[16a,19] is one of well-known noninnocent bidentate ligands since 1970s (Scheme 4).[20]

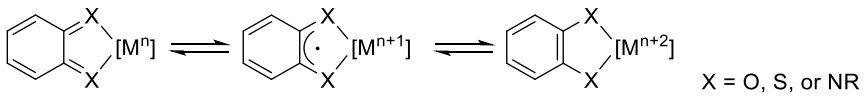

Scheme 4. Resonance structures of complexes bearing a catecholate/*o*-quinone redox noninnocent ligand.

As shown in Scheme 4, such ligands can coordinate with a metal center tightly through a formation of a five-member ring. The redox ability of catecholate/*o*-quinone sequence allow complexes to exhibit three resonance structures. As a result, the redox properties of metal catecholate complexes has been widely applied to study, such as those on Fe-based intradiol dioxygenases,[21] Cu-dependent amine oxidases,[22] and others.[23]

As time goes on, more complicated ligand systems have been developed by introducing a new concept of metal-ligand corporation (MLC).[24] In this concept, incoming substrates interact with both a metal center and a ligand in a cooperative manner.[14a] Therefore, the substrate can be activated in a synergetic manner. One of the famous examples was reported by Noyori *et al.*, and their work has been nowadays recognized as one of the most important studies in ligand-assisted hydrogenation of polar bonds (Scheme 5).[25]

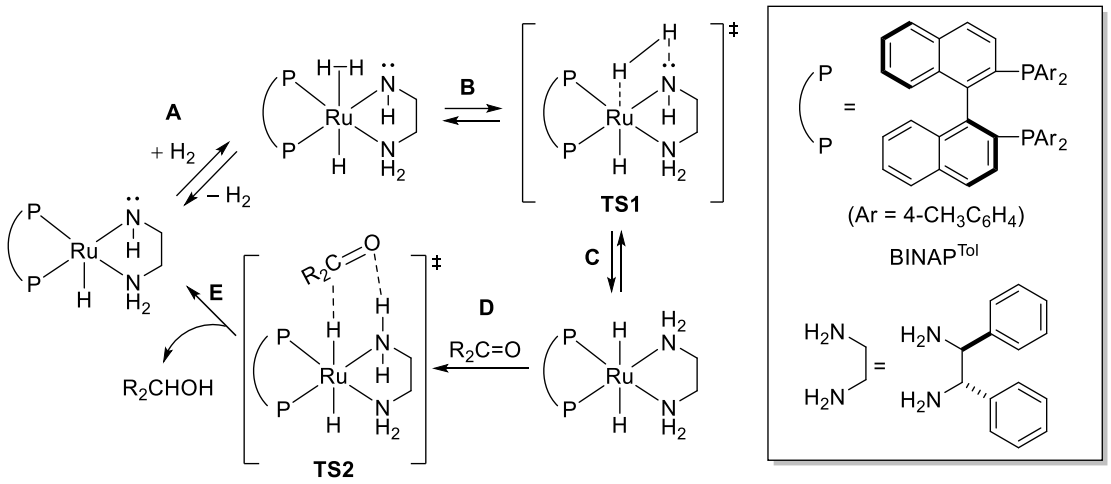

Scheme 5. H_2 activation and hydrogenation of a ketone via MLC of a BINAP^{Tol}-Ru(II)-diamine complex.

In the case of BINAP^{Tol}-Ru(II)-diamine complex (BINAP^{Tol} = 2,2'-bis(di-4-tolylphosphino)-

1,1'-binaphthyl), not only the metal center but also a neighboring amido moiety at the primary coordination sphere can participate in the activation of H_2.[26] During the reaction, heterolytic cleavage of the H–H bond proceeds to form a hydride ligand (through **TS1** in Scheme 5). Simultaneously, a proton (H^+) is formed on the N atom of the chelating-diamine ligand (Scheme 5 step C). Thus, H–H bond cleavage can be facilitated.

The resulting Ru *trans*-dihydrido complex successively achieve hydrogenation of ketones through an outer-sphere mechanism (Scheme 5 step D to E). In this step, a ketone molecule is incorporated into the reaction sphere via interaction of the carbonyl group with the hydride and amino proton. Thus, the reaction proceeds via a six-membered transition state (**TS2** in scheme 5), leading to the formation of the corresponding alcohol. The reaction is accomplished with high turnover frequency (TOF > 200,000 h^{-1}) and high enantioselectivity (ee > 98%).[27]

1-3. Metal-ligand cooperation of pincer systems

As mentioned above, chelating modes, which can influence the electronic structures and thermodynamic stability of complexes, are considered as one of key factors for catalyst design. Among various types of chelating systems, pincer ligands were found as suitable candidates to fulfil the two factors, π conjugate structure and chelating ability, and thus they are one of famous ligand systems enabling MLC.[14]

In 1970s, design of pincer ligands was pioneered by Nelson, Shaw and van Koten,[28] and the concept has arrested great attention in area of homogeneous catalysts since then. Pincer ligands with a planar multidentate chelating ability usually afford a rigid meridional coordination mode to endow reactive complexes with good thermostability[29] and sometimes even with moisture and/or air stability.[30] Moreover, the design of pincer ligands can be easily tuned to render precise control of a steric circumstance, hemilability, and noninnocent nature.[29]

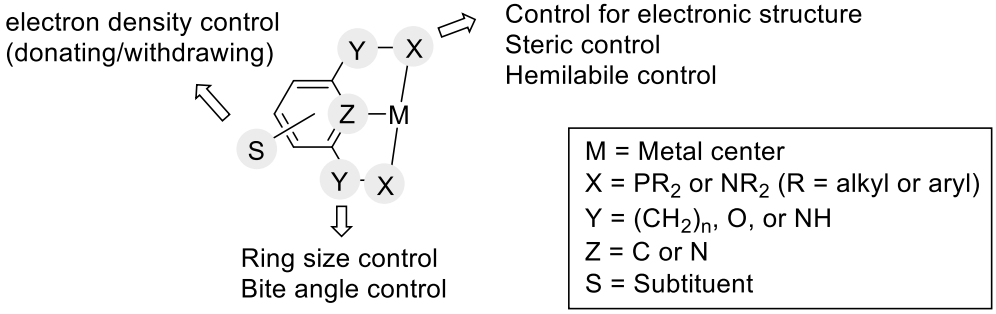

Figure 2. Design of pincer ligand with an aromatic motif.

As shown in Figure 2, a classical pincer ligand with an aromatic motif contains several sections, each of which plays some distinct roles. The side-arm group X, which are usually

composed of phosphanyl-groups (PR_2) and/or amino-groups (NR_2), can tune the electronic nature of the metal center. Furthermore, the R substituents can further control the steric circumstances and the chirality of metal complexes. According to the coordinating strength of the X groups, they sometimes exhibit hemilabile behaviors. The group Y is normally CH_2, O, or NH moieties, which can tune a chelate-ring size and a bite angle. The length of the side arms and the chirality at the metal center can be also adjusted by the Y group. As a coordination site, group Z, which locates at the *trans* position to an incoming substrate, significantly influence an electronic nature of the metal atom. Group S as the substituent(s) on the backbone can directly modify the electron density of the aromatic ring, enabling fine tuning of the donating ability of Z.

So far, detailed ligand design has been provided for in pincer-complex systems. In addition to classical oxidative addition/reductive elimination, in Scheme 6, two other important reaction modes are shown.[2b] In Scheme 6 (i), activation of substrates in a primary coordination sphere (via direct coordination) is well-established. Because the amine side-arm is hemilabile, the side-arm NEt_2 group dissociates from the metal center at the initial stage, and a ketone can coordinate to the metal center and then be inserted into the M–H bond.

The outer sphere substrate activation via MLC is also reported, such as hydrogenolysis of esters (Scheme 6 (ii)). The reaction initiates with the formation of a weak hydrogen bond between the lone pair electrons on the oxygen atom of the carbonyl group and the hydrogen at the ligand backbone. Simultaneously, the carbonyl carbon interacts with the hydride ligand. The reaction completes with the formation of a hemiacetal and an imido complex.

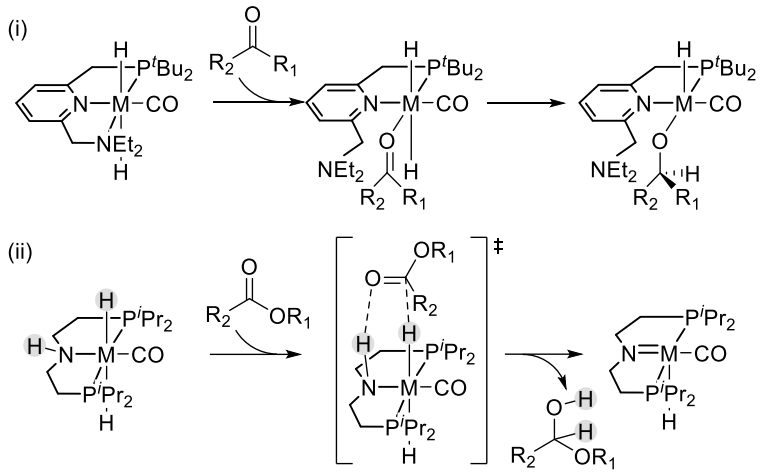

Scheme 6. Two common activating modes: (i) inner-sphere approach (hydrogenation of ketone), (ii) outer-sphere approach (hydrogenation of ester).

Another approach based on MLC has portrayed a unique and promising reactivity and a mechanism, which is different from the aformentioned two approaches (Scheme 7). As mentioned

above, pincer complexes can often exhibit MLC behavior. In pincer complexes with an aromatic moiety, particularly in the pyridine-based (also lutidine-based) pincer complexes, the switch between the aromatized form and the dearomatized form enables bond activation of small molecules, such as C–H, O–H, N–H, etc. (Scheme 7).[14b] For example, on the treatment with a base, one H atom at the methylene carbon atom on the ligand side arm is deprotonated, causing the dearomatization of the pyridine ring. Then, the metal center and the exomethylene carbon act as an acid and a base, respectively. Accordingly, H–X (H–X = H–H, H–OH, H–OR, H–N(H)R, etc.) bond is heterolytically cleaved via a bridged-transition state with the interaction between H–X and both the metal center and the *exo*-methylene carbon atom.

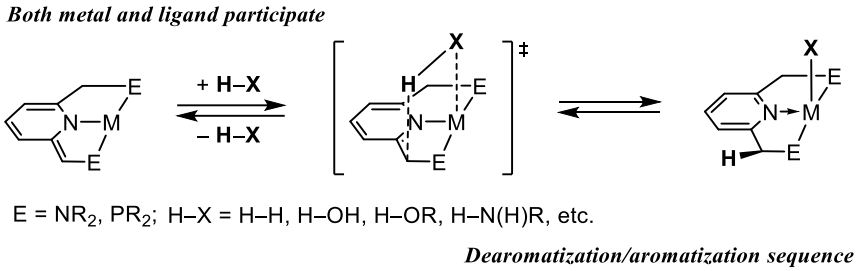

Scheme 7. Activation of small molecules via pyridine-based complexes applying MLC.

For these pyridine-based PNP or PNN complexes, some specific catalytic reactivity or unprecedented reactions were reported (Scheme 8).[31, 32] For example, Milstein *et al.* reported formation of amides directly from primary amines and alcohols along with H_2 liberation catalyzed by a PNP-Ru complex in 2007,[31] and his group also published a consecutive thermal H_2 and light-induced O_2 revolution from water via a PNN-Ru pincer complex in 2009.[32] Both of these reactions showed high reactivity based on the MLC with a dearomatization/rearomatization sequence. Hence, this thesis focuses on the systems with aromatic backbones.

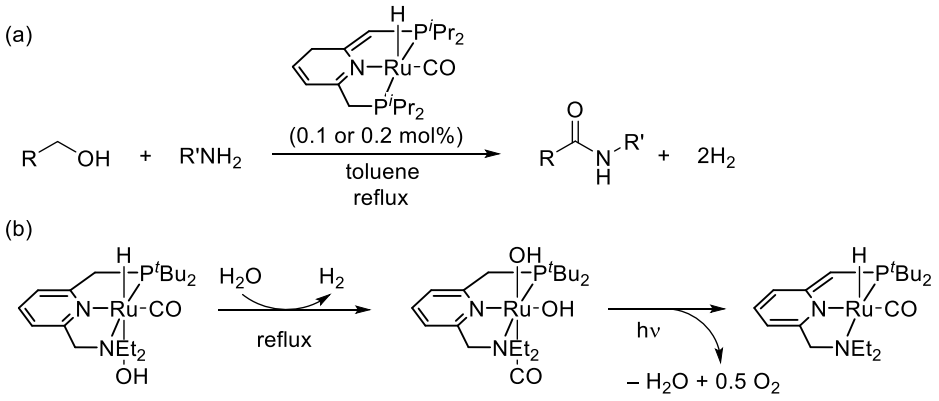

Scheme 8. (a) Amide formation and H_2 liberation from primary amines and alcohols

catalyzed by a PNP-Ru complex. (b) Sequential H_2 and O_2 revolution from water via a PNN-Ru complex.

Recently, long-range MLC has been reported. In 2010, two independent studies of long-range MLC were reported by Milstein's group[33] and Song's group[34], respectively (Scheme 9). In the Milstein's system, H_2 activation was achieved by an acridine-based Ru complex in refluxing toluene under 5 bar H_2 atmosphere. Bond cleavage of H_2 was achieved heterolytically. In the resulting complex, one H atom was coordinated to Ru and the other one attached to a 9-position of the acridine framework. In the Song's system, H_2 activation occurred via a diazafluorene-based Ru complex at 60 °C in THF or benzene under 1 bar of H_2. Similarly, Ru–H was formed, and another H attached to the 9-position of the diazafluorene framework. Thus, both of these two studies showed the occurrence of the heterolytic cleavage of H–H to afford one hydride at the Ru atom and one hydrogen atom at the terminal sites of the ligand backbone in each case.

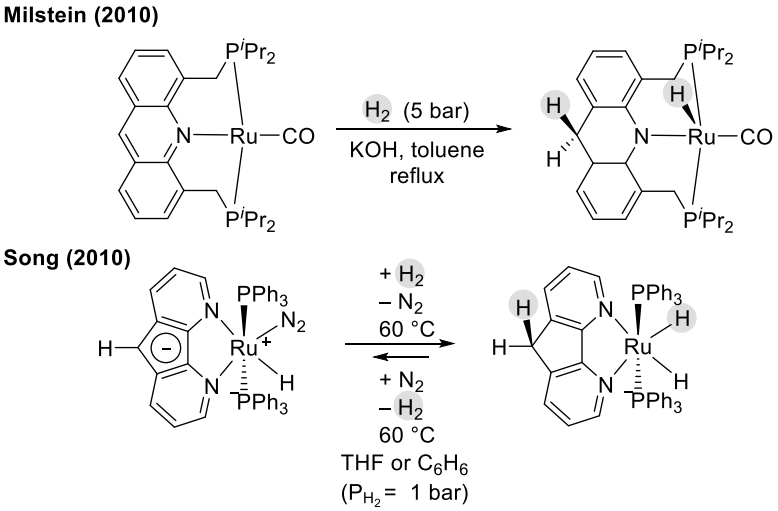

Scheme 9. Hydrogen activation via long-rang MLC developed by Milstein's and Song's groups, respecctively.

Overall, MLC has provided a new concept of design of complexes, and the unique activating modes lead to various reaction pathways, which then offered distinct reactivity in catalytic reactions.[14b]

1-4. Co(I) pincer complexes

Among the miscellaneous systems, the low valent cobalt complexes, especially cobalt(I) complexes are of great interest because they can cleavage various bonds. It was revealed that the reactions proceed via both radical mechanism[35] and ionic mechanism (two-electron redox

mechanism)[2b, 36] (Figure 3).

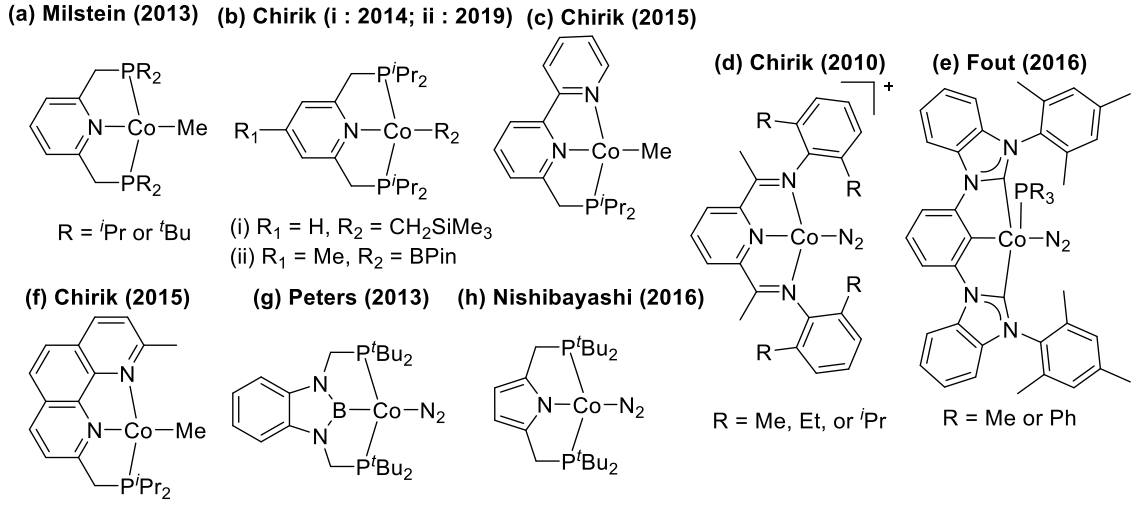

Figure 3. Selected Co(I) pincer complexes as catalysts in literature.

With a specific electronic nature, excellent catalytic performance can be achieved by Co(I) pincer complexes. In addition to the PNP pyridine-based Co(I) complexes,[36,37] Chirik's group reported PDI-Co(I) complexes (PDI = bisimino(pyridine); Figure 3d),[38] bipyridine-based (Figure 3c),[38] and phenanthroline-based (Figure 3f) Co(I) complexes,[39] which could be applied as catalysts for borylation,[37b,37d,37e,38b,39] hydrosilylation of carbon dioxide (CO_2),[37a] and Suzuki−Miyaura cross coupling.[37c] Moreover, other tridentate PNP and CCC type Co (I) pincer complexes were introduced by Nishibayashi's group (Figure 3h)[40] and Fout's group (Figure 3e)[41]. Nishibayashi's PNP Co(I) complex was utilized as a catalyst for the direct transformation of molecular nitrogen (N_2) into ammonia (NH_3),[40] while Fout *et al.* made use of CCC type Co(I) complexes with two NHC (NHC = N-heterocyclic carbenes) side groups to achieve catalytic olefin hydrogenation.[41] Besides, a pentadentate PBP-Co(I) complex, which shows a similar structure to Nishibayashi's complex reported by Peters's group (Figure 3g), can be applied as a catalyst to (de)hydrogenation and transfer hydrogenation.[42]

Surprisingly, to the best of my knowledge, MLC behavior has been not reported so far in most of the above-mentioned Co(I) complexes. However, in 2013, Milstein reported syntheses of PNP-Co(I)-methyl complexes bearing a pyridine-based pincer ligand (Figure 3a) by the reaction of PNP-Co(II)-dichloride with methyllithium (MeLi). It was revealed that the resulting methyl complex underwent a formal loss of H· radical, resulting in the formation of a Co(I) complex with a ligand-centered radical (Scheme 10a-i). In this study, the radical behavior of Co(I) methyl complex demonstrated not only the occurrence of a long-range MLC behavior but also hydrogenation of diphenylacetylene (Scheme 10b-i).[35] In a different study, Chirik's group also

reported the same reaction: i.e. reaction of PNP-Co(II) chloride with excess MeLi one year later. In contrast to Milstein's study, it was reported that the PNP-Co(II)-dichloride underwent methylation, methane (CH_4) generation, and again methylation, thus the resulting complex was assigned to a PNP-Co(II)-methyl complex with a dearomatized PNP ligand (Scheme 10a-ii). They also revealed that the reaction of PNP-Co(I) methyl complex with diphenylacetylene proceeded at elevated temperature to form PNP-Co(II)-Ar complex, which was generated via insertion of diphenylacetylene followed by orthometalation (Scheme 10b-ii).[36]

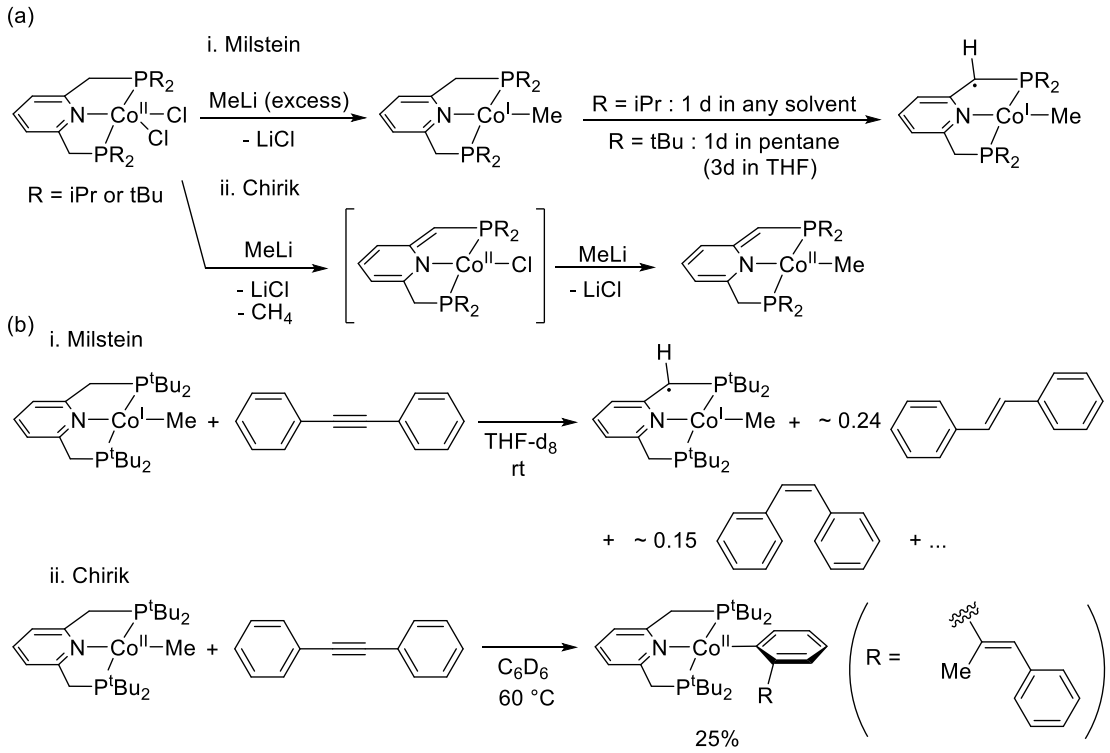

Scheme 10. (a) Syntheses of the PNP-Co-methyl complexes with excess amount of MeLi by Milstein and Chirk. (b) Reactions of PNP^{tBu}-Co-methyl complex with biphenylacetylene by Milstein and Chirik.

Overall, although these Co(I) pincer complexes behave as good catalysts in the reactions mentioned above, MLC behavior was rarely found in these systems. Thus, there is still a huge space for chemists to search on Co(I) complexes with MLC.

1-5. Complexes bearing a tetradentate phenanthroline-based PNNP ligand

Even with abundant pincer systems as a chemists' tool kit, a journey to search new and powerful ligands has not yet been stopped. To develop new ligand system, Ziessel introduced a series of PNP and PNNP pincer ligands in 1989 (Figure 4).[43]

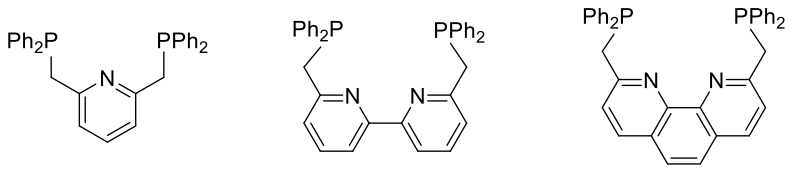

Figure 4. Examples of Ziessel's ligands.

All of these ligands contain two diphenylphosphanyl methyl groups built on the backbone of pyridine-, bipyridine-, and phenanthroline-moiety, respectively. Among them, the third one ((2,9-bis ((diphenylphosphanyl)methyl)-1,10-phenanthroline, PNNP ligand) with four coordinate sites and a more rigid conjugated backbone, behave as a strong-field ligand to stabilize the metal center and enable MLC by the dearomatization/rearomatization sequence.[44] Complexes synthesized from Ru precursors and a tailored PNNP ligand (with *tert*-butyl groups on the phosphine atoms; 2,9-bis ((di-*tert*-butylphosphanyl)methyl)-1,10-phenanthroline, PNNP-^{t}Bu ligand) were reported by Milstein's group in 2013 (Scheme 11).[45] Saito *et al.* utilized a tailored bipyridine based PCY2 ligand (6,6'-bis((dicyclohexylphosphaneyl)methyl)-2,2'-bipyridine, PCY2), which possesses a mesityl group at the 4 position of each pyridine moiety and two cyclohexyl group on each phsophino terminal, to synthesize a Mes-IrPCY2 complex which allowed the selective formation of formic acid from carbon dioxide (CO_2).[46]

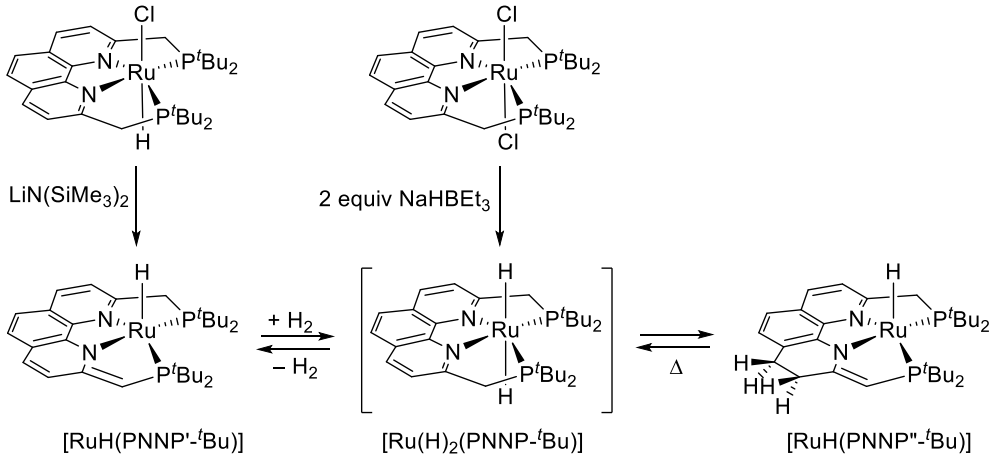

Scheme 11. H_2 activation by a Ru complex with a dearomatized PNNP-^{t}Bu ligand.

With PNNP-^{t}Bu, a square pyramidal complex was synthesized on the treatment of its octahedral precursor ([RuHCl(PNNP-^{t}Bu)]) with lithium bis(trimethylsilyl)amide ($LiN(SiMe_3)_2$) to proceed deprotonation affording a dearomatized backbone, [RuH(PNNP'-^{t}Bu)] (Scheme 11). After the introduction of H_2 (1atm), [RuH(PNNP'-^{t}Bu)] was partially converted to a complex with

PNNP"-^{t}Bu, which had a hydrogenated phenanthroline framework (Scheme 11). Since no *trans*-dihydride intermediate ([Ru(H)$_2$(PNNP-^{t}Bu)]) was observed, further investigation from direct synthesis of the dihydride species was performed by applying 2 equiv of sodium triethylborohydride (NaHBEt$_3$) to [RuCl$_2$(PNNP-^{t}Bu)] complex (Scheme 11). Although there was an evidence to prove the initial existence of a small amount of Ru dihydride species,[47] the final product was a mixture including [RuH(PNNP'-^{t}Bu)] and [RuH(PNNP"-^{t}Bu)]. Accordingly, the Ru dihydride species, though it was not fully identified, was proposed to be the intermediate during the hydrogenation of [RuH(PNNP'-^{t}Bu)] (Scheme 11). Collectively, even the hydrogen source to the phenanthroline framework was still not clear, which can be from either hydride source (e.g. NaHBEt$_3$) or H_2 gas, the experimental results still demonstrated a new mode of long-range MLC. Upon applying this complex as a catalyst, catalytic dehydrogenative coupling of alcohols was performed via the mode of MLC (Scheme 12).

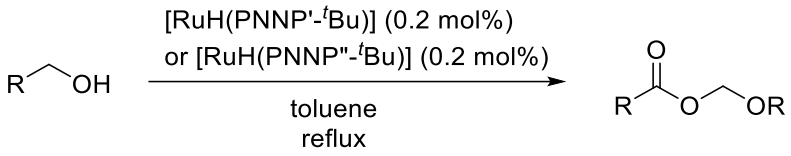

Scheme 12. Dehydrogenative coupling of alcohols using Ru complexes with a dearomatized PNNP-^{t}Bu ligand as catalysts.

As shown in Scheme 13, the dehydrogenative coupling of alcohols was achieved with 0.2 mol% of [RuH(PNNP'-^{t}Bu)] or [RuH(PNNP"-^{t}Bu)] in refluxing toluene after 6 to 72 h. However, the proposed mechanism suggested that there were only coordination and transfer hydrogenation from the alcohols to the ligand of the complex. No further application of hydrogenation by PNNP-Ru system has not yet be reported.

In 2018, our group reported a series of Fe complexes bearing a PNNP ligand (Scheme 13a).[48] A dichloro PNNP-Fe complex, [FeCl$_2$(PNNP)], in a pentacoordinate distorted trigonal bipyramidal structure was converted to the dihydride complex, [Fe(H)$_2$(PNNP)] upon treatment with 2 equiv NaHBEt$_3$ (Scheme 13a, path I).[48a] Furthermore, the hydrido complex underwent reductive elimination under N_2 atmosphere to generate a N_2-bridged dinuclear Fe complex, [{Fe(PNNP)}$_2$(μ-N$_2$)]. It was also found that dehydogenative coupling of silanols with silanes catalyzed by [FeCl$_2$(PNNP)]/NaHBEt$_3$ proceeded to afford hydrotrisiloxanes selectively (Scheme 13b).[48a]

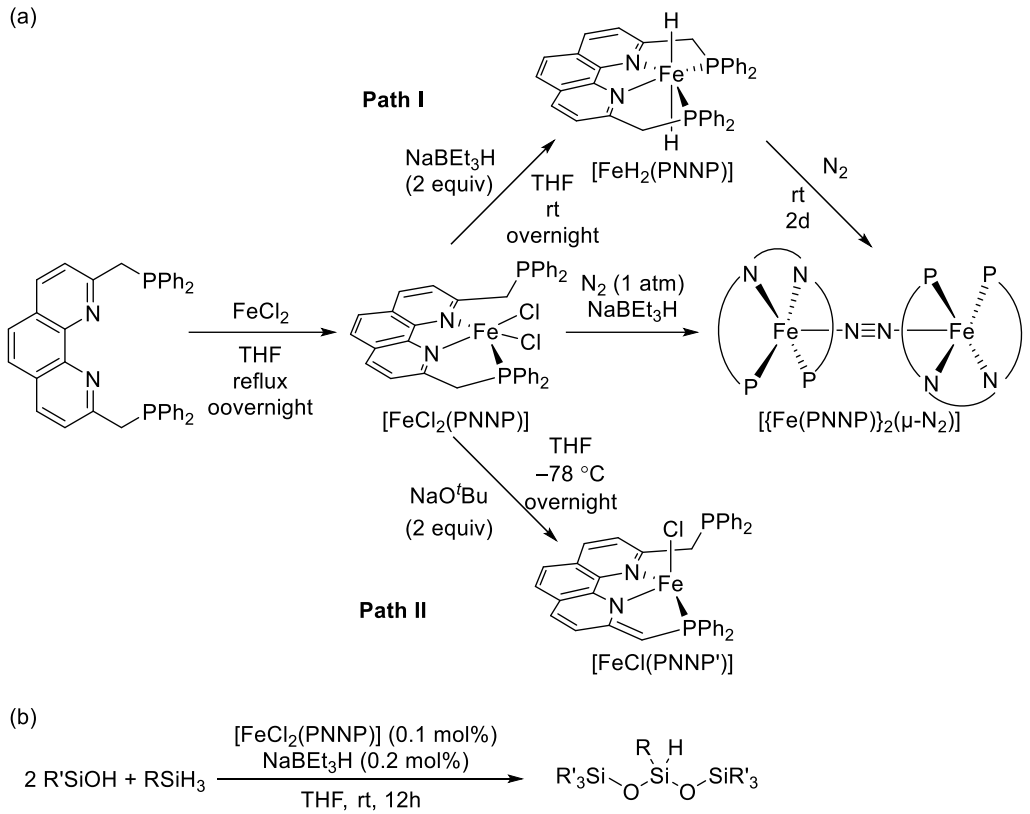

Scheme 13. (a) Syntheses of [$FeCl_2$(PNNP)], [FeH_2(PNNP)], [FeCl(PNNP')], and [{Fe(PNNP)}$_2$(μ-N_2)]. For the [{Fe(PNNP)}$_2$(μ-N_2)] complex, structural detail of PNNP ligand was replaced by P-N-N-P for clarity. (b) Dehydrogenative coupling of silanols with silanes catalyzed by [$FeCl_2$(PNNP)].

In addition, it was revealed that treatment of [$FeCl_2$(PNNP)] with 2 equiv sodium *tert*-butoxide (NaO^{t}Bu) at –78 °C in THF resulted in the formation of an iron complex bearing a dearomatized phenanthroline framework, [FeCl(PNNP')], as a major product (Scheme 13a, Path II).[48b] It is worth mentioning that the X-ray crystallographic study of [FeCl(PNNP')] revealed a significantly shorter C1–P1 bond than its counterpart on another side.[49] Along with the results of DFT calculation, it was suggested that there is a resonance structure of the metallacycle moiety which contains P1, C1, C2, N1, and the Fe center (Scheme 14). In this system, the redox active P atom and the Fe atom play pivotal roles. Overall, it is likely that the PNNP ligand established a broad π-conjugation system involving the Fe atom, thus facilitating the stability of [FeCl(PNNP')].

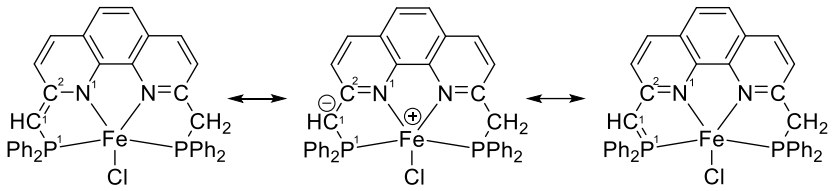

Scheme 14. Possible resonance structures of [FeCl(PNNP')].

The MLC behaviors of PNNP-Fe system were also observed (Scheme 15).[50] While treating with 2 equiv NaO^{t}Bu to [Fe(CH_3)I(PNNP)], which was prepared from [{Fe(PNNP)}$_2$(μ-N_2)] and 4 equiv CH_3I, afforded [Fe(CH_3)(PNNP')] bearing a dearomatized PNNP' ligand. Interestingly, on the treatment of [Fe(CH_3)(PNNP')] with 1 atm H_2 atmosphere for 20 min, an octahedral *trans* methyl hydrido complex with a rearomatized PNNP ligand ([Fe(CH_3)(H)(PNNP)]) was formed (Scheme 15a). Thus, conventional MLC was demonstrated in the PNNP-Fe system.

Recently, an iron dihydride complex bearing PNNP-Cy ligand, [Fe$(H)_2$(PNNP-Cy)] (2,9-bis ((dicyclohexylphosphanyl)methyl)-1,10-phenanthroline, PNNP-Cy ligand), was prepared by the reaction of a dibromide precursor with 2 equiv $NaHBEt_3$. The resulting Fe-hyderido complex can be spontaneously transformed into a new iron complex with a doubly-hydrogenated phenanthroline ligand, demonstrating a new long-range MLC behavior (Scheme 15b).[51] Moreover, [Fe$(H)_2$(PNNP-Cy)] can react with benzophenone to afford an insertion product [Fe($OCHPh_2$)(PNNP'-Cy)].[50] In this reaction, partial dearomatization of the phenanthroline framework proceeded. As a result, the resulting complex was supported by an unsymmetrical PNNP'-Cy, in which two phosphanyl groups are connected to the ligand backbone via one methylene carbon and one *exo*-methylene carbon (Scheme 15b). Thus, the reaction also demonstrated the occurrence of a long-range MLC in the PNNP-Fe system.

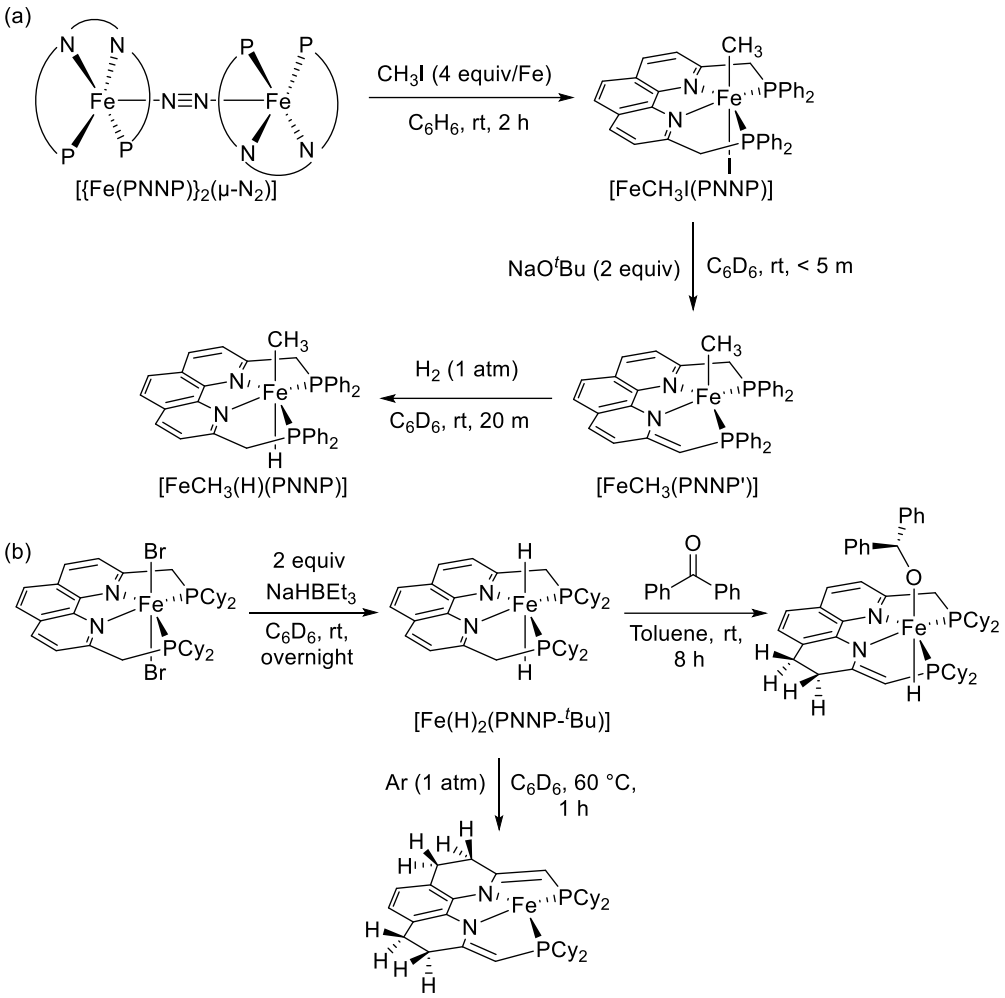

Scheme 15. MLC in a PNNP-Fe system: (a) a conventional mode and (b) a long-range mode.

1-6. Purpose of this research

In this thesis, study on fundamental reactions of PNNP-Co(I) complexes are described. Based on the properties of the PNNP ligands, two characteristic aspects can be expected: (1) The low valent Co(I) center could be stabilized by the PNNP ligand via a rigid coordination as well as the electron accepting ability of the phenanthroline framework. (2) PNNP-Co complexes could render intrinsic MLC behaviors via the dearomatization/rearomatization sequence of a broader conjugation system with the phenanthroline-based ligand than that with the pyridine-based ligand. Based on these two concepts, it is expected that a square planar 16-electron PNNP-Co(I) complex with two vacant sites (Figure 5), which can be potentially synthesized, might demonstrates novel reactivity.

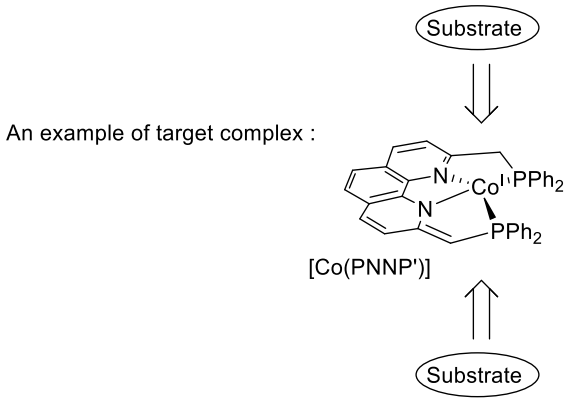

Figure 5. Expected PNNP'-Co(I) complex.

The outlines of chapters are as follows:

In Chapter 2, motivated by the importance of PNP-Co(I) alkyl complexes in various catalytic reactions,[37, 39] the syntheses of PNNP-Co(I) alkyl complexes and their potential MLC behavior were described (Scheme 16). In addition, a long-range MLC behavior was also observed during the heating reaction of a PNNP-Co(I) alkyl complex, which underwent homolysis of Co–C bond and benzylic hydrogen atom abstraction.

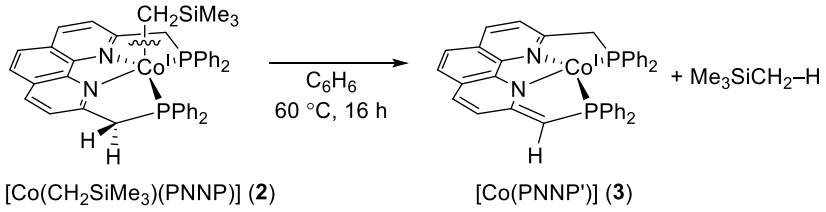

Scheme 16. Structural transformation of **2** into **3**.

In Chapter 3, mechanistic study on H_2 activation by the PNNP-Co(I) system is described (Scheme 17). In order to gain mechanistic insight into H–H activation by the PNNP-Co(I) complex, mechanistic study was performed including a deuterium labeling experiment and stoichiometric reactions.

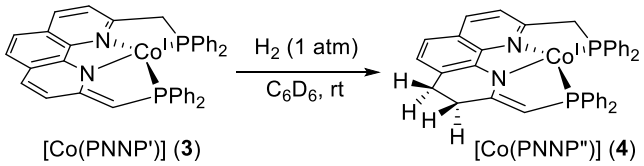

Scheme 17. H_2 activation via **3**.

In Chapter 4, catalytic hydrodehalogenation of aryl halides catalyzed by a PNNP-Co(I) complex is discussed (Scheme 18). The reactions were proceeded under milder conditions (e.g. under 1 atm H_2) in comparison with previous reports. Moreover, mechanistic study including kinetic study is also included to uncover the reaction mechanism. Based on the mechanistic study, the catalytic cycle was suggested to be based on the specific long-range MLC behaviors via a series of structural transformation of the PNNP ligand which has been elucidated in the previous chapters.

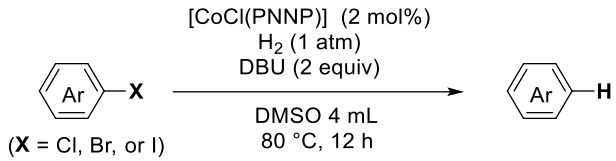

Scheme 18. Hydrodehaloation of aryl halides catalyzed via a PNNP-Co(I) catalyst.

Chapter 5 describes the summary of this thesis.

Reference

(1) (a) Bolm, C.; Legros, J.; Le Paih, J.; Zani, L. *Chem. Rev.* **2004**, *104*, 6217–6254. (b) Bauer, I.; Knölker, H.-J. *Chem. Rev.* **2015**, *115*, 3170–3387. (c) Fürstner, A. *ACS Cent. Sci.* **2016**, *2*, 778–789. (d) Gandeepan, P.; Müller, T.; Zell, D.; Cera, G.; Warratz, S.; Ackermann, L. *Chem. Rev.* **2018**, *119*, 2192–2452. (e) Irrgang, T.; Kempe, R. *Chem. Rev.* **2018**, *119*, 2524–2549. (f) Alig, L.; Fritz, M.; Schneider, S. *Chem. Rev.* **2018**, *119*, 2681–2751. (g) Taylor, L. J.; Kays, D. L. *Dalton Trans.* **2019**, *48*, 12365–12381.

(2) (a) Debuigne, A.; Poli, R.; Jérôme, C.; Jérôme, R.; Detrembleur, C. *Prog. Polym. Sci.* **2009**, 34, 211–239. (b) Junge, K.; Papa, V.; Beller, M. *Chem. Eur. J.* **2019**, *25*,122–143. (c) Michiyuki, T.; Komeyama, K. *Asian J. Org. Chem.* **2020**, *9*, 343–358. (d) Kyne, S. H.; Lefèvre, G.; Ollivier, C.; Petit, M.; Cladera, V.-A. R.; Fensterbank, L. *Chem. Soc. Rev.* **2020**, *49*, 8501–8542.

(3) (a) Oukaci, R.; Singleton, A. H.; Goodwin, J. G. *Appl. Catal. A Gen.* **1999**, *186*, 129–144. (b) Balonek, C. M.; Lillebø, A. H.; Rane, S.; Rytter, E.; Schmidt, L. D.; Holmen, A. *Catal. Lett.* 2010, 138, 8–13. (c) de Klerk, A., Fischer−Tropsch Process. *Kirk-Othmer Encyclopedia of Chemical Technology*; Wiley-VCH: Weinheim, 2013. (d) Kwak, G.; Kim, D.-E.; Kim, Y. T.; Park, H.-G.; Kang, S. C.; Ha, K.-S.; Jun, K.-W.; Lee, Y.-J. *Catal. Sci. Technol.* **2016**, *6*, 4594–4600. (e) Jeske, K.; Kizilkaya, A. C.; López-Luque, I.; Pfänder, N.; Bartsch, M.; Concepción, P.; Prieto, G. *ACS Catal.* **2021**, *11*, 4784–4798.

(4) Franke, R.; Selent, D.; Börner, A. *Chem. Rev.* **2012**, *112*, 5675–5732.

(5) Cornils, B.; Herrmann, W. A.; Rasch, M. *Angew. Chem. Int. Ed.* **1994**, *33*, 2144–2163.

(6) Heck, R. F.; Breslow, D. S. *J. Am. Chem. Soc.* **2002**, *83*, 4023–4027.
(7) Evans, D.; Osborn, J. A.; Wilkinson, G. *J. Chem. Soc. A Inorg. Phys. Theor.* **1968,** *62*, 3133–3142.
(8) Hood, D. M.; Johnson, R. A.; Carpenter, A. E.; Younker, J. M.; Vinyard, D. J.; Stanley, G. G. *Science* **2020**, *367*, 542–548.
(9) (a) Gruber, K.; Puffer, B.; Kräutler, B. *Chem. Soc. Rev.* **2011**, *40*, 4346–4363. (b) Giedyk, M.; Goliszewska, K.; Gryko, D. *Chem. Soc. Rev.* **2015**, *44*, 3391–3404.
(10) Pattenden, G. *Chem. Soc. Rev.* **1988**, *17*, 361–382.
(11) (a) Choi, H. Y.; Chi, D. Y. *J. Am. Chem. Soc.* **2001**, *123*, 9202–9203. (b) Effenberger, F. *Angew. Chem. Int. Ed.* **2002**, *41*, 1699–1700.
(12) (a) Payne, K. A. P.; Quezada, C. P.; Fisher, K.; Dunstan, M. S.; Collins, F. A.; Sjuts, H.; Levy, C.; Hay, S.; Rigby, S. E. J.; Leys, D. *Nature* **2014**, *517*, 513–516. (b) Kunze, C.; Bommer, M.; Hagen, W. R.; Uksa, M.; Dobbek, H.; Schubert, T.; Diekert, G. *Nat. Commun.* **2017**, *8*, 15858. (c) Chen, C.; Zuo, H.; Chan, K. S. *Tetrahedron* **2019**, *75*, 510–517. (d) Shimakoshi, H.; Shichijo, K.; Tominaga, S.; Hisaeda, Y.; Fujitsuka, M.; Majima, T. *Chem. Lett.* **2020**, *49*, 820–822.
(13) Smith, M. H.; Woods, S. L. *Appl. Environ. Microbiol.* **1994**, *60*, 4111–4115.
(14) (a) Grützmacher, H. *Angew. Chem. Int. Ed.* **2008**, *47*, 1814–1818. (b) Khusnutdinova, J. R.; Milstein, D. *Angew. Chem. Int. Ed.* **2015**, *54*, 12236–12273.
(15) Jørgensen, C. K. *Coord. Chem. Rev.* **1966**, *1*, 164–178.
(16) (a) Kaim, W.; Schwederski, B. *Coord. Chem. Rev.* **2010**, *254*, 1580–1588. (b) Hoffmann, R.; Alvarez, S.; Mealli, C.; Falceto, A.; Cahill, T. J.; Zeng, T.; Manca, G. *Chem. Rev.* **2016**, *116*, 8173–8192. (c) Ganguly, S.; Ghosh, A. *Acc. Chem. Res.* **2019**, *52*, 2003–2014.
(17) Kaim, W. *Coord. Chem. Rev.* **2002**, *230*, 127–139.
(18) (a) Prakash, G. K. S.; Wang, F.; Zhang, Z.; Haiges, R.; Rahm, M.; Christe, K. O.; Mathew, T.; Olah, G. A. *Angew. Chem. Int. Ed.* **2014**, *53*, 11575−11578. (b) Yamada, C.; Hirota, E. *J. Chem. Phys.* **1983**, *78*, 1703−1711.
(19) (a) Pierpont, C.G. *Coord. Chem. Rev.* **2001**, *2217*, 99–125. (b) Ray, K.; Petrenko, T.; Wieghardt, K.; Neese, F. *Dalton Trans.* **2007**, 1552–1566. (c) Eisenberg, R.; Gray, H. B. Inorg. Chem. 2011, 50, 9741–9751.
(20) (a) Balch, A. L. *J. Am. Chem. Soc.* **1973**, *95*, 2723–2724. (b) Griffith, W. P. *Trans. Met. Chem.* **1993**, *18*, 250–256. (c) Pierpont, C. G.; Lange, C.W. *Prog. Inorg. Chem.* **1994**, *41*, 331. (d) Pierpont, C. G. *Coord. Chem. Rev.* **2001**, *216–217*, 99–125. (e) Bhattacharya, S.; Gupta, P.; Basuli, F.; Pierpont, C. G. *Inorg. Chem.* **2002**, *41*, 5810–5816.
(21) (a) Borowski, T.; Siegbahn, P. E. M. *J. Am. Chem. Soc.* **2006**, *128*, 12941–12953. (b) Pau, M. Y. M.; Davis, M. I.; Orville, A. M.; Lipscomb, J. D.; Solomon, E. I. *J. Am. Chem. Soc.* **2007**, *129*, 1944–1958. (c) Bugg, T.D.H.; Ramaswamy, S. *Curr. Opin. Chem. Biol.* **2008**, *12*, 134–140.

(22) W. Kaim, B. Sarkar, G.K. Lahiri, in: W. Kaim, A. Klein *Spectroelectrochemistry*; Royal Society of Chemistry, Cambridge, 2008, pp 68.
(23) Other applications, for example, (a) as anti-cancer drugs: Koyama, J. *Recent Pat. Anti-Infect. Drug Discov.* **2006**, *1*, 113–125.; (b) as a model study for pathogenic research on Parkinson's disease: Arreguin, S.; Nelson,P.; Padway, S.; Shirazi, M.; Pierpont, C. J. *Inorg. Biochem.* **2009**, *103*, 87–93.
(24) Lyaskovskyy, V.; de Bruin, B. *ACS Catal.* **2012**, *2*, 270−279.
(25) (a) Clapham, S. E.; Hadzovic, A.; Morris, R. H. *Coord. Chem. Rev.* **2004**, *248*, 2201−2237. (b) Muñiz, K. *Angew. Chem. Int. Ed.* **2005**, *44*, 6622−6627.
(26) Sandoval, C.A.; Ohkuma, T.; Muñiz, K.; Noyori, R. *J. Am. Chem. Soc.* **2003**, *125*, 13490–13503.
(27) (a) Noyori, R.; Ohkuma, T. *Angew. Chem. Int. Ed.* **2001**, *40*, 40–73. (b) Noyori, R.; Yamakawa, M.; Hashiguchi, S. *J. Org. Chem.* **2001**, *66*, 7931–7944.
(28) (a) Kelly, W. S. J.; Ford, G. H.; Nelson, S. M. *J. Chem. Soc. A Inorg. Phys. Theor.* **1971**, *0*, 388–396. (b) Dahlhoff, W. V.; Nelson, S. M. *J. Chem. Soc. A Inorg. Phys. Theor.* **1971**, *0*, 2184–2190. (c) J. Moulton, C.; L. Shaw, B. *J. Chem. Soc. Dalt. Trans.* **1976**, *0*, 1020–1024. (d) van Koten, G.; Timmer, K.; Noltes, J. G.; Spek, A. L. *J. Chem. Soc. Chem. Commun.* **1978**, *6*, 250–252.
(29) Peris, E.; Crabtree, R. H. *Chem. Soc. Rev.* **2018**, *47*, 1959–1968.
(30) Selander, N.; Szabó, K. J. *Chem. Rev.* **2010**, *111*, 2048–2076.
(31) Gunanathan, C.; Ben-David, Y.; Milstein, D. *Science* **2007**, *317*, 790–792.
(32) Kohl, S. W.; Weiner, L.; Schwartsburd, L.; Konstantinovski, L.; Shimon, L. J. W.; Ben-David, Y.; Iron, M. A.; Milstein, D. *Science* **2009**, *324*, 74–77.
(33) Gunanathan, C.; Gnanaprakasam, B.; Iron, M. A.; Shimon, L. J. W.; Milstein, D. *J. Am. Chem. Soc.* **2010**, *132*, 14763–14765.
(34) Stepowska, E.; Jiang, H.; Song, D. *Chem. Commun.* **2010**, *46*, 556–558.
(35) Khaskin, E.; Diskin-Posner, Y.; Weiner, L.; Leitus, G.; Milstein, D. *Chem. Commun.* **2013**, *49*, 2771–2773.
(36) Semproni, S. P.; Milsmann, C.; Chirik, P. J. *J. Am. Chem. Soc.* **2014**, *136*, 9211–9224.
(37) (a) Scheuermann, M. L.; Semproni, S. P.; Pappas, I.; Chirik, P. J. *Inorg. Chem.* **2014**, *53*, 9463–9465. (b) Obligacion, J. V.; Semproni, S. P.; Chirik, P. J. *J. Am. Chem. Soc.* **2014**, *136*, 4133–4136. (c) Neely, J. M.; Bezdek, M. J.; Chirik, P. J. *ACS Cent. Sci.* **2016**, *2*, 935–942. (d) Obligacion, J. V.; Semproni, S. P.; Pappas, I.; Chirik, P. J. *J. Am. Chem. Soc.* **2016**, *138*, 10645–10653. (e) Pabst, T. P.; Obligacion, J. V.; Rochette, É.; Pappas, I.; Chirik, P. J. *J. Am. Chem. Soc.* **2019**, *141*, 15378–15389.
(38) (a) Bowman, A. C.; Milsmann, C.; Atienza, C. C. H.; Lobkovsky, E.; Wieghardt, K.; Chirik,

P. J. *J. Am. Chem. Soc.* **2010**, *132*, 1676–1684. (b) Obligacion, J. V.; Chirik, P. J. *J. Am. Chem. Soc.* **2013**, *135*, 19107–19110.

(39) Schaefer, B. A.; Margulieux, G. W.; Small, B. L.; Chirik, P. J. *Organometallics* **2015**, *34*, 1307–1320.

(40) Kuriyama, S.; Arashiba, K.; Tanaka, H.; Matsuo, Y.; Nakajima, K.; Yoshizawa, K.; Nishibayashi, Y. *Angew. Chem. Int. Ed.* **2016**, *55*, 14291–14295.

(41) Tokmic, K.; Markus, C. R.; Zhu, L.; Fout, A. R. *Am. Chem. Soc.* **2016**, *138*, 11907–11913.

(42) Lin, T.-P.; Peters, J. C. *J. Am. Chem. Soc.* **2013**, *135*, 15310–15313.

(43) Ziessel, R. *Tetrahedron Lett.* **1989**, *30*, 463–466.

(44) Gunanathan, C.; Milstein, D. *Acc. Chem. Res.* **2011**, *44*, 588–602

(45) Langer, R.; Fuchs, I.; Vogt, M.; Balaraman, E.; Diskin-Posner, Y.; Shimon, L. J. W.; Ben-David, Y.; Milstein, D. *Chem. Eur. J.* **2013**, *19*, 3407–3414.

(46) Kamada, K.; Jung, J.; Wakabayashi, T.; Sekizawa, K.; Sato, S.; Morikawa, T.; Fukuzumi, S.; Saito, S. *J. Am. Chem. Soc.* **2020**, *142*, 10261−10266.

(47) A triplet signal was found at −8.65 ppm in a ^{1}H NMR spectrum (in C_6D_6). The detailed experimental results can be referred to ref. 45.

(48) (a) Takeshita, T.; Sato, K.; Nakajima, Y. *Dalton Trans.* **2018**, *47*, 17004–17010. (b) Takeshita, T.; Nakajima, Y. *Chem. Lett.* **2019**, *48*, 364–366.

(49) The bond length of C1−P1 bond is 1.777(4) Å, and the bond length of C−P bond on another side arm is 1.849(4) Å. The detailed experimental results can be referred to ref. 48b.

(50) Gautam, M.; Yatabe, T.; Tanaka, S.; Satou, N.; Takeshita, T.; Yamaguchi, K.; Nakajima, Y. *ChemistrySelect* **2020**, *5*, 15–17.

(51) Gautam, M.; Tanaka, S.; Sekiguchi, A.; Nakajima Y. *Organometallics* **2021**, *40*, 3697–3702.

Chapter 2 Synthesis and Reactivity of Cobalt(I) Alkyl Complexes with a Tetradentate Phenanthroline-Based PNNP Ligand

2-1. Introduction

As mentioned in Chapter 1, on the basis of the unique electronic structures, the cobalt(I) alkyl complexes with a tridentate pincer ligands often demonstrate diverse reactivities.[1] Polymerization of ethylene catalyzed by PDI-Co complexes (PDI = 2,6-bis(1-(2,6-diisopropyphenyllimino)ethyl)pyridine) were surveyed by Brookhard[2] and Gibson[3], and the mechanistic study suggested the presence of a reactive Co(I) species. More solid evidence based on the detailed mechanistic study was reported independently by Gibson[4] and Gal[5] in 2001, showing a PDI-Co(I) methyl complex behaved as a key intermediate.

Several leading reports on Co(I)-alkyl complexes with a series of pyridine-based PNP pincer ligands (PNP = 2,6-bis((dialkylphosphanyl)methyl)pyridine) were launched by Chirik *et al.*[6] For, example, CO_2 hydrosilylation was achieved catalyzed by a PNP-Co(I) (trimethylsilyl)methyl complex, which converts CO_2 into silyl formate, bis(silyl)acetyl, silyl ether, and siloxanes (Scheme 1a).[6a] This Co(I) alkyl complex was also found to be active for C–H borylation reaction of furan, thiophene, pyridine, benzene, and their derivatives (Scheme 1b).[6b,6d] Thus, miscellaneous catalytic abilities of Co(I) alkyl complexes can be expected by the introduction of pincer ligands.

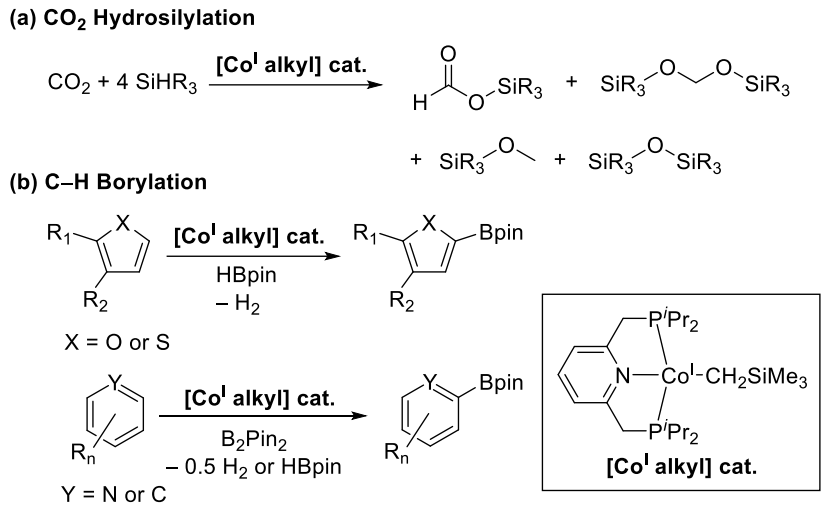

Scheme 1. Selected examples of catalytic reaction via Co(I) pincer complexes reported by Chirik's group. (a) CO_2 hydrosilylation. (b) C–H borylation.

It has been known that metal-ligand cooperation (MLC) further expands the reactivity of pincer complexes in various reactions.[7] Some specific reports has been reveal in Chapter 1, such

as Milstein's works on the direct synthesis of amides from alcohols and amines,[8] and consecutive H_2 and O_2 evolution from water,[9] both of which were mediated by MLC of Ru pincer complexes. However, in the chemistry of cobalt pincer complexes, examples to exhibit MLC behavior still remain rare. One distinct example is a formal loss of a H˙ radical from PNP-Co(I) methyl complexes via homolysis of benzylic C–H bond at the ligand side-arm (Chapter 1, Scheme 10).[10]

Recent study on a tetradentate PNNP ligand ((2,9-bis ((diphenylphosphanyl)methyl)-1,10-phenanthroline), which has the phenanthroline framework and renders MLC behavior via the dearomatization/rearomatization sequence of the phenanthroline framework, has demonstrated their applicability for catalysts, such as PNNP-Ru[11] and PNNP-Fe[12] systems (Chapter 1, Schemes 13 and 14). In this context, the preparation of the first PNNP-Co(I) alkyl complex [Co(CH_2SiMe_3)(PNNP)] (**2**) was achieved in our laboratory by the reaction of PNNP-Co(I) chloride (**1**) with 1 equiv of the corresponding Grignard reagent in 27% yield (Scheme 2).[13]

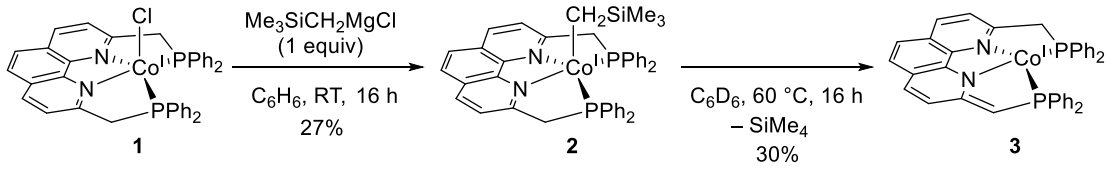

Scheme 2. Synthesis of **3**.

It is well known that the four low-coordinate Co(I) alkyl species are applicable for C–H bond cleavage.[14] For example, Chirik's group reported that PNP-Co(I) methyl complex successfully proceed an oxidative addition reaction of benzene at 80 °C.[15] In contrast, complex **2** was transformed to **3**, which possesses asymmetric dearomatized PNNP' ligand, upon heating at 60 °C. Concomitant formation of tetramethylsilane ($SiMe_4$) was also confirmed by ^1H NMR. This reaction strongly supports a long-range MLC behavior of the PNNP-Co system. To shed light on this phenomenon, mechanistic study was performed in this chapter.

2-2. Preparation of PNNP-Co(I) alkyl complexes

First of all, synthesis of **2** was re-examined. The reaction of **1** with Me_3SiCH_2MgCl was similarly performed. After several trials, it was revealed that the reduction of the reaction time to 1 h significantly improved the yield of **2** to 89%. By applying this method, the reaction of **1** with MeMgBr was also performed, affording another reaction platform of the PNNP-Co(I) alkyl, [CoMe(PNNP)] (**5**) with the isolated yield of 49% (Scheme 3). Complex **5** slowly decomposed at ambient temperature to form a complex mixture. However, it could be identified by NMR spectroscopy.

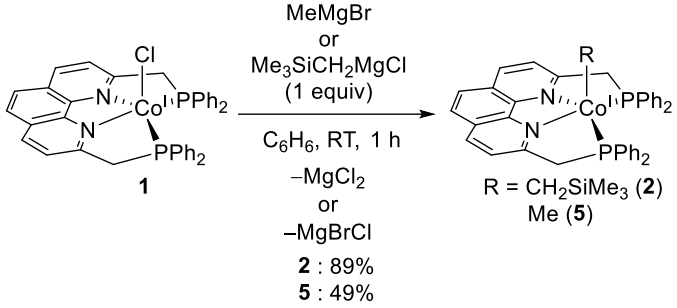

Scheme 3. Synthesis PNNP-Co(I) alkyl complexes **2** and **5** from **1**.

In $^{31}P\{^{1}H\}$ NMR spectrum, **5** exhibits one singlet at 76.9 ppm, which is similar to that of **2** (75.7 ppm). In ^{1}H NMR spectrum, the methyl group attached to the Co metal appears in the typical high-field region, −0.36 ppm ($^{3}J_{PH}$ = 3.3 Hz). Two side-arms (PCH_2) were found at 3.93 (m) and 4.42 ppm (d, $^{2}J_{PH}$ = 16.3 Hz).

2-3. Mechanistic study of PNNP-Co(I) alkyl complexes

To shed light on the mechanism of the transformation of **2** to **3**, further consideration is necessary.[16] Therefore, reaction of **2** with TEMPO ((2,2,6,6-tetramethylpiperidin-1-yl)oxyl) as a radical scavenger was examined (Scheme 4).[17]

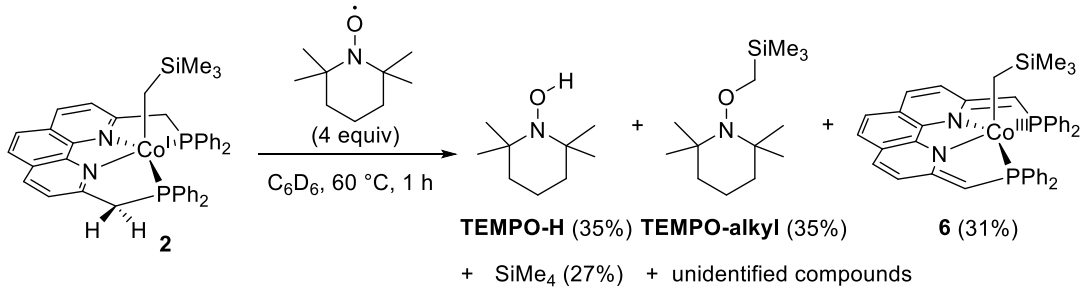

Scheme 4. Reaction of **2** with TEMPO.

Complex **2** reacted with excess amount of TEMPO (4 equiv) at 60 °C for 1 h. The reaction mixture was examined by ^{1}H NMR, showing a formation of a new Co complex (**6**), TEMPO-H, TEMPO-alkyl, and $SiMe_4$ in 31%, 35%, 35%, and 27% yield, respectively, along with some unidentified species. Based on the formation of TEMPO-alkyl, it was suggested that Co–C homolysis proceeded to generate $(Me_3Si)CH_2^{\bullet}$ radical during this reaction. The formation of $SiMe_4$ and TEMPO-H should be formed via H atom abstraction by $(Me_3Si)CH_2^{\bullet}$ radical and TEMPO radical, respectively.

Considering these observations, it is likely that the Co–C homolysis proceeds during the

transformation from **2** to **3**, where the resulting alkyl radical further underwent benzylic H atom abstraction to afford $SiMe_4$ (Scheme 5). In this process, the delocalized π-system composed of the Co metal and the PNNP ligand, which was evidenced in the PNNP-Fe system (Chapter 1, Scheme 14), should facilitate the benzylic H atom abstraction.

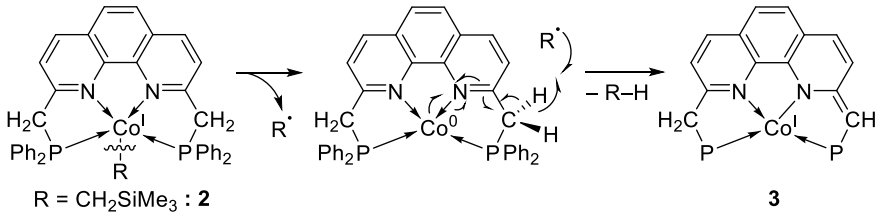

Scheme 5. Possible reaction path for the formation of **3** from **2**.

Complex **6** was identified by NMR. Complex **6** exhibits one singlet signal at 33.9 ppm in the $^{31}P\{^1H\}$ NMR spectrum, which can be assigned to the PCH groups. In the ^1H NMR spectrum, the CH_2SiMe_3 group appears at −0.17 (s, 9H) and −0.29 (t, 2H). There is a singlet signal of the PCH groups at 4.68 ppm with the integral intensity of 2 H. In the $^{13}C\{^1H\}$ NMR spectrum, the PCH groups exhibit one singlet signal at 82.7 ppm. All these observed NMR spectra are consistent with the assignment of **6** as a Co(III) alkyl complex (alkyl = CH_2SiMe_3) with a symmetrically doubly-deprotonated PNNP''' ligand. It is likely that the doubly C–H bond homolysis occurred on the treatment of **2** with TEMPO to afford **6**. It should be mentioned that all the above-mentioned reaction processes include benzylic H atom abstraction from the ligand side-arms, strongly supporting the occurrence of long-rang MLC.

Single crystals of **6** were formed from its cold hexane solution, therefore structural determination of **6** was performed by a single-crystal X-ray study (Figure 1).

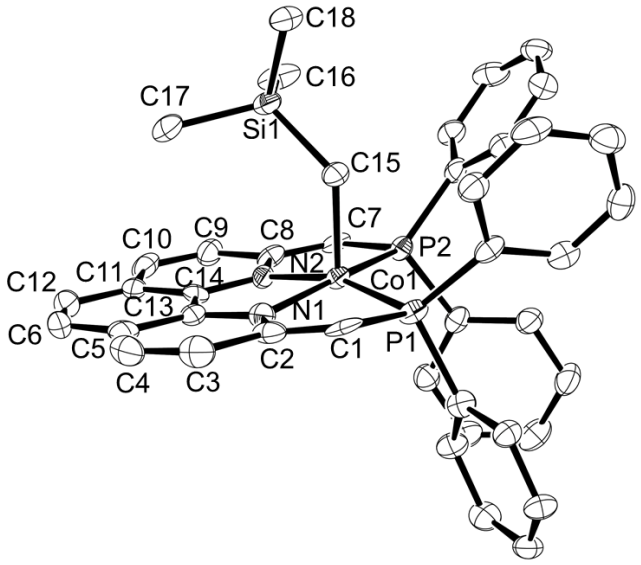

Figure 1. ORTEP drawing of **6** with 50% probability ellipsoids.[16] Hydrogen atoms are omitted for clarity. Selected bond lengths (Å) and angles (°): Co–C15, 2.017(5); Co–P1, 2.2196(15); Co–P2, 2.2207(15); Co1–N1, 1.894(4); Co–N2, 1.884(4); P1–Co–P2, 110.68(6); P1–Co–N1, 82.02(14); N1–Co–N2, 83.31(19); N2–Co–P2 82.36(13).

The C1−C2 (1.361(7) Å) and C7−C8 (1.357(7) Å) bonds exhibit double bond character.[17] Moreover, the bond lengths of C2−C3 and C3−C4 are 1.451(7) and 1.354(7) Å, which can be assigned to a single bond and a double bond, respectively. A similar trend was observed in C8−C9 (1.449(7) Å) and C9−C10 (1.339(7) Å) bonds on the other side. Collectively, all values of the X-ray result are consistent with the NMR spectral data.

2-4. Conclusion

In this chapter, two PNNP-Co(I) alkyl complexes, **2** and **5**, were synthesized in good yields. Owing to the stable diamagnetic characteristics of these complexes, **5** was fully characterized by NMR spectroscopy. Mechanistic study was performed to shed light on the transformation of **2** to **3**. On the treatment of **2** with TEMPO as a radical scavenger as well as a hydrogen atom acceptor, both alkyl group and H atom were trapped. Based on this observation, it was concluded that formation of **3** from **2** initiated by the Co–C homolysis to form an alkyl radical, where the resulting alkyl radical further underwent benzylic H atom abstraction to afford $SiMe_4$. In the TEMPO reaction, a new Co(III) alkyl complex **6**, which possesses doubly-dearomatized PNNP''' ligand, was formed. It is likely that the double C−H bond homolysis occurred on the treatment of **2** with TEMPO to afford **6**. Based on these results, occurrence of the facile benzylic-H atom abstraction of the PNNP ligand was evidenced, supporting the potential capability of a long-range

MLC of **2**, which could be promising to develop new catalytic reactions.

2-5. Experimental Details

2-5-1. Synthesis of [Co(CH_2SiMe_3)(PNNP)] (**2**)[13, 16]

1 (19.9 mg, 0.030 mmol) was dissolved in benzene (35 mL) and stored in a 50 mL Schlenk tube. Trimethylsilylmethylmagnesium chloride (30.0 μL of 1 M THF solution, 0.030 mmol) was added dropwise. The mixture was stirred at room temperature for 1 h. The resulting solution was dried under vacuum. The residue was extracted with Et_2O and filtered using a Celite pad. The filtrate was concentrated to dryness under vacuo to afford **2** as a purple solid (18.7 mg, 0.026 mmol, 87 %).

^{1}H NMR (C_6D_6, 25 °C) δ 7.35 (d, 2H, Phen-*H*, $^3J_{HH}$ = 7.0 Hz), 7.32 (m, 4H, P*Ph*$_2$), 7.13 (vt, 4H, Phen-*H* (2H) + P*Ph*$_2$ (2H)), 7.04 (vq, 6H, Phen-*H* (2H) + P*Ph*$_2$ (4H)), 6.75 (m, 4H, PPh_2), 6.64 (t, 2H, PPh_2, $^3J_{HH}$ = 7.4 Hz), 6.49 (t, 4H, P*Ph*$_2$, $^3J_{HH}$ = 7.7 Hz), 4.81 (d, 2H, PC*H*$_2$, $^3J_{HH}$ = 15.8 Hz), 3.95 (m, 2H, PC*H*$_2$), –0.57 (s, 9H, C*H*$_2$SiMe$_3$), –0.60 (t, 2H, CH_2SiMe_3, $^3J_{PH}$ = 4.4 Hz). ^{13}C{^{1}H} NMR (C_6D_6, 25 °C) 157.0, 140.0, 138.7, 134.2, 133.5, 131.7, 131.4, 129.5, 128.6 (×2), 128.3, 126.3, 117.2, 113.7, 45.4, 2.9, –22.2. ^{31}P{^{1}H} NMR (C_6D_6, 25 °C) δ 75.72. ^{29}Si{^{1}H} NMR (C_6D_6, 25 °C) δ 7.46 (t, $^3J_{SiP}$ = 3.6 Hz). HRMS (ESI) Calculated: ($C_{42}H_{42}CoN_2P_2Si$) 723.1919 ([M+H]$^+$), Found: 723.1907.

2-5-2. Synthesis of [CoMe(PNNP)] (**5**)[19]

1 (50.0 mg, 0.074 mmol) was dissolved in benzene (5 mL) and stored in a 30 mL Schlenk tube. Methylmagnesium bromide (29 μL of 3.0 M Et_2O solution, 0.090 mmol) was added dropwise at room temperature. The mixture was stirred at room temperature for 1 h. The resulting solution was dried under vacuum, and the residue was extracted with ether. The solution was filtered using a Celite pad, and the filtrate was concentrated to dryness under vacuo to afford **5** as a purple solid (23.2 mg, 0.036 mmol, 49 %).

^{1}H NMR (C_6D_6, 25 °C) δ 7.69 (br, 2H, Phen-*H*), 7.29 (br, 4H, P*Ph*$_2$), 7.12 (m, 2H, Phen-*H*), 7.08 (s, 2H, Phen-*H*), 7.02 (brm, 4H, P*Ph*$_2$), 6.91 (m, 6H, P*Ph*$_2$), 6.73 (t, 2H, P*Ph*$_2$, $^3J_{HH}$ = 7.0 Hz), 6.61 (t, 4H, P*Ph*$_2$, $^3J_{HH}$ = 7.3 Hz), 4.42 (d, 2H, PC*H*$_2$, $^3J_{HH}$ = 16.3 Hz), 3.93 (m, 2H, PC*H*$_2$), –0.36 (t, 3H, CoC*H*$_3$, $^3J_{PH}$ = 3.3 Hz). ^{13}C{^{1}H} NMR (C_6D_6, 25 °C) 156.4, 140.8, 138.0, 133.7, 133.4, 131.9, 131.8, 129.3, 128.6, 126.3, 116.3, 112.5, 45.4, –15.2. Two Ar signals were obscured in a residual benzene signal. ^{31}P{^{1}H} NMR (C_6D_6, 25 °C) δ 76.92. HRMS (ESI) Calculated: ($C_{39}H_{33}CoN_2P_2$) 651.1524 ([M+H]$^+$), Found: 651.1511.

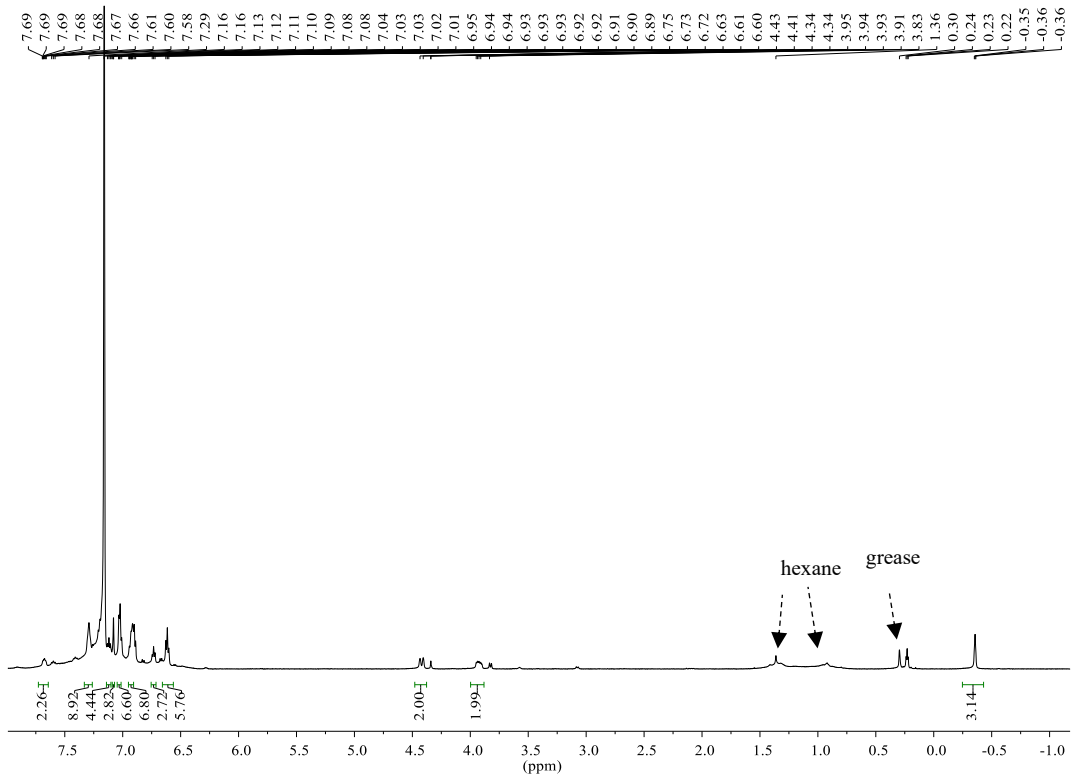

Figure 2. ^{1}H NMR spectrum of **5** in C_6D_6.

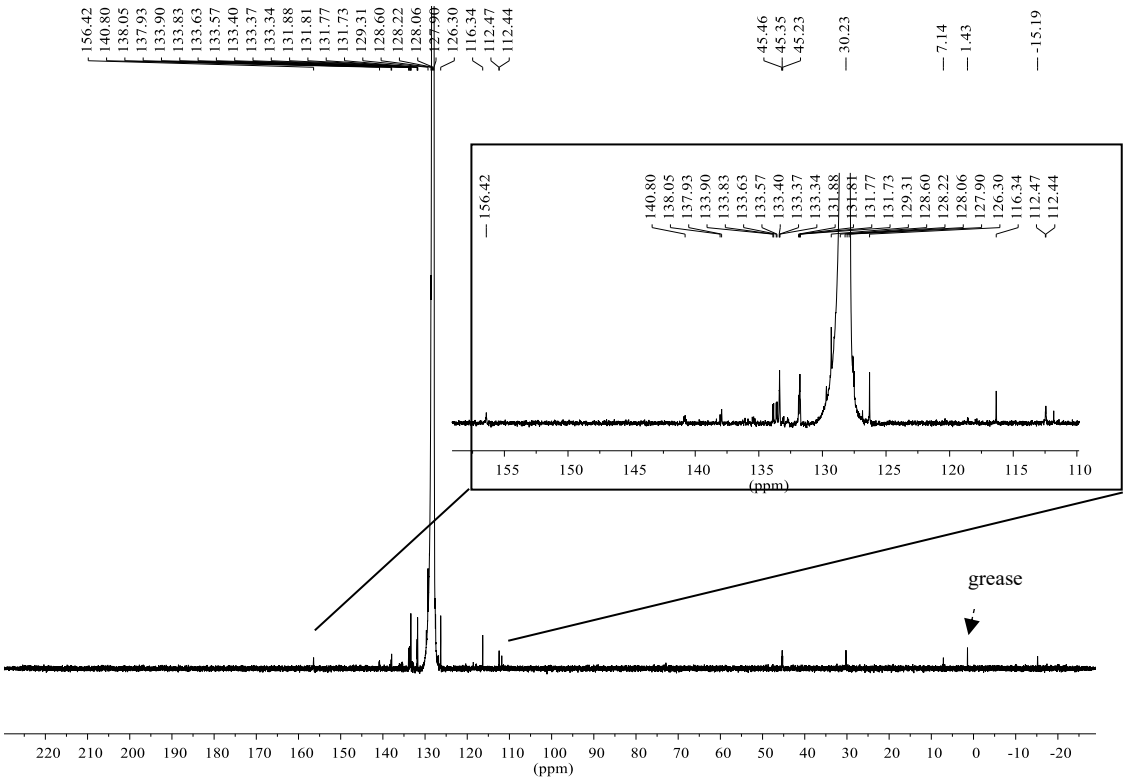

Figure 3. $^{13}C\{^{1}H\}$ NMR spectrum of **5** in C_6D_6.

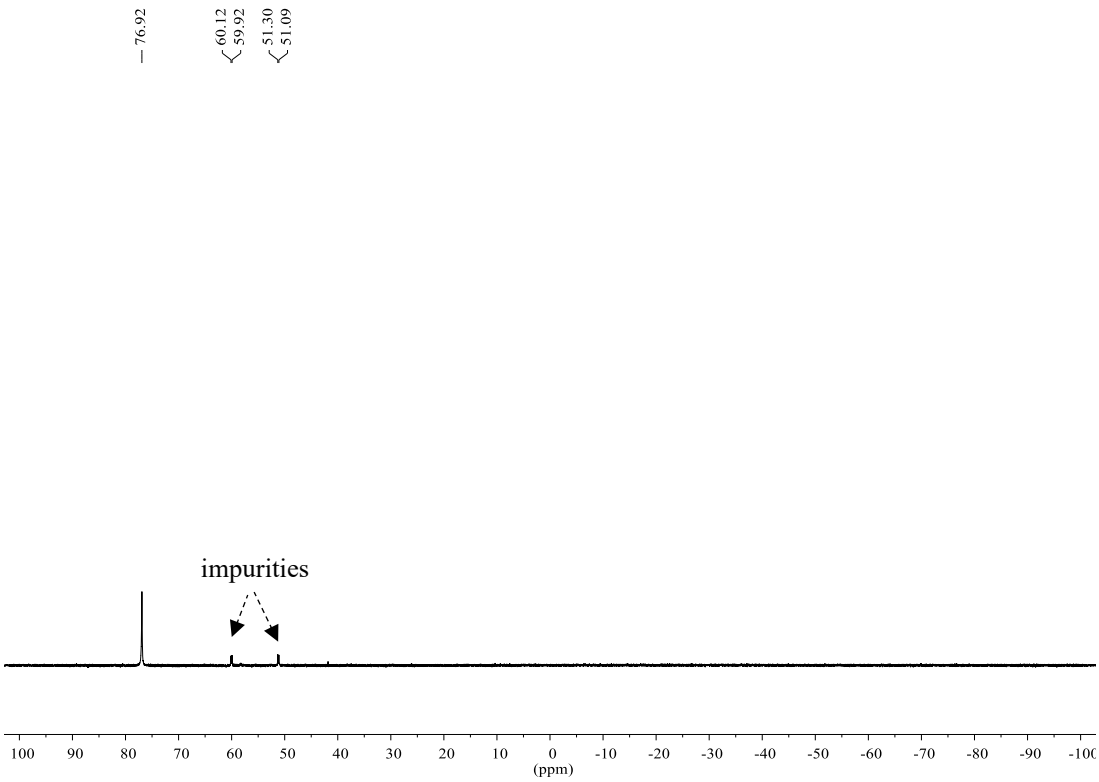

Figure 4. $^{31}P\{^{1}H\}$ NMR spectrum of **5** in C_6D_6.

2-5-3. Synthesis of [Co(PNNP')] (**3**)[13, 16]

Method 1[13]: **2** (24.3 mg, 0.034 mmol) was charged in a 50 mL Schlenk tube and dissolved in benzene (10 mL). The solution was stirred at 60 °C for 16 h to form a deep green crystalline precipitate. After filtration, **3** was obtained as an analytically pure form (14.2 mg, 0.029 mmol, 86%). Single crystals of **3** was obtained by slow evaporation of saturated C_6H_6 solution of **3** at room temperature.

Method 2[16]: To a benzene solution (10 mL) of **1** (15.2 mg, 0.023 mmol), was added sodium tert-butoxide (2.2 mg, 0.023 mmol). The solution was stirred at room temperature for a few minutes. The solution was filtered with a Celite pad to give **3** as a deep green solid (13.8 mg, 0.022 mmol, 96%).

^{1}H NMR (C_6D_6, 25 °C) δ 7.60 (t, 4H, P*Ph*$_2$, $^{3}J_{HH}$ = 8.6 Hz), 7.56 (d, 1H, Phen-*H*, $^{3}J_{HH}$ = 8.3 Hz), 7.41 (t, 4H, P*Ph*$_2$, 3JHH = 8.6 Hz), 7.00 (m, 4H, P*Ph*$_2$), 6.88-6.93 (m, 9H, Phen-*H* (1H) + P*Ph*$_2$ (8H)), 6.65 (m, 2H, Phen-*H*), 6.55 (d, 1H, Phen-*H*, $^{3}J_{HH}$ = 8.0 Hz), 6.28 (d, 1H, Phen-*H*, $^{3}J_{HH}$ = 8.5 Hz), 4.33 (brs, 1H, PC*H*), 3.08 (d, 2H, PC*H*$_2$, $^{2}J_{PH}$ = 12.0 Hz). $^{13}C\{^{1}H\}$ NMR (DMSO-*d*$_6$, 25 °C) δ 165.8, 151.3, 146.0, 143.6, 139.4, 133.9, 132.6, 130.8, 130.7, 129.4, 127.9, 127.7, 127.6, 127.2, 126.1, 124.0, 121.6, 117.1, 114.2, 111.2, 70.9, 46.7. $^{31}P\{^{1}H\}$ NMR (C_6D_6, 25 °C) δ 52.8 (br), 38.2 (br). HRMS (ESI) Calculated: ($C_{38}H_{29}CoN_2P_2$) 634.1132 ([M+H]$^{+}$), Found: 634.1148.

Anal. Calculated for $CoN_2P_2C_{38}H_{29}$: C, 71.93; H, 4.61; N 4.41. Found: C, 72.24; H, 4.96; N, 4.58.

2-5-4. Reaction of **2** with TEMPO[16]

A C_6D_6 solution (0.4 mL) of **2** (9.1 mg, 0.013 mmol) was charged in a J-Young NMR tube, and TEMPO (2,2,6,6-tetramethylpiperidin-1-yl)oxyl) (7.7 mg, 0.049 mmol) was then added to the solution. The solution was left to stand at 60 °C for 1 h, and the resulting solution was analyzed by ^{1}H NMR by comparing with 1 euqiv. 1,4-dioxane (1.1 mg, 0.013 mmol) as the internal standard to determine the yield of each product. TEMPO-H[20] and TEMPO-CH_2SiMe_3[21] were identified by comparison of their spectral data with those of authentic samples. The yields of **6**, TEMPO-H, TEMPO-CH_2SiMe_3 and $SiMe_4$ were 31%, 35%, 35%, and 27%, respectively. After removal of all the volatiles, the resultant was extracted with hexane. The extract was concentrated to dryness to give **6** (trace amount).

TEMPO-H: ^{1}H NMR (C_6D_6, 25 °C) δ 3.74 (br, 1H, O*H*), 1.39 (m, 4H, CH_2), 1.30 (m, 2H, CH_2), 1.15 (s, 12H, CH_3).

TEMPO-CH_2SiMe_3: ^{1}H NMR (C_6D_6, 25 °C) δ 3.54 (s, 2H, OCH_2), 1.48 (m, 4H, CH_2), 1.33 (m, 2H, CH_2), 1.16 (br, 6H, CH_3), 1.08 (br, 6H, CH_3), 0.06 (s, 9H, Si(CH_3)$_3$).

6: 1H NMR (C_6D_6, 25 °C) δ 7.44 (m, 4H, P*Ph*$_2$), 7.40 (m, 4H, P*Ph*$_2$), 7.07 (t, 2H, P*Ph*$_2$, $^3J_{HH}$ = 7.3 Hz), 7.00 (t, 4H, P*Ph*$_2$, $^3J_{HH}$ = 7.4 Hz), 6.89 (t, 2H, P*Ph*$_2$, $^3J_{HH}$ = 7.3 Hz), 6.72 (d, 2H, Phen-*H*, $^3J_{HH}$ = 9.2 Hz), 6.67-6.63 (m, 6H, Phen-*H* (2H) + P*Ph*$_2$ (4H)), 6.62 (d, 2H, Phen-H, $^3J_{HH}$ = 9.2 Hz), 4.68 (s, 2H, PC*H*), –0.17 (s, 9H, Si*Me*$_3$), –0.29 (t, 2H, CH_2SiMe_3, $^3J_{PH}$ = 9.2 Hz). ^{13}C{^{1}H} NMR (C_6D_6, 25 °C) δ 167.5, 146.8, 133.7, 132.7, 132.1, 132.0, 131.9, 131.7, 129.9, 129.4, 128.5, 121.1, 121.0, 117.7, 82.7, 0.60 (×2). HSQC (C_6D_6, 25 °C) δ_H-δ_C –0.17 (δ_H), –0.29 (δ_H) - 0.60 (δ_C). ^{31}P{^{1}H} NMR (C_6D_6, 25 °C) δ 33.9 (br). ^{29}Si{^{1}H} NMR (C_6D_6, 25 °C) δ 9.24 (t, $^3J_{SiP}$ = 1.2 Hz). HRMS (ESI) Calculated: ($C_{42}H_{39}CoN_2P_2Si$) 721.1763 ([M]$^+$), Found: 721.1764. Single crystal of **6** was obtained from cold hexane solution at –35 °C.

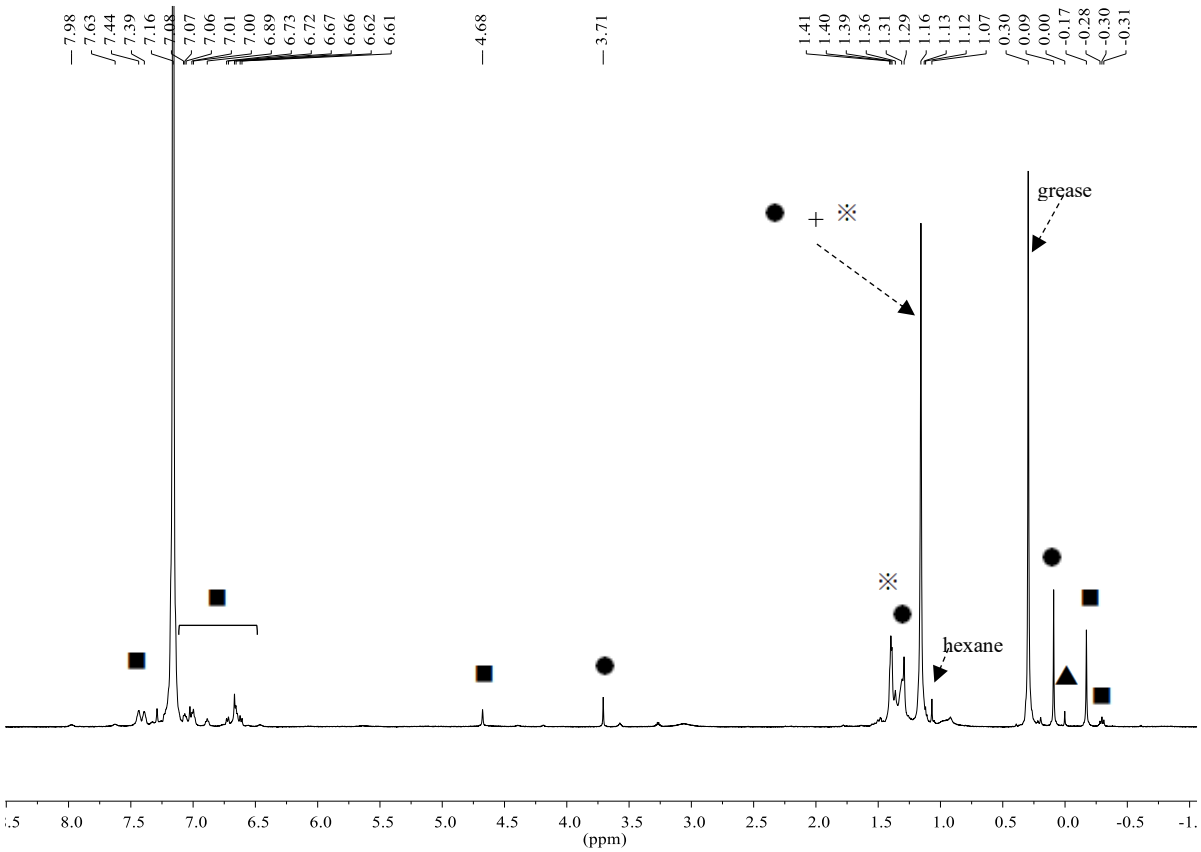

Figure 5. ^{1}H NMR spectrum of the reaction mixture in C_6D_6; ■ : 6; ● : TEMPO-CH_2SiMe_3;

▲ : $SiMe_4$; ※: TEMPO-H.

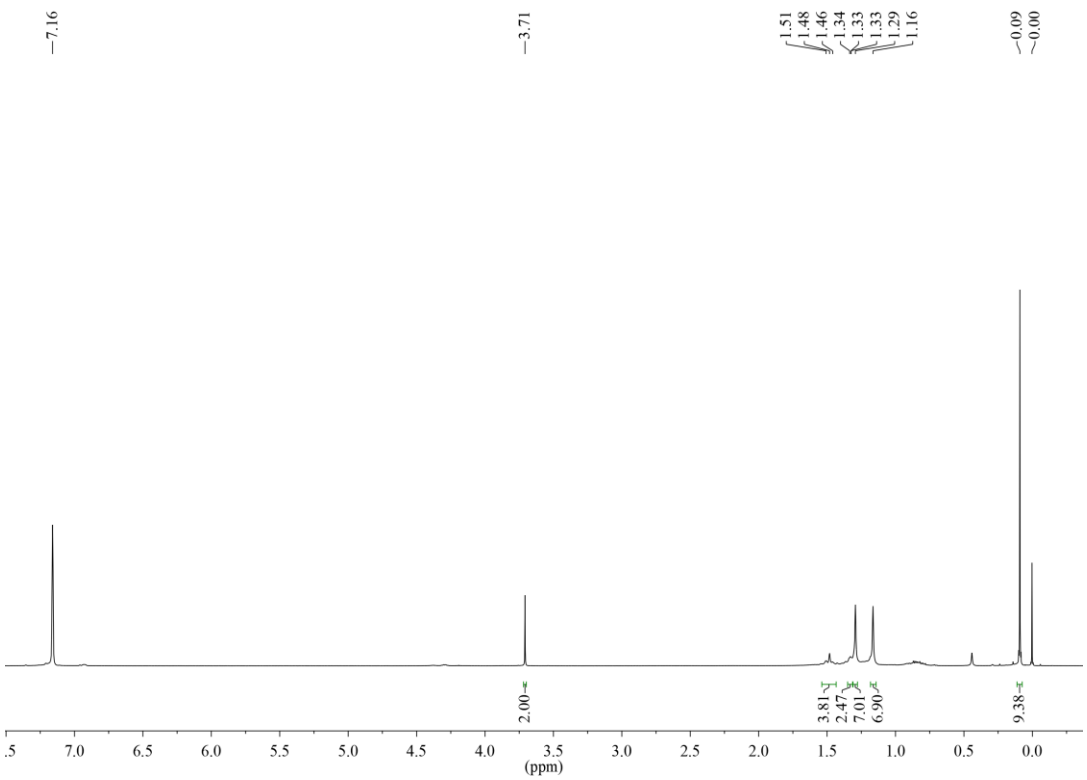

Figure 6. ^{1}H NMR of TEMPO-CH_2SiMe_3 in C_6D_6.

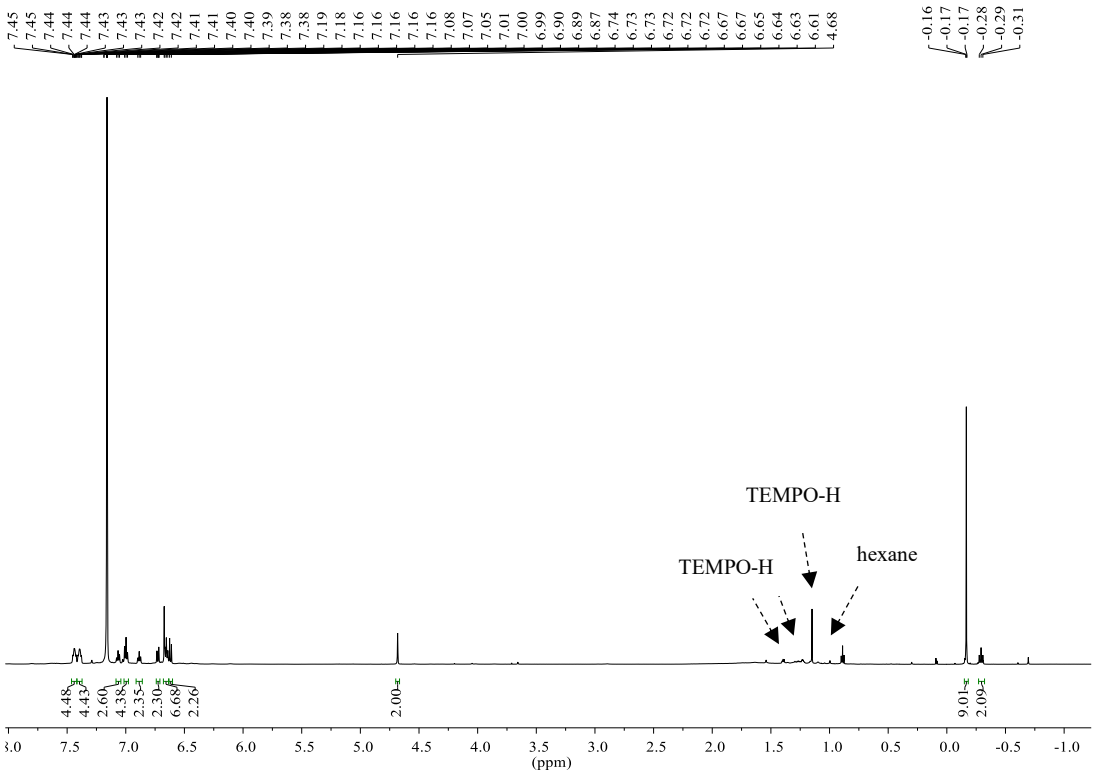

Figure 7. ^{1}H NMR of **6** in C_6D_6.

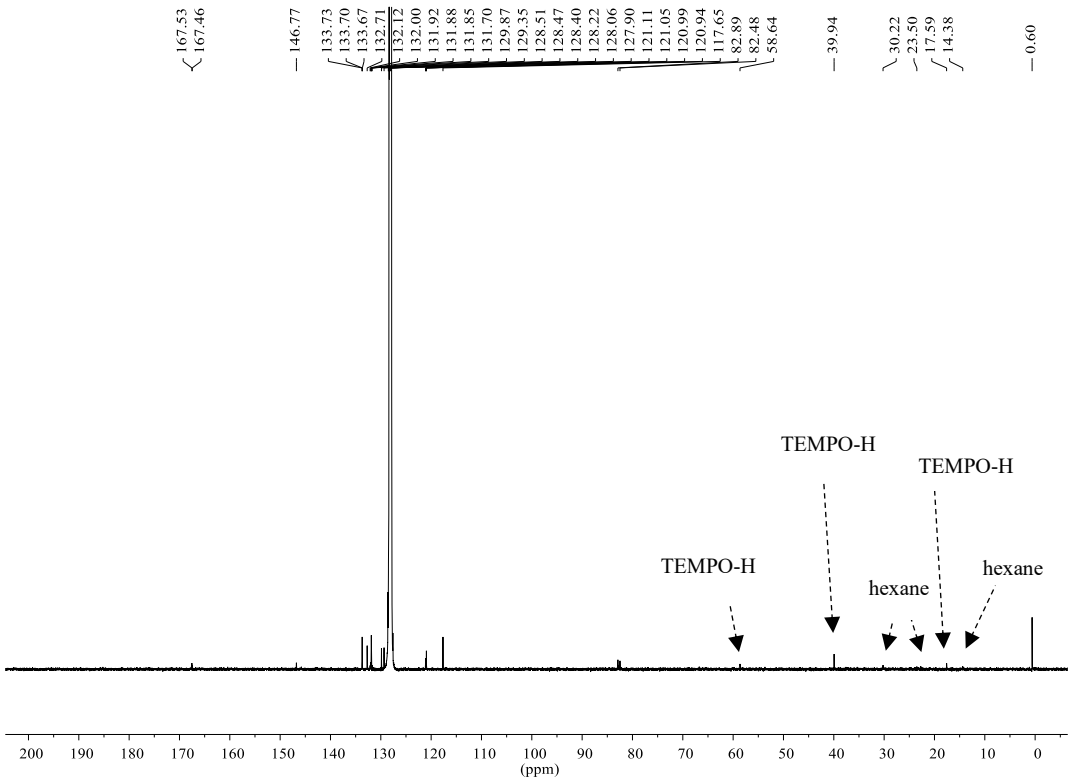

Figure 8. $^{13}C\{^{1}H\}$ spectrum of **6** in C_6D_6.

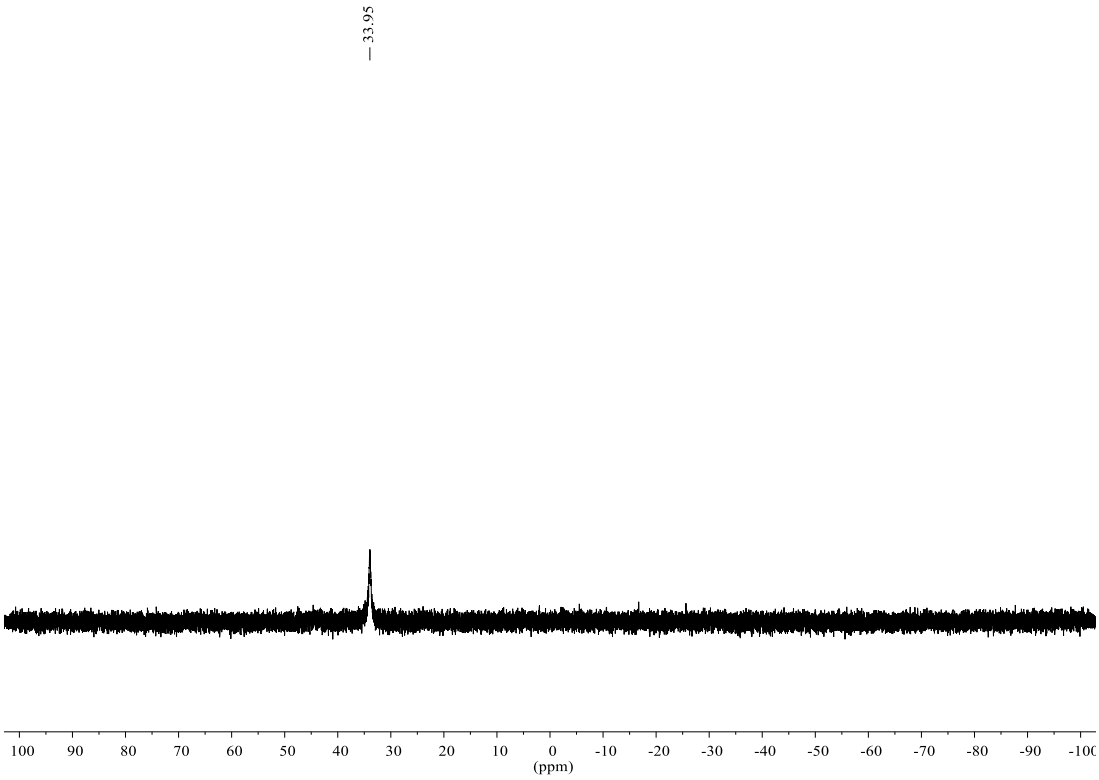

Figure 9. $^{31}P\{^{1}H\}$ spectrum of **6** in C_6D_6.

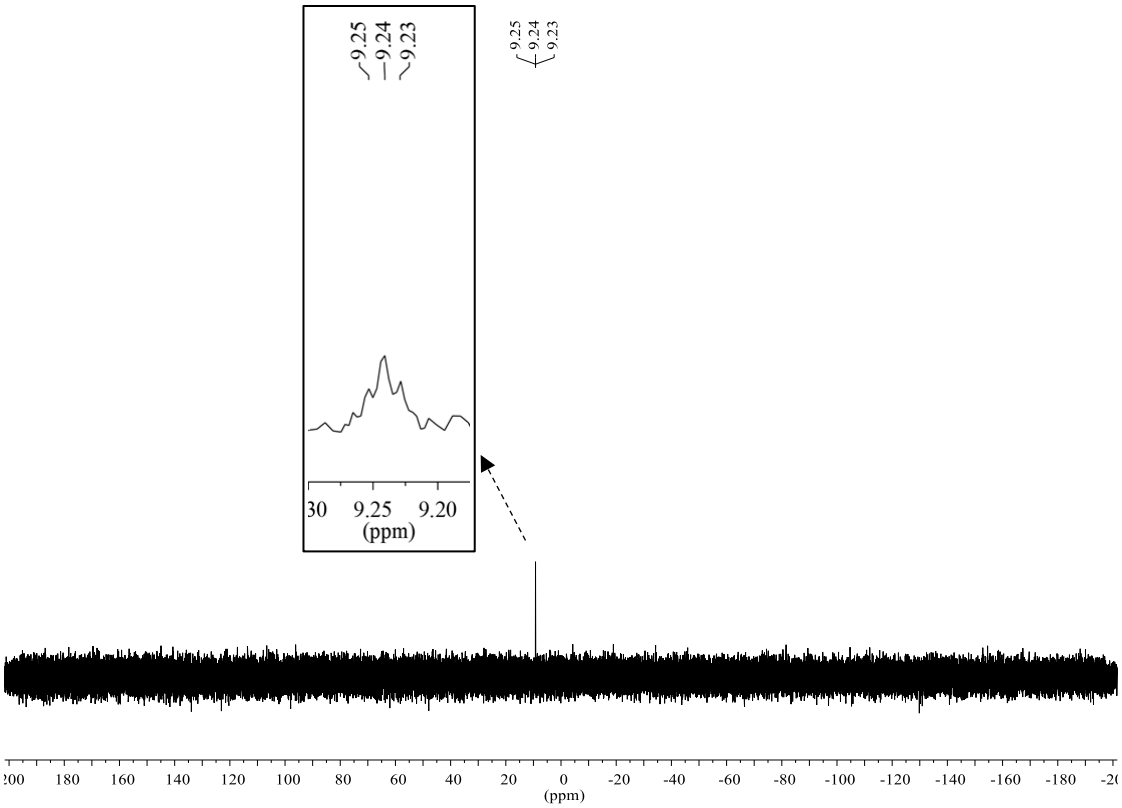

Figure 10. $^{29}Si\{^{1}H\}$ spectrum of **6** in C_6D_6.

2-5-5. X-ray Crystallographic Data

All single-crystal X-ray diffraction measurements of **6** was performed under a cold nitrogen stream on a Rigaku XtaLAB P200 diffractometer with a Pilatus 200K detector using multi-layer mirror monochromated Mo-Kα radiation (λ = 0.71073 Å, 50 kV/24 mA). The determination of crystal systems and unit cell parameters were performed with the CrystalClear program package. Data processing was performed with the CrystalClear program package or CrysAlisPro program package. All structures were solved by direct methods using SIR2014 program[22], and refined by full-matrix least squares calculations on F2 for all reflections (SHELXL-2014/7)[23], using Yadokari-XG 2009 program[24]. The X-ray crystallographic data for **6** has been deposited at the Cambridge Crystallographic Data Centre (CCDC) under deposition no. CCDC 2013569. These data can be obtained free of charge from the CCDC (www.ccdc.cam.ac.uk/data_request/cif).

Table 1. Crystallographic parameters of **6**.

Empirical formula	$C_{42}H_{39}CoN_2P_2Si$	α/deg	90 °
Formula weight	720.71	β/deg	103.596(8) °
Temperature	93(2) K	γ/deg	90 °
Crystal system	monoclinic	Volume	3526.3(5) $Å^3$
Space group	$P2_1/c$	Z	4
a/Å	15.4631(12) Å	Goodness-of-fit on F^2	1.038
b/Å	12.4153(11) Å	Final R indices [I>2sigma(I)]	$R1$ =0.0577, $wR2$ = 0.1107
c/Å	18.8980(12) Å	R indices (all data)	$R1$ = 0.1227, $wR2$ = 0.1564

Reference

(1) (a) Liu, W.; Shahoo, B.; Junge, K.; Beller, M. *Acc. Chem. Res.* **2018**, *51*, 1858−1869. (b) Junge, K.; Papa, V.; Beller, M. *Chem. Eur. J.* **2019**, *25*,122–143.

(2) (a) Johnson, L. K.; Killian, C. M.; Brookhart, M. *J. Am. Chem. Soc.* **1995**, *117*, 6414–6415. (b) Small, B. L.; Brookhart, M.; Bennett, A. M. A. *J. Am. Chem. Soc.* **1998**, *120*, 4049–4050. (c) Small, B. L.; Brookhart, M. *J. Am. Chem. Soc.* **1998**, *120*, 7143–7144. (d) Ittel, S. D.; Johnson, L. K.; Brookhart, M. *Chem. Rev.* **2000**, 100, 1169–1204.

(3) (a) Britovsek, J. P.; Gibson, V. C.; Kimberley, B. S.; Maddox, P. J.; McTavish, S. J.; Solan, G. A.; White, A. J. P.; Williams, D. J. *Chem. Commun.* **1998**, *7*, 849 –850. (b) Britovsek, G. J. P.; Bruce, M.; Gibson, V. C.; Kimberley, B. S.; Maddox, P. J.; Mastroianni, S.; McTavish, S. J.; Redshaw, C.; Solan, G. A.; Strömberg, S.; White, A. J. P.; Williams, D. J. *J. Am. Chem. Soc.* **1999**, *121*, 8728–8740.

(4) Gibson, V. C.; Humphries, M. J.; Tellmann, K. P.; Wass, D. F.; White, A. J. P.; Williams, D. J. *Chem. Commun.* **2001**, 2252–2253.

(5) Kooistra, T. M.; Knijnenburg, Q.; Smits, J. M. M.; Horton, A. D.; Budzelaar, P. H. M.; Gal, A. W. *Angew. Chem. Int. Ed.* **2001**, *40*, 4719–4722.

(6) (a) Scheuermann, M. L.; Semproni, S. P.; Pappas, I.; Chirik, P. J. *Inorg. Chem.* **2014**, *53*, 9463–9465. (b) Obligacion, J. V.; Semproni, S. P.; Chirik, P. J. *J. Am. Chem. Soc.* **2014**, *136*, 4133–4136. (c) Neely, J. M.; Bezdek, M. J.; Chirik, P. J. *ACS Cent. Sci.* **2016**, *2*, 935–942. (d) Obligacion, J. V.; Semproni, S. P.; Pappas, I.; Chirik, P. J. *J. Am. Chem. Soc.* **2016**, *138*, 10645–10653. (e) Pabst, T. P.; Obligacion, J. V.; Rochette, É.; Pappas, I.; Chirik, P. J. *J. Am. Chem. Soc.* **2019**, *141*, 15378–15389.

(7) (a) Grützmacher, H. *Angew. Chem. Int. Ed.* **2008**, *47*, 1814–1818. (b) Khusnutdinova, J. R.; Milstein, D. *Angew. Chem. Int. Ed.* **2015**, *54*, 12236–12273.
(8) Gunanathan, C.; Ben-David, Y.; Milstein, D. *Science* **2007**, *317*, 790–792.
(9) Kohl, S. W.; Weiner, L.; Schwartsburd, L.; Konstantinovski, L.; Shimon, L. J. W.; Ben-David, Y.; Iron, M. A.; Milstein, D. *Science* **2009**, *324*, 74–77.
(10) Khaskin, E.; Diskin-Posner, Y.; Weiner, L.; Leitus, G.; Milstein, D. *Chem. Commun.* **2013**, *49*, 2771–2773.
(11) Langer, R.; Fuchs, I.; Vogt, M.; Balaraman, E.; Diskin-Posner, Y.; Shimon, L. J. W.; Ben-David, Y.; Milstein, D. *Chem. Eur. J.* **2013**, *19*, 3407–3414.
(12) (a) Takeshita, T.; Sato, K.; Nakajima, Y. *Dalton Trans.* **2018**, *47*, 17004–17010. (b) Takeshita, T.; Nakajima, Y. *Chem. Lett.* **2019**, *48*, 364–366. (c) Gautam, M.; Yatabe, T.; Tanaka, S.; Satou, N.; Takeshita, T.; Yamaguchi, K.; Nakajima, Y. *ChemistrySelect* **2020**, *5*, 15–17. (e) Gautam, M.; Tanaka, S.; Sekiguchi, A.; Nakajima Y. *Organometallics* **2021** ASAP.
(13) Ishizaka, Y. Master thesis in February 2019.
(14) (a) Hung-Low, F.; Krogman, J. P.; Tye, J. W.; Bradley, C. A. *Chem. Commun.* **2012**, *48*, 368–370. (b) Marinescu, S. C.; Winkler, J. R.; Gray, H. B. *Proc. Natl. Acad. Sci. U. S. A.* **2012**, *109*, 15127–15131. (c) Reinaud, O. M.; Theopold, K. H. *J. Am. Chem. Soc.*
1994, *116*, 6979–6980. (d) Sung, S.; Wang, Q.; Krämer, T.; Young, R. D. *Chem. Sci.* **2018**, *9*, 8234–8241.
(15) Semproni, S. P.; Hojilla Atienza, C. C.; Chirik, P. J. *Chem. Sci.* **2014**, *5*, 1956–1960.
(16) Jheng, N.Y.; Ishizaka, S.; Naganawa, Y.; Sekiguchi, A.; Nakajima, Y. *Dalton Trans.* **2020**, *49*, 14592–14597.
(17) The bond length of C1–P1 bond is 1.788(2) Å, and the bond length of C–P bond on another side arm is 1.867(2) Å. The detailed experimental results can be referred to ref. 16.
(18) Takeshita, T.; Nakajima, Y. *Chem. Lett.* **2019**, *48*, 364–366.
(19) Considering the relative instability of **5**, the reaction of **5** with TEMPO was not performed.
(20) Henry-Riyad, H.; Tidwell, T. T. *J. Phys. Org. Chem.* **2003**, *16*, 559–563.
(21) Kurandina, D.; Parasram, M.; Gevorgyan, V. *Angew. Chem. Int. Ed.* **2017**, *56*, 14212–14216.
(22) Burla, M.C.; Caliandro, R.; Carrozzini, B.; Cascarano, G. L.; Cuocci, C.; Giacovazzo, C.; Mallamo, M.; Mazzone, A.; Polidori, G. *J. Appl. Cryst.* **2015**, *48*, 306.
(23) M.Sheldrick, G. *Acta Crystallogr. Sect. A Found. Crystallogr.* **2008**, *64*, 112–122.
(24) Kabuto, C.; Akine, S.; Nemoto, T.; Kwon, E. Release of software (Yadokari-XG 2009) for crystal structure analyses. *Nippon Kessho Gakkaishi* **2009**, *51*, 218.

Chapter 3 Hydrogen Activation via Metal-Ligand Cooperation of PNNP-Cobalt(I) Complexes

3-1. Introduction

Hydrogen activation is considered as an important method to utilize molecular hydrogen (H_2) to various areas, such as hydrogenation reactions[1] and hydrogen storage[2]. Among various approaches to activate H_2, H–H bond cleavage by metal complexes undergoes oxidative addition, and the reverse reaction proceeds via reductive elimination (Scheme 1).[3]

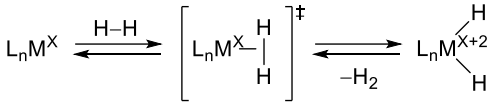

Scheme 1. Reversible hydrogen activation via a metal complex.

In comparison with the above classical model of hydrogen activation, metal-ligand cooperation (MLC) utilizes both metal centers and ligand moieties to achieve H–H cleavage.[4] One leading report was achieved via a $BINAP^{Tol}$-Ru(II)-diamine complex ($BINAP^{Tol}$ = 2,2'-bis(di-4-tolylphosphino)-1,1'-binaphthyl) by Noyori *et al.*[5] as mentioned in Chapter 1.

In the cobalt(I) pincer complexes, the reaction pattern of H_2 activation varies depending on the ligand system. For example, Chirik *et al.* reported activation of atmospheric H_2 with a CNC-Co(I) methyl complex (CNC = bis(arylimidazol-2-ylidene)pyridine) to afford a CNC-Co(I) hydride complex in 2013 (Scheme 2a). The application of this CNC-Co(I) methyl complex as the pre-catalyst to hydrogenation of alkenes was also reported.[6] Thomas *et al.* reported the first H_2 activation across 3d metal–P bond via MLC in 2018 (Scheme 2b).[7] The heterolytic H–H bond cleavage was achieved in THF under 1 atm H_2 by a PPP-Co(I) complex (PPP = 1,3-bis(2-(diphenylphosphino)phenyl)-1,3,2-diazaphospholidine). Unfortunately, the PPP-Co(I) complex was found to exhibit poor reactivity in catalytic hydrogenation of alkenes due to the steric hinderance of its trimethylphosphine group (PMe_3).[7] To the best of my knowledge, Thomas's report is the only example to achieve H_2 activation, mediated via MLC of a Co(I) pincer complex.

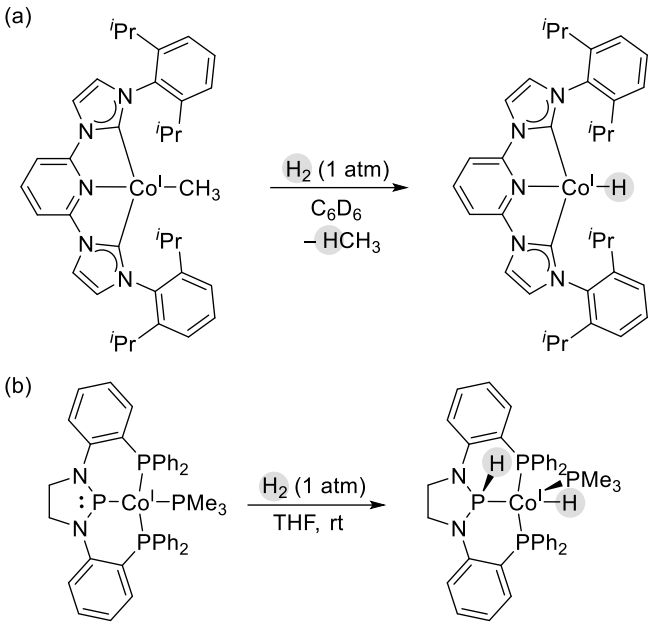

Scheme 2. (a) Hydrogen via a CNC-Co(I) methyl complex. (b) H_2 activation via a PPP-Co(I) complex.

With the consideration to develop a new mode of MLC other than traditional pincer systems, the PNNP ligand (2,9-bis ((diphenylphosphanyl)methyl)-1,10-phenanthroline) and its tailored derivatives were introduced in several ruthenium and iron complexes as shown in Chapter 1.[8,9] In those studies, [Ru(PNNP'-^{t}Bu)] complex and [FeCH$_3$(PNNP')] complex, both of which possess the dearomatized ligand backbone, can achieve H_2 activation via MLC (Chapter 1, Schemes 11 and 15).[8c, 9] Recently, our group also reported H_2 activation using PNNP-Co(I) system (Scheme 3).[10]

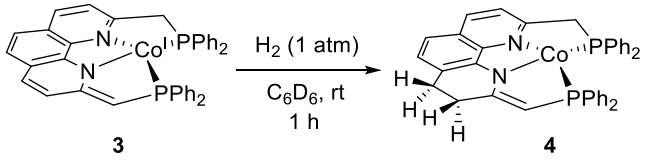

Scheme 3. H_2 activation via complex **3** in C_6D_6.

In this reaction, [Co(PNNP')] (**3**) undergoes H–H bond cleavage, and the two H atoms were incorporated in the endocyclic double bond of the ligand backbone to form a new Co(I) complex, [Co(PNNP")] (**4**), which possesses partially hydrogenated phenanthroline framework. The results suggested a long-range MLC behavior of **3**.

Although the result indicated that H_2 activation can occur via MLC, the detailed mechanism

is still unclear. Therefore, in this chapter, mechanistic study on H_2 activation by **3** was performed

3-2. Synthesis of 3 via deprotonation of 1

The previous method to synthesize **3** includes two steps, alkylation and structural transformation. In this study, reactions of **1** with various bases were first of all examined to establish a facile synthetic route for **3**. In C_6D_6, **1** did not react with amine type bases, such as DBU (1,8-diazabicyclo(5.4.0)undec-7-ene) and triethylamine (Et_3N). Treatment of 1 equiv sodium *tert*-butoxide as a strong base afforded **3** as a major product (96% isolated yield) along with *tert*-butyl alcohol (^{t}BuOH) (Scheme 4).

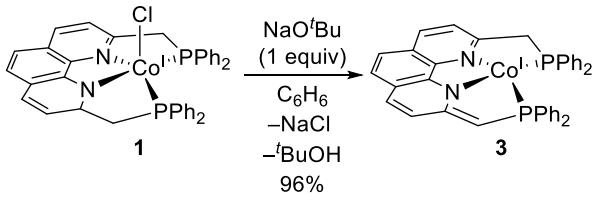

Scheme 4. Preparation of **3** from **1** with NaO^{t}Bu.

Interestingly, **1** was found to release the Cl ligand easily in a polar solvent DMSO-d_6 to become a cationic specie $[Co(PNNP)]^+Cl^-$ (**1**$^+$). This structural transformation was evidenced by ^{1}H NMR spectroscopy. In ^{1}H NMR spectrum, the two benzylic CH_2 groups of **1** exhibited one set of diastereotopic signals at 5.23 ppm and 4.17 ppm in C_6D_6, whereas one singlet benzylic CH_2 signal appeared at 4.83 ppm in DMSO-d_6. As a result of being an ionic form, **1**$^+$ can easily undergo deprotonation with an organic base in DMSO (Scheme 5). Therefore, **1**$^+$ was partially converted to **3** (56% NMR yield) upon treatment with 10 equiv DBU.

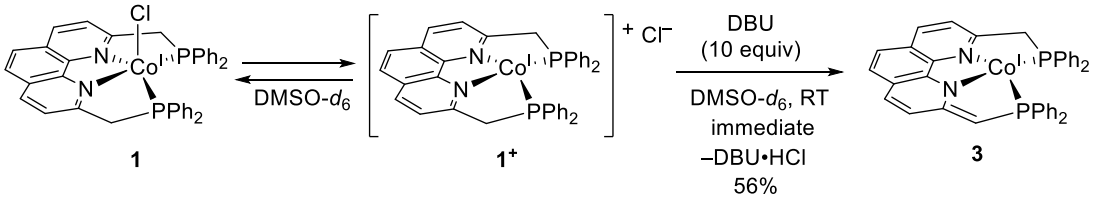

Scheme 5. Deprotonation **1** with DBU in DMSO-d_6.

3-3. Mechanistic study on H_2 activation by 3

With a more facile pathway to prepare **3,** H_2 activation by **3** was further examined. It was found out that **4** underwent dehydrogenation to recover **3** upon heating. After heating a toluene

solution of **4** at 110 °C for 24 h, partial conversion of **3** (24% by NMR) was observed along with a small amount of unidentified species (Scheme 6).

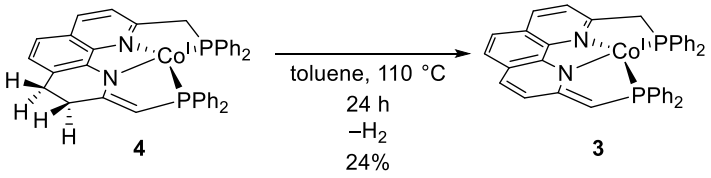

Scheme 6. Conversion of **4** to **3** at 110 °C in toluene.

This result supported reversibility of the H_2 activation via **3**, thus suggesting an intrinsic properties of the PNNP–Co(I) system as a H_2 reservoir. Similar reversibility of H_2 activation was also observed in Ru complexes with a PNNP-^{t}Bu ligand, however the reaction required high pressure of H_2 (6 atm).[9]

Next, reaction of **3** with deuterium (D_2) was performed (Scheme 7).

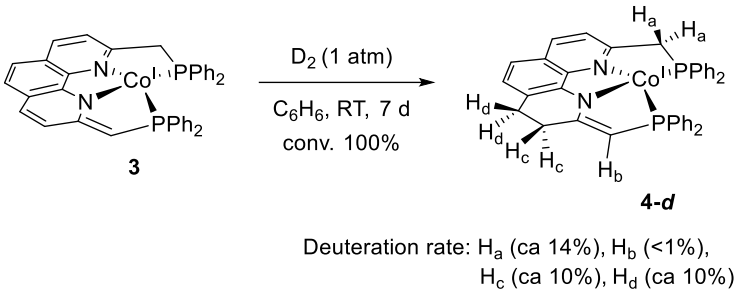

Scheme 7. Deuteration of **3**.

After the introduction of D_2 gas (1 atm) into a benzene solution of **3**, the reaction was kept and stirred at room temperature. It was found that the full conversion of **3** into the deuterated **4** after seven days.[12] As shown in Scheme 4, the deuterated ***4-d*** was formed with the deuteration ratio of ca. 14% for the H_a and ca. 10% for H_c/H_d atoms.[13] No obvious deuteration (<5%) was detected. According to the mechanism mentioned below, D incorporation at the H_b position should occur, however it was obscured due to the low signal intensity in the ^{1}H NMR.

It should be noted that deuteration of H_a occurred, excluding the occurrence of a simple hydrogenation of the PNNP-ligand backbone during the reaction. Therefore, it was suggested that the transformation of **3** to **4** in the presence of H_2 involves the H_2 activation by conventional MLC,[7] whereby both the Co center and the *exo*-methylene carbon synergistically cleave H–H bond in a heterolytic manner to form the hydride intermediate [CoH(PNNP)] (**A**) (Scheme 8).

Intermediate **A** underwent similar structural transformation as PNNP-cobalt alkyl complex **2** via Co–H homolysis (Chapter 2, Scheme 5) to form **4**.

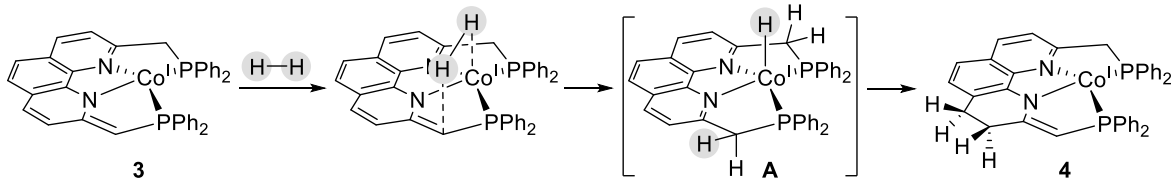

Scheme 8. Possible pathway for H–H bond cleavage by MLC of **3**.

One might notice that the observed deuteration rate in **4-*d*** was low than expected (the expected vs. observed total deuteration rates: >99% vs. 34%). The result suggested the occurrence of the H atom abstraction not only from D_2 but also from *in situ* existing other molecules. One possible reason for this is that after the Co–H homolysis, the reactive H radical is trapped by the PNNP-Co complex as well as other molecules. Then, the resulting complex can abstract a H atom contaminated molecules other than D_2-originated D-sources. These steps should lead to a significant decrease in the deuteration ratio in **4-*d***. This process is summarized in Scheme 9.

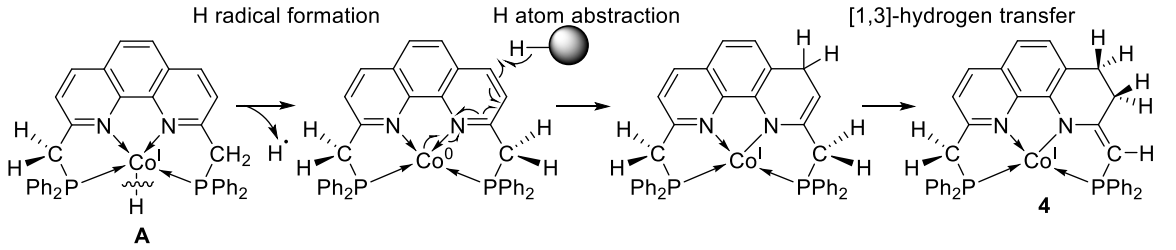

Scheme 9. Possible routes for the formation of **4** from **A**.

In order to confirm the proposed reaction path from **A** to **4**, several hydride sources (e.g., NaH and $NaHBEt_3$) were applied to **1** to prepare the hydride intermediate **A**. However, such reactions afforded **3** and/or **4** along with a complicated mixture. Thus, another route to prepare **A** was examined using PNNP-Co ethyl complex [CoEt(PNNP)] (**7**), which could generate **A** via β-H elimination.

Complex **7** was synthesized by following the similar procedure for the formation of **2**: i.e. reaction of **1** with ethylmagnesium bromide (EtMgBr) resulted in the quantitative formation of **7**. Next, **7** was dissolved in C_6D_6 and heated at 60 °C, and the process was monitored by NMR. After 5 h, **7** was completely consumed, and **4** was observed in 35% NMR yield along with **3** in 26% NMR yield. In addition, formation of ethene (C_2H_4; major), ethane (C_2H_6; minor), and some

unidentified species were also confirmed (Scheme 10).

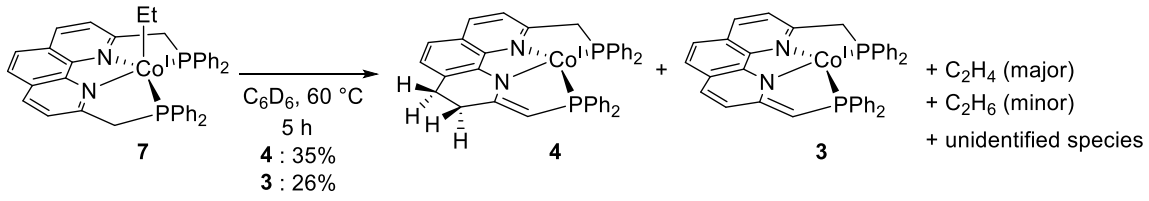

Scheme 10. Transformation of **7** in C_6D_6 at 60 °C.

The resulting product **4** and C_2H_4 supported the *in situ* formation of a hydride intermediate **A**, which successively undergoes transfer of hydride and one of hydrogen atoms at the benzylic moiety to the PNNP backbone (Scheme 11a). Furthermore, the formation of **3** might be derived from the Co–C bond homolysis and the following hydrogen abstraction at the benzylic carbon by the resulting ethyl radical (Scheme 11b). The similar transformation of [Co(CH_2SiMe_3)(PNNP)] (**2**) was also reported (Chapter 2, Scheme 2). Collectively, these results implied that the formation of **A** from **7** could also be mediated via homolysis of both the benzylic C–H bond and the Co–H bond.

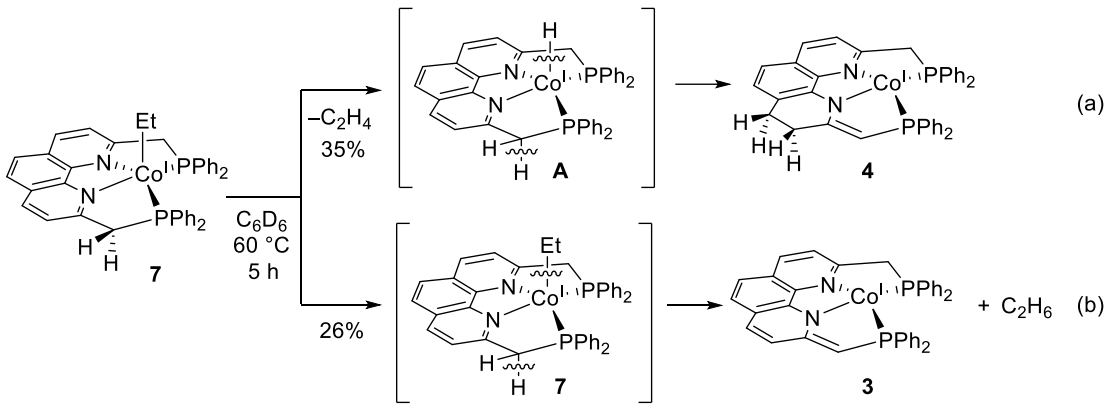

Scheme 11. Possible pathways for the transformation of **7** to **4** (a) and **3** (b).

3-4. Conclusion

In this chapter, the deuterium labeling experiment of **3** was performed to support the occurrence of heterolytic cleavage of H–H bond mediated via MLC. In this process, a hydride precursor, which further undergoes H atom transfer to form **4**, is expected. PNNP-Co(I) ethyl complex **7** as a hydride precursor was synthesized, and transformation of **7** to **4** was confirmed. This experimental result also supported the postulated H_2 activation process. It is to be mentioned that reversibility of H_2 activation by **3** was indicated. All the study discussed in this chapter

strongly support that the PNNP-Co(I) system can exhibit long-range MLC behavior as a H_2 reservoir.

3-5. Experimental Details

3-6-1. Another synthetic approach of [Co(PNNP')] (**3**)[11]

To a benzene solution (10 mL) of [CoCl(PNNP)] (**1**) (15.2 mg, 0.023 mmol), was added sodium tert-butoxide (2.2 mg, 0.023 mmol). The solution was stirred at room temperature for a few minutes. The solution was filtered with a Celite pad to give **3** as a deep green solid (13.8 mg, 0.022 mmol, 96%).

^{1}H NMR (C_6D_6, 25 °C) δ 7.60 (t, 4H, P*Ph*$_2$, $^3J_{HH}$ = 8.6 Hz), 7.56 (d, 1H, Phen-*H*, $^3J_{HH}$ = 8.3 Hz), 7.41 (t, 4H, P*Ph*$_2$, $^3J_{HH}$ = 8.6 Hz), 7.00 (m, 4H, P*Ph*$_2$), 6.88-6.93 (m, 9H, Phen-*H* (1H) + P*Ph*$_2$ (8H)), 6.65 (m, 2H, Phen-*H*), 6.55 (d, 1H, Phen-*H*, $^3J_{HH}$ = 8.0 Hz), 6.28 (d, 1H, Phen-*H*, $^3J_{HH}$ = 8.5 Hz), 4.33 (brs, 1H, PC*H*), 3.08 (d, 2H, PC*H*$_2$, $^2J_{PH}$ = 12.0 Hz). ^{13}C{^{1}H} NMR (DMSO-*d*$_6$, 25 °C) δ 165.8, 151.3, 146.0, 143.6, 139.4, 133.9, 132.6, 130.8, 130.7, 129.4, 127.9, 127.7, 127.6, 127.2, 126.1, 124.0, 121.6, 117.1, 114.2, 111.2, 70.9, 46.7. ^{31}P{^{1}H} NMR (C_6D_6, 25 °C) δ 52.8 (br), 38.2 (br). HRMS (ESI) Calculated: ($C_{38}H_{29}CoN_2P_2$) 634.1132 ([M+H]$^+$), Found: 634.1148. Anal. Calculated for $CoN_2P_2C_{38}H_{29}$: C, 71.93; H, 4.61; N 4.41. Found: C, 72.24; H, 4.96; N, 4.58.

3-6-2. Reaction of **1** with 10 equiv DBU in DMSO-*d*$_6$

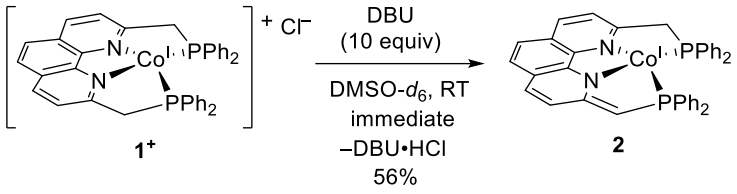

Complex **1** (2.7 mg, 4.0 mmol) was dissolved in DMSO-*d*$_6$ (0.40 mL). To the solution, was added 10 equiv DBU (6.0 μL, 40 mmol). The reaction was followed by ^{1}H and ^{31}P{^{1}H} NMR spectroscopy, showing the partial conversion of **1**$^+$ to **2** (conv. 56%). After removal of the solvent, the residue was analyzed by ^{1}H and ^{31}P{^{1}H} NMR using C_6D_6 as a solvent to support complete recovery of **1**.

1$^+$: ^{1}H NMR (DMSO-*d*$_6$, 25 °C) δ 8.68 (d, 2H, Phen-*H*, $^3J_{HH}$ = 6.0 Hz), 8.02 (m, 4H, Phen-*H*), 7.36 (vt, 4H, P*Ph*$_2$, *J* = 9.0 Hz), 7.16 (t, 8H, P*Ph*$_2$, $^3J_{HH}$ = 9.0 Hz), 7.11 (br, 8H, P*Ph*$_2$), 4.83 (s, 4H, C*H*$_2$PPh$_2$). ^{31}P{^{1}H} NMR (DMSO-*d*$_6$, 25 °C) δ 65.1 (s).

2: ^{1}H NMR (DMSO-*d*$_6$, 25 °C) δ 7.96 (d, 1H, Phen-*H*, $^3J_{HH}$ = 6.0 Hz), 7.41 (t, 4H, P*Ph*$_2$, $^3J_{HH}$ = 9.0 Hz), 7.35 (t, 2H, P*Ph*$_2$, $^3J_{HH}$ = 9.0 Hz), 7.22 (m, 5H, P*Ph*$_2$ (4H) + Phen-*H* (1H)), 7.12 (m, 8H, P*Ph*$_2$ (6H) + Phen-*H* (2H)), 7.02 (t, 4H, P*Ph*$_2$, $^3J_{HH}$ = 6.0 Hz), 7.00 (d, 1H, Phen-*H*, $^3J_{HH}$ = 6.0 Hz),

6.75 (d, 1H, Phen-*H*, $^{3}J_{HH}$ = 12.0 Hz), 4.29 (s, 1H, C*H*PPh$_2$), 4.06 (d, 2H, C*H*$_2$PPh$_2$, $^{2}J_{PH}$ = 6.0 Hz). ^{31}P{^{1}H} NMR (DMSO-d_6, 25 °C) δ 66.2 (d, $^{2}J_{PP}$ = 41.3 Hz), 44.0 (m).

3-6-3. Reaction of **3** with H_2

A C_6D_6 solution (0.5 mL) of [Co(PNNP')] (**3**) (4.1 mg, 0.0065 mmol) was charged in a J-Young NMR tube. H_2 (1 atm) was introduced to the NMR tube. The solution was kept at room temperature overnight. Full conversion of **4** and clean formation of **4** were confirmed by NMR analysis. The solution was concentrated to dryness under vacuum and washed with hexane to give 6 as a brown solid (2.2 mg, 0.0035 mmol, 53%). Single crystals of **4** was obtained by slow evaporation of saturated C_6H_6 solution of **4** at room temperature.

4: ^{1}H NMR (C_6D_6, 25 °C) δ 7.74 (d, 1H, Phen-*H*, $^{3}J_{HH}$ = 8.3 Hz), 7.62 (m, 4H, P*Ph*$_2$), 7.49 (m, 4H, P*Ph*$_2$), 7.10 (d, 1H, Phen-*H*, $^{3}J_{HH}$ = 7.9 Hz), 7.00 (m, 2H×2, P*Ph*$_2$), 6.96 (m, 4H, P*Ph*$_2$), 6.92 (m, 4H, P*Ph*$_2$), 6.84 (d, 1H, Phen-*H*, $^{3}J_{HH}$ = 7.9 Hz), 6.48 (d, 1H, Phen-*H*, $^{3}J_{HH}$ = 8.3 Hz), 4.64 (m, 1H, PC*H*), 3.25 (d, 2H, PC*H*$_2$, $^{2}J_{PH}$ = 9.4 Hz), 2.89 (t, 2H, C*H*$_2$, $^{3}J_{HH}$ = 7.0 Hz), 2.67 (t, 2H, C*H*$_2$, $^{3}J_{HH}$ = 7.2 Hz). ^{13}C{^{1}H} NMR (C_6D_6, 25 °C) δ 166.0, 155.7, 149.9, 143.0, 138.8, 137.1, 132.9, 132.8, 130.0, 128.6, 128.3* (×2), 128.2*, 127.9*, 119.6, 118.7, 110.5, 89.7, 49.4, 26.9, 25.5. One *ipso*-carbon was obscured due to low intensity. * signals were determined based on HSQC. HSQC (C_6D_6, 25 °C) δ_H-δ_C 7.00 (δ_H) - 128.2 (δ_C), 128.3(δ_C); 6.96 (δ_H) - 128.3 (δ_C); 6.92 (δ_H) - 127.9 (δ_C). ^{31}P{^{1}H} NMR (C_6D_6, 25 °C) δ 55.6 (br), 44.5 (br). Anal. Calculated for $CoN_2P_2C_{38}H_{31}$: C, 71.70; H, 4.91; N 4.40. Found: C, 72.13; H, 4.87; N, 4.28.

3-6-4. Deuteration of **3**

A benzene solution (5 mL) of [Co(PNNP')] (**3**) (24.9 mg, 39 mmol) was charged in a Schlenk tube with a Teflon cock. D_2 (1 atm) was introduced to the Schlenk tube, and the solution was kept at room temperature with stirring for a week. The solution was passed through a Celite pad and concentrated to dryness under vacuum. The residue was analyzed by ^{1}H NMR spectrum[12], supporting full conversion of **3** to **4-*d***. Incorporation of deuteride was confirmed at H_a in 14%, and H_c and H_d in 10%. Significant decrease in the integral intensity of H_b was not observed.

3-6-5. Synthesis of **7**

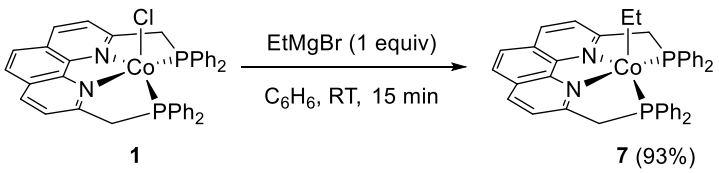

1 **7** (93%)

A benzene solution (2.0 mL) of **1** (7.9 mg, 0.012 mmol) was charged in a vial. To the solution, was added EtMgBr (12.0 μL, 1 M THF soln, 0.012 mmol) slowly at ambient temperature. The solution was stirred at room temperature for 15 minutes. The solution was concentrated to dryness under vacuum, and the resulting residue was extracted with benzene (3 mL) and filtered through a Celite pad. The filtrate was concentrated to dryness under vacuo to afford **7** as a purple solid (7.3 mg, 0.011 mmol, 93 %).

^{1}H NMR (C_6D_6, 25 °C) δ 7.24 (m, 4H, P*Ph*$_2$), 7.12 (t, 2H, P*Ph*$_2$, $^{3}J_{HH}$ = 9.0 Hz), 7.08 (m, 4H, Phen-*H*), 7.02 (t, 4H, P*Ph*$_2$, $^{3}J_{HH}$ = 9.0 Hz), 6.89 (m, 4H, P*Ph*$_2$), 6.86 (d, 2H, Phen-*H*, $^{3}J_{HH}$ = 6.0 Hz), 6.72 (t, 2H, P*Ph*$_2$, $^{3}J_{HH}$ = 6.0 Hz), 6.60 (t, 4H, P*Ph*$_2$, $^{3}J_{HH}$ = 6.0 Hz), 4.32 (d, 2H, PC*H*$_2$, $^{2}J_{PH}$ = 18.0 Hz), 3.87 (m, PC*H*$_2$), 1.21 (m, 2H, -C*H*$_2$CH$_3$), 0.23 (t, 3H, -CH$_2$*CH*$_3$, $^{3}J_{HH}$ = 9.0 Hz). ^{31}P{^{1}H} NMR (C_6D_6, 25 °C) δ 76.3 (s). ^{13}C{^{1}H} NMR δ 156.0, 140.8, 137.4, 135.3, 133.4, 131.7, 131.6, 129.3, 128.6, 128.1 (×2), 126.4, 115.8, 112.1, 46.0, 14.9, –4.9. HRMS (ESI) Calculated: ($C_{40}H_{35}CoN_2P_2$) 664.1602 ([M]$^{+}$), Found: 664.1574.

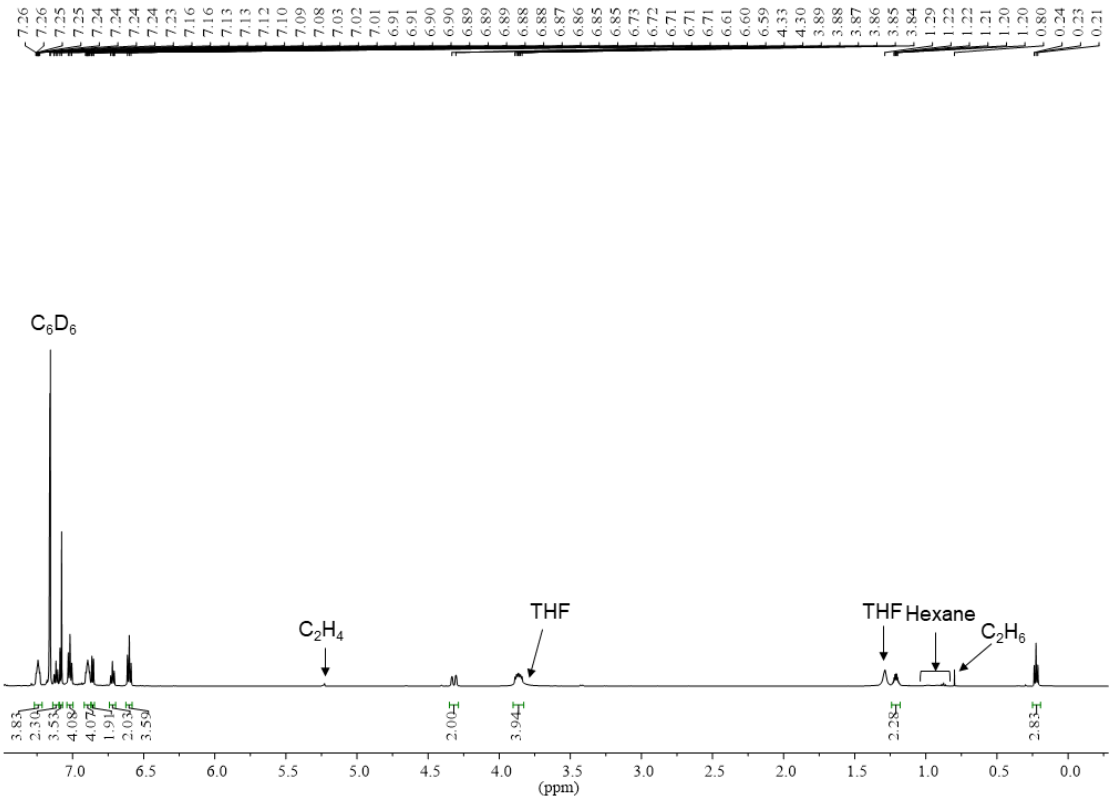

Figure 1. ^{1}H NMR of **7** in C_6D_6.

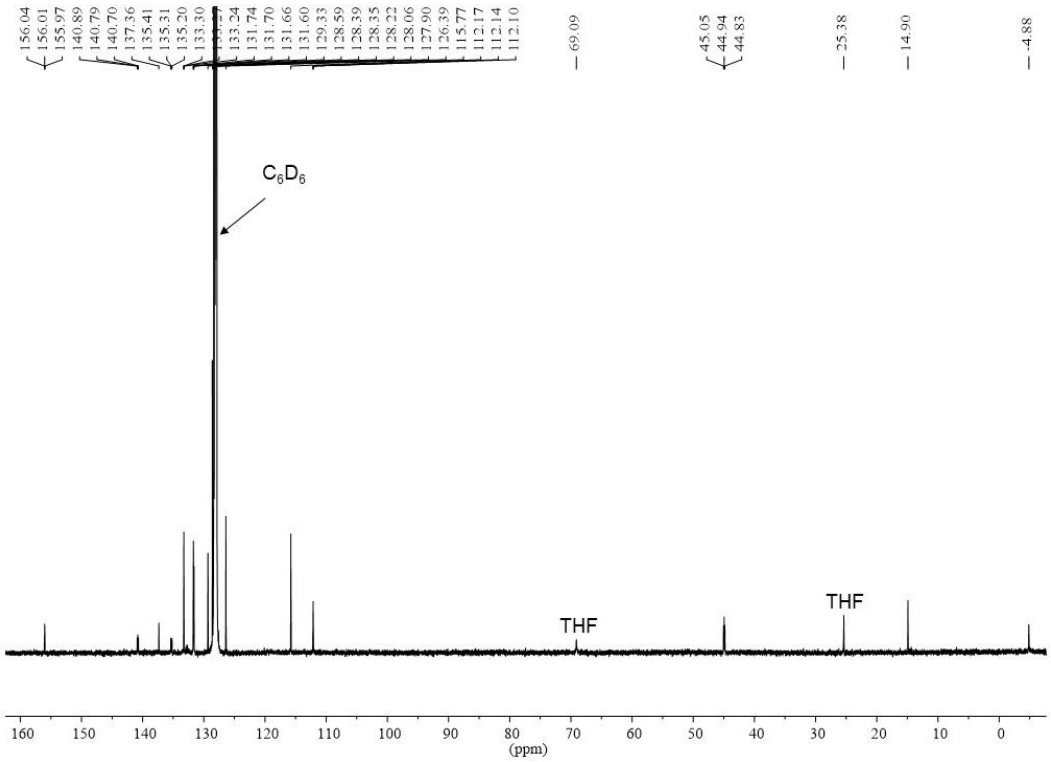

Figure 2. $^{13}C\{^{1}H\}$ NMR of **7** in C_6D_6.

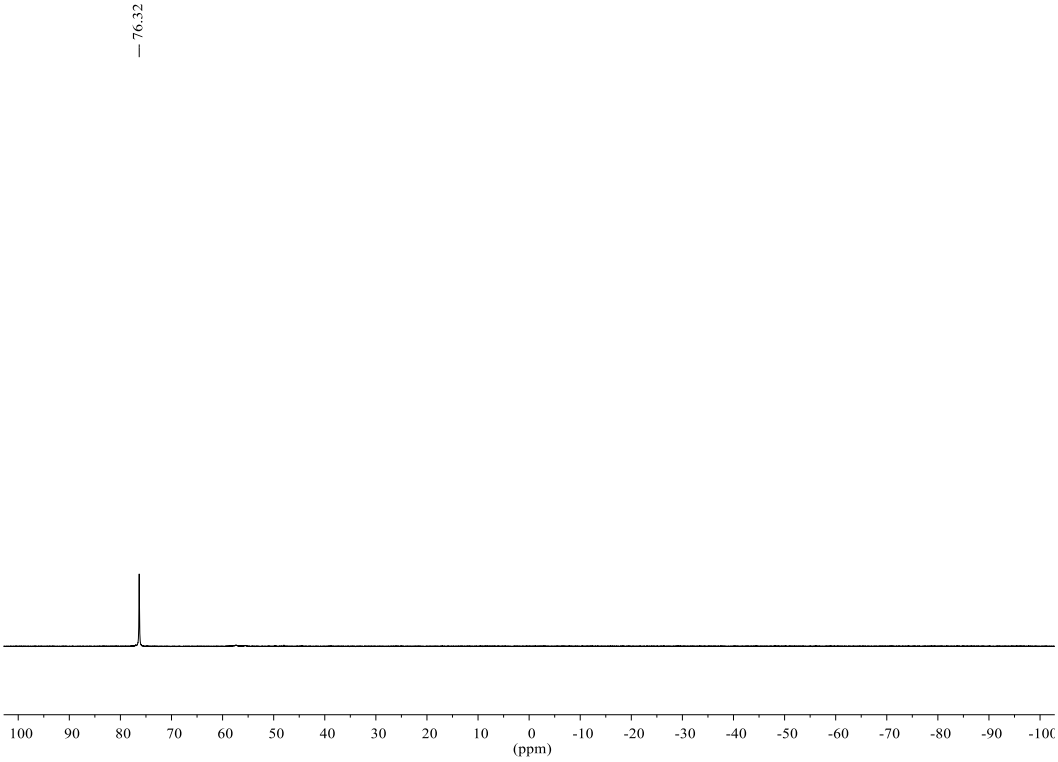

Figure 3. $^{31}P\{^{1}H\}$ NMR of **7** in C_6D_6.

3-6-6. Heating C_6D_6 solution of **7**

Complex **7** (6.3 mg, 0.0095 mmol) was dissolved in C_6D_6 (0.6 mL) and transferred into a J-Young NMR tube. 1,4-dioxane (0.9 mg, 0.10 mmol) was added as an internal standard. The solution was kept at 60 °C. After 5 h, **7** was fully consumed, and **3** and **4** were formed in 26% and 35% NMR yields, respectively. Unidentified products, which exhibit singlets at 77.0, 57.5, and 48.0 ppm in $^{31}P\{^1H\}$ NMR spectrum, were slightly formed.

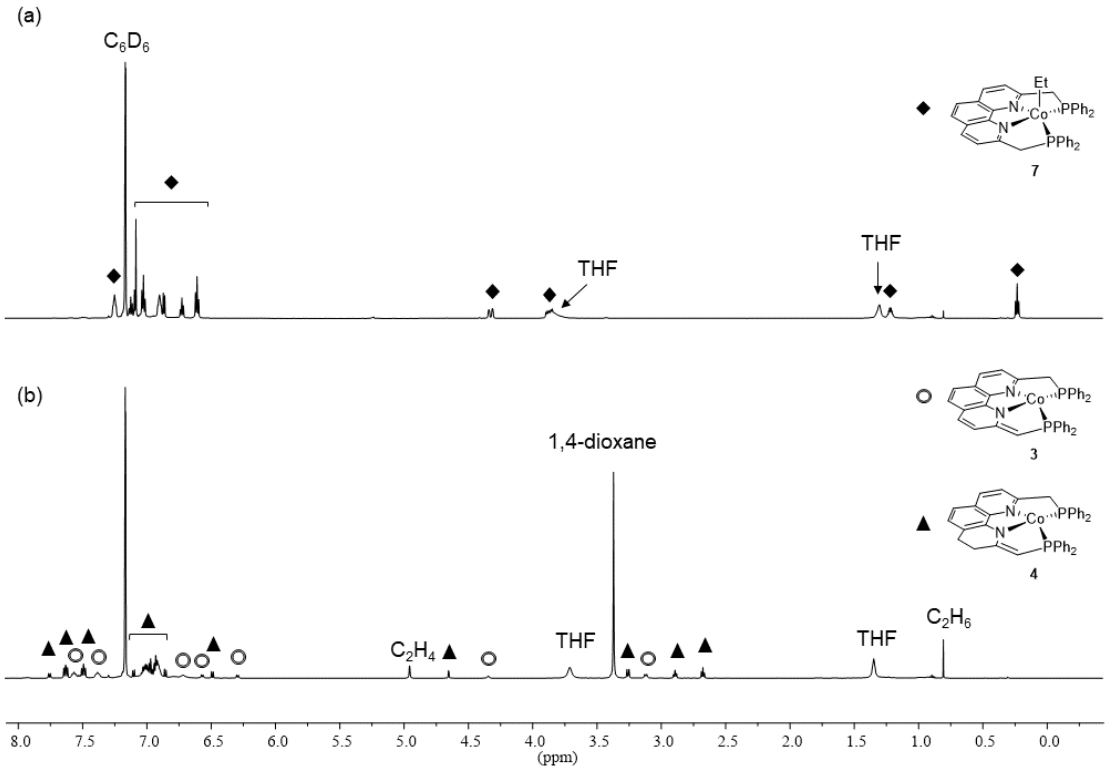

Figure 4. ^1H NMR spectrum of **7** before (a) and after (b) heating in C_6D_6. The signals marked with ○, ▲, ◆ are **3**, **4**, and **7**, respectively.

Reference

(1) (a) Bullock, R. M. *Science* **2013**, *342*, 1054-1055. (b) Werkmeister, S.; Neumann, J.; Junge, K.; Beller, M. *Chem. Eur. J.* **2015**, *21*, 12226 – 12250. (c) Stoffels, M. A.; Klauck, F. J. R.; Hamadi, T.; Glorius, F.; Leker, J. *Adv. Synth. Catal.* **2020**, *362*, 1258 – 1274.

(2) (a) Sordakis, K.; Tang, C.; Vogt, L. K.; Junge, H.; Dyson, P. J.; Beller, M.; Laurenczy, G. *Chem. Rev.* **2018**, *118*, 372−433. (b) Shao, Z.; Li, Yang; Liu, C.; Ai, W.; Luo, S.-P.; Liu, Q. *Nat. Commun.* **2020**, *11*, 591. (c) Tan, K. C.; He, T.; Chua, Y.S.; Chen, P. J. *Phys. Chem. C* **2021**, *125*, 18553−18566.

(3) Craabtree, R. H. Oxidative Addition and Reductive Elimination. In *The Organometallic Chemistry of the Transition Metals*, 7th ed.; John Wiley & Sons, 2019; pp 147−168.
(4) (a) Grützmacher, H. *Angew. Chem. Int. Ed.* **2008**, *47*, 1814–1818. (b) Khusnutdinova, J. R.; Milstein, D. *Angew. Chem. Int. Ed.* **2015**, *54*, 12236–12273.
(5) Sandoval, C.A.; Ohkuma, T.; Muñiz, K.; Noyori, R. *J. Am. Chem. Soc.* **2003**, *125*, 13490–13503.
(6) Yu, R. P.; Darmon, J. M.; Milsmann, C.; Margulieux, G. W.; Stieber, S. C. E.; DeBeer, S,; Chirik, P. J. *J. Am. Chem. Soc.* **2013**, *135*, 13168–13184.
(7) Poitras, A. M.; Knight, S. E.; Bezpalko, M. W.; Foxman, B. M.; Thomas, C.M. *Angew. Chem. Int. Ed.* **2018**, *57*,1497–1500.
(8) (a) Takeshita, T.; Sato, K.; Nakajima, Y. *Dalton Trans.* **2018**, *47*, 17004–17010. (b) Takeshita, T.; Nakajima, Y. *Chem. Lett.* **2019**, *48*, 364–366. (c) Gautam, M.; Yatabe, T.; Tanaka, S.; Satou, N.; Takeshita, T.; Yamaguchi, K.; Nakajima, Y. *ChemistrySelect* **2020**, *5*, 15–17. (d) Gautam, M.; Tanaka, S.; Sekiguchi, A.; Nakajima Y. *Organometallics* **2021** ASAP.
(9) Langer, R.; Fuchs, I.; Vogt, M.; Balaraman, E.; Diskin-Posner, Y.; Shimon, L. J. W.; Ben-David, Y.; Milstein, D. *Chem. Eur. J.* **2013**, *19*, 3407–3414.
(10) Ishizaka, Y. Master thesis in February 2019.
(11) Jheng, N.Y.; Ishizaka, S.; Naganawa, Y.; Sekiguchi, A.; Nakajima, Y. *Dalton Trans.* **2020**, *49*, 14592–14597.
(12) ^{2}H NMR Measurement of **4-*d*** was not successful probably due to the relatively low solubility of **4-*d*** in benzene to afford good resolution.

Chapter 4 Radical Hydrodehalogenation of Aryl Halides with H_2 Catalyzed by a PNNP-Cobalt(I) Complex

4-1. Introduction

Degradation of environmentally hazardous chemicals holding structures of aryl halides, such as insecticides and fire retardants, is a long-lasting issue for scientists.[1] Conventionally, transition metal complexes are utilized to proceed hydrodehalogen of aryl halides.[1] However, the reactions have been usually performed using via noble-metal complexes as catalysts.[1] Recently, radical hydrodehalogenation, which usually proceeds successively with the formation of aryl radicals and hydrogen atom transfer (HAT), arrests much more attention due to the radical pathway with considerably lower intrinsic barrier.[2] Accordingly, the reaction can be performed in milder reaction conditions and apply broader substrate scope than other transition-metal-mediated approaches.[3] For example, König *et al.* reported a visible-light photocatalytic hydrodehalogenation of aryl halides catalyzed by *N*,*N*-bis(2,6-diisopropylphenyl)perylene-3,4,9,10-bis(dicarboximide) (PDI) as a metal-free photoredox-active catalyst to render successive photoinduced electron transfer (PET) at 40 °C in dimethyl sulfoxide (DMSO) or *N*,*N*-dimethylformamide (DMF) (Figure 1a).[4]

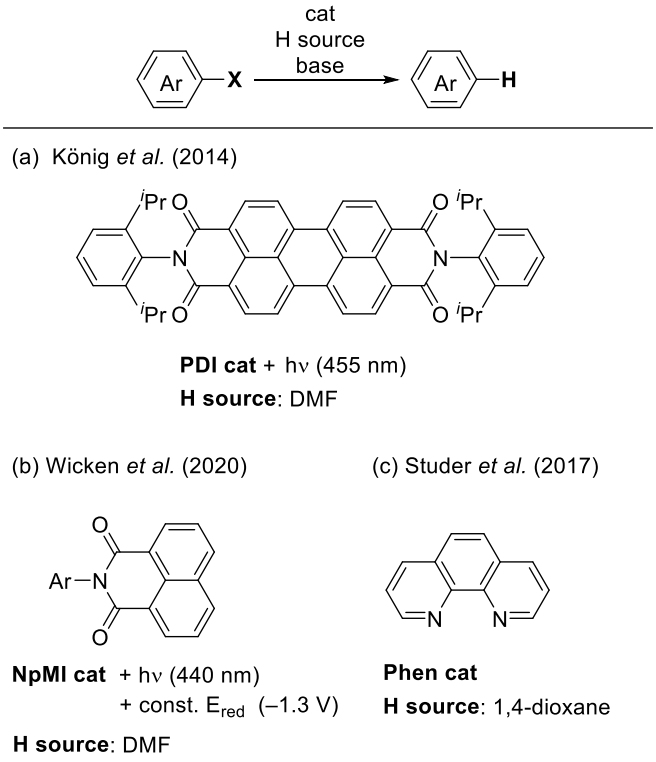

Figure 1. Selected examples of catalytic radical hydrodehalogenation

Inspired by König's work, several groups further expanded the concept. One of important reports from Wickens's group utilized a combination of electrochemical and light-irradiation stimulation to activate photoredox catalysts and thus achieved hydrodehalogenation of various aryl bromides (Figure 1b).[5] In addition to the approaches using photoredox catalysts, it was revealed that aryl radicals can be generated by 1,10-phenanthroline (Phen) with Strong base like potassium *tert*-butoxide (KO^{t}Bu) or sodium hydride (NaH)[6], which can be applied to hydrodehalogenation[7] or cross-coupling reactions of aryl halides with various unactivated arenes[8]. One of leading works to apply this chemistry to radical hydrodehalogenation was reported by Studer *et al.* (Figure 1c)[8]. The radicals, generating from NaH and Phen, effectively convert aryl halides along with 1,4-dioxane as the solvent and the hydrogen source into the corresponding arenes. Most importantly, even aryl fluorides can be converted via Studer's approach.

Albeit these radical approaches showed nice performance of hydrodehalogenation of aryl halides, the hydrogen sources in these methods were limited to solvents, such as DMF or 1,4-dioxane, which may cause potential health problems.[9] In comparison with such solvents, molecular hydrogen (H_2) is an environmentally benign and atom economical hydrogen source; however, there is no report to utilize H_2 as the hydrogen source for radical hydrodehalogenation, because aryl radicals can not proceed H abstraction from H_2 with a BDE of 103.8 kcal/mol.[10]

In the previous chapters, fundamental reactivity of PNNP-Co(I) complexes was surveyed. PNNP-Co(I) complexes undergo Co–C bond homolysis via MLC to generate the corresponding alkyl radicals *in situ*. This is the crucial step for the cobalamins to afford alkyl radicals in radical dehalogenation of alkyl halides.[11] Inspired by this chemistry, hydrodehalogenation of organic halides was performed using the PNNP-Co system. It is to be mentioned that [Co(PNNP')] (**3**) undergoes H_2 activation to afford [Co(PNNP")] (**4**) via long-range MLC, where activated H terminus were incorporated into the ligand backbone (Chapter 3, Scheme 3). Based on this phenomenon, it is expected that once organic radical is formed *in situ* from organohalides by **3**, the formed organic radicals could undergo hydrogen atom transfer (HAT) from the activated H_2, which is stored at the ligand backbone of **3**. Indeed, hydrodehalogenation of various aryl halides proceeded under mild conditions via PNNP-Co(I) complexes. Based on the foundation of several stoichiometric reactions of PNNP-Co(I) complexes and further mechanistic study including kinetic study for this catalytic reaction, it was revealed that the reaction was achieved via a radical mechanism utilizing atmospheric pressure of H_2. It is also to be mentioned that the reaction was catalyzed via PNNP-Co(I) as a base metal catalyst, which enjoys unique long-range MLC.

4-2. Reaction of 4 with chlorobenzene

In order to scrutinize the proposal to achieve hydrodehalogenation of aryl halides via PNNP-Co(I) complexes, a model study by performing reaction of **4** with chlorobenzene was performed

at 80 °C in C_6D_6 (Scheme 1).

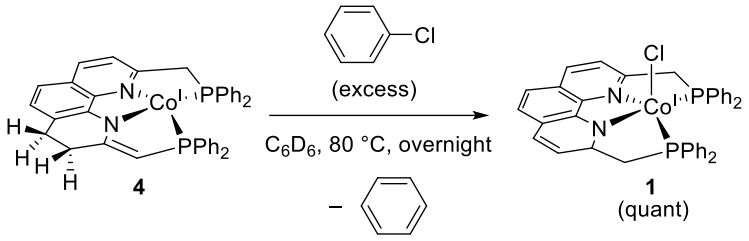

Scheme 1. Reaction of **4** with chlorobenzene.

As shown in Scheme 1, the quantitative formation of **1** and benzene were observed by ^{1}H NMR. Accordingly, this preliminary result supported the activation of C–Cl bond of chlorobenzene and hydrogen abstraction along with structural rearrangement of PNNP" ligand. Hence, a catalytic cycle was postulated: (i) formation of **3** via deprotonation of **1**, (ii) hydrogen activation by **3** to afford **4**, and (iii) hydrodehalogenation of aryl halides by **4** (Scheme 2).

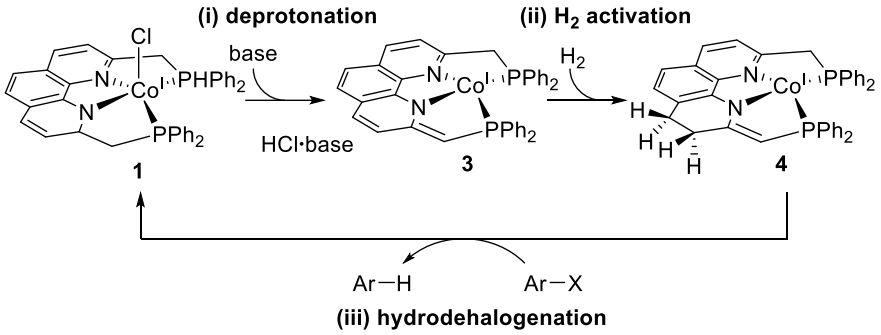

Scheme 2. Proposed reaction cycle of the hydrodehalogenation of aryl halides (ArX).

4-3. Optimization of reaction conditions

Optimization of reaction conditions using 1-bromonanpfthalene as a substrate was performed (Table 1).

Firstly, various bases were screened in the presence of 2 mol% of **1** and 1 atm H_2 in DMSO. With 2 equiv NaO^{t}Bu, only 6% yield of naphthalene as the hydrodebrominated product was formed (entry 1, Table 1). With another inorganic base, potassium carbonate (K_2CO_3), only trace amount of naphthalene was observed probably due to poor solubility of K_2CO_3 in DMSO (entry 2, Table 1). In the presence of triethylamine (NEt_3)[12] or dimethyl-4-aminopyridine (DMAP)[13], only limited yield (<5%) of the product was formed (entry 3 and 4, Table 1). In contrast, higher yields were achieved to 43% and 97% when stronger bases, pyrrolidine[13] and 1,8-diazabicyclo[5.4.0]undec-7-ene (DBU)[12] were applied, respectively (entry 5 and 6, Table 1). The

highest yield (>99%) was observed by applying a stronger base, 7-methyl-1,5,7-triazabicyclo[4.4.0]dec-5-ene (MTBD)[12] (entry 7, Table 1). Lower temperature (room temperature) and reduced amount of base (1 equiv) and catalyst loading (0.2 mol%) resulted in lower yields (entry 8 ~ 10, Table 1). Moreover, solvents with less polarity suppressed the performance of catalytic reactions (entry 11- 14, Table 1), and this phenomenon was congruous with the behavior of deprotonation of **1**, which is reluctant in non-polar solvent, as revealed in the previous chapter (Chapter 3).

Table 1. Optimization of reaction conditions for hydrodebromination of 1-bromonaphthalene[1]

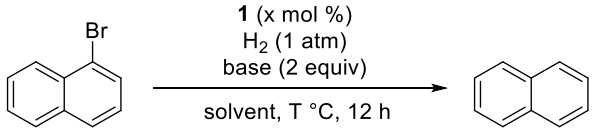

Entry	Solvent	Base	**1** (x mol %)	T (°C)	Yield (%)[2]
1	DMSO	NaO^{t}Bu	2	80	6
2	DMSO	K_2CO_3	2	80	trace
3	DMSO	Et_3N	2	80	<5
4	DMSO	DMAP	2	80	<5
5	DMSO	Pyrrolidine	2	80	43
6	DMSO	DBU	2	80	97
7	DMSO	MTBD	2	80	>99
8	DMSO	DBU	2	r.t.	35
9	DMSO	DBU[3]	2	80	82
10	DMSO	DBU	0.2	80	<5
11	MeCN	DBU	2	80	33
12	DMF	DBU	2	80	21
13	THF	DBU	2	80	6
14	Benzene	DBU	2	80	Trace

[1]Reaction conditions: Aryl halides (0.5 mmol), base (1.0 mmol), and **1** (2 or 0.2 mol %) in DMSO (4 mL) under a H_2 atmosphere. [2]GC yield. [3]1.1 equiv of DBU.

4-4. Substrate scope

After the investigation of the reaction conditions (Table 1), the high performance (97%) was found in entry 6 by a relatively inexpensive base, DBU in DMSO. Thus, this condition was applied as the optimal catalytic conditions to scan substrate scope (Table 2). In the reactions of bromobenzene and iodobenzene, benzene was afforded in similar yields, 88% and 87%, respectively. In both cases, trace biphenyl as a homocoupling product was detected by GC analyses. By contrast, no benzene was furnished from phenyl triflate under the optimal reaction conditions, which might imply the radical mechanism involved in this catalytic system (vide infra).[14] 2-, 3-, and 4-Hydrodehalogenation of bromotoluenes also proceeded to form toluene in good yields. For 1-bromo-4-trifluoromethylbenzene, 78% yield of the corresponding product was observed. Bulky substrate, such as 1-bromo-4-*t*-butylbenzene and 1-bromo-2,4,6-trimethylbenzene also afforded the corresponding dehalogenated products in good yields. Similarly, reaction of 4-bromobiphenyl achieved good product yield. For other functional groups, such as amino-, alkoxy-, hydroxy-, keto-, ester groups, and boronic acid ester, the reaction was also applicable to achieve good product yields (72 ~ 85% yield), suggesting a widely adoptable functional scope. The formation of benzaldehyde (66%) along with benzyl alcohol (33%) as a fully hydrogenated product were achieved in the reaction of 4-bromobenzaldehyde. Reaction of 1-bromo-4-chlorobenzene achieved good yielding to 1-chlorobenzene (87% yield) along with a slight amount of benzene (10% yield) as a further hydrogenated product. In contrast, 1-bromo-4-fluorobenzene mainly afforded 1-fluorobenze (85% yield) without the observation of bromobenzene and benzene. For multi-fluoro-substituted aryl bromide, 1-bromo-2,4,6-trifluorobenzene afforded 1,3,5-trifluobenze in high yield (92%). There were some cases that showed relative limited performance. For example, 1-bromo-4-cyanobenzene did not fully convert to the corresponding product (54% yield). 5-Bromo-1,3-benzodioxole resulted in 25% product yield, and complicated mixture of byproducts were concomitantly formed probably due to the decomposition of the methylenedioxy group. In the reaction of 4-bromo-*N*-methylphthalimide, 71% yield of the corresponding product was achieved. In the cases with heteroaromatic and fused aromatic rings, the reactions were also good yielding.

Table 2. Substrate scope of hydrodehalogenation of aryl halides catalyzed by **1**[1]

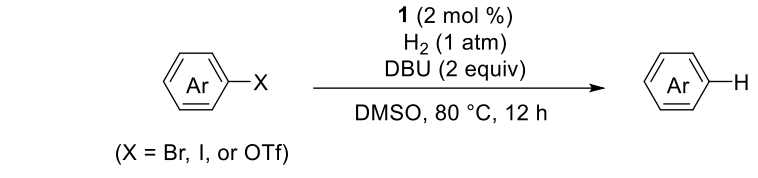

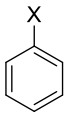	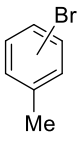	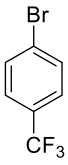	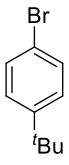	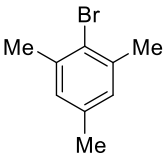
X = Br : 88%[*2] X = I : 87%[*2] X = OTf : N.D.	o : 91% m : 80% p : 80%[*2]	78%	89%[*2]	92%
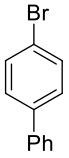	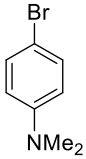	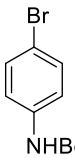	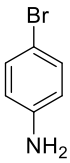	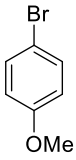
81%[*2]	90%[*2]	87%	85%	83%[*2]
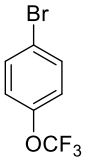	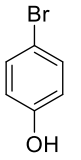	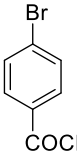	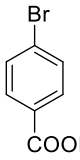	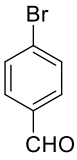
77%	84%	72%[*3]	85%	66%[*4]
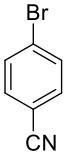	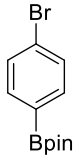	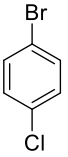	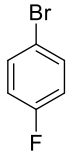	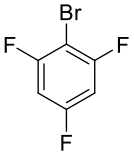
54%[*2]	72%	87% Ph-Cl[*2] 10% Ph-H	85%	92%
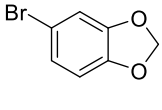	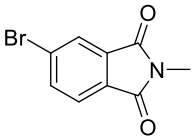	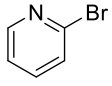	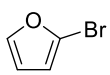	
25%	71%	93%	63%[*5]	
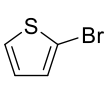	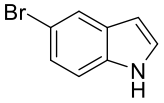	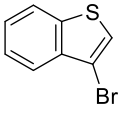	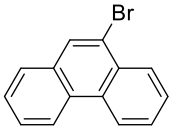	
88%	79%[*2]	>99%	95%	

[1]Reaction conditions: aryl halides (0.5 mmol), DBU (1.0 mmol), and 1 (2 mol %) in DMSO (4 mL) under a H_2 atmosphere. Yields were determined by GC. [2]Trace homocoupling products were observed. [3]Trace 1-phenylethanol was formed. [4]Benzyl alcohol was also formed in 33%. [5]The yield was low due to the low

boiling point (bp 31.3 °C) of furan.

Collectively, this catalytic system demonstrated excellent performance and good functional group tolerance in hydrodehalogenation of aryl bromides.

In the case of aryl chlorides, catalytic reactions were achieved with higher loading of **1** (Table 3). Chlorobenzene was reduced to benzene in 80% yield with 15 mol% of **1** after 16 h. For substrates with electron-donating groups, such as 4-chlorotoluene, 1-chloro-4-*t*-butylbenzene, and 1-chloro-4-methoxybenzene, moderate yields of the corresponding products (55 ~ 67% yield) were achieved under the same conditions. In contrast, 1-chloro-4-trifluoromethylbenzene and 1-chloronaphthalene showed good performance to form the corresponding dehalogenated products in 80% and 95% yields, respectively, while applying lower loading of **1** (10 mol%).

Table 3. Substrate scope of hydrodehalogenation of aryl chlorides catalyzed by **1**[1]

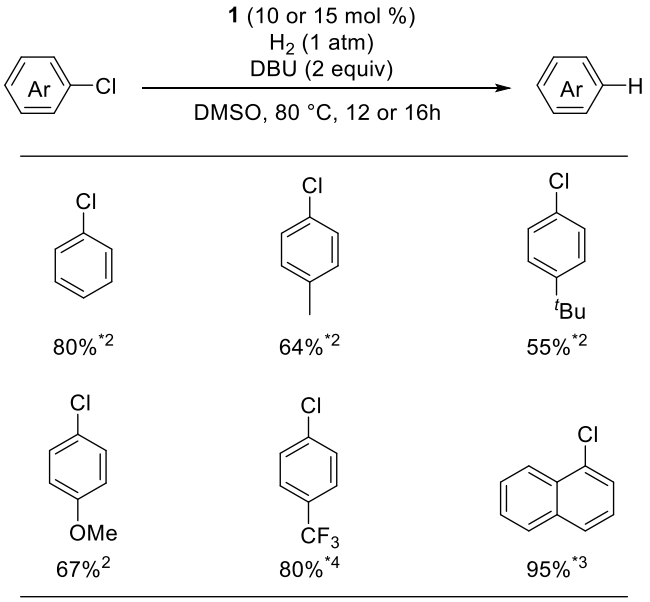

[1]Reaction conditions: aryl halides (0.5 mmol), DBU (1.0 mmol), and 1 (10 or 15 mol %) in DMSO (4 mL) under a H_2 atmosphere. Yields were determined by GC. [2]15 mol %, 16 h. [3]10 mol %, 12 h. [4]10 mol %, 16 h.

Moreover, this system was applicable for degradation of brominated fire retardants. Hydrodebromination of hexabromobenzene was achieved 61% yield of benzene along with trace of 1-bromobenze and dibromobenzene (a mixture of isomers) via 20 mol% of **1** and 12 equiv DBU in 0.5 mL DMSO at 80 °C after 24 h (Scheme 3). Another multisubstituted aryl bromide, decabromodiphenyl ether (deca-BDE) also as a fire retardant (unify), was treated with H_2 (1 atm)

in the presence of 10 mol % of **1** and 11 equiv DBU in 4 mL DMSO at 80 °C. After 12h, GC-MS analysis revealed that tri- and tetrabromodiphenyl ether were predominantly formed as a mixture of several isomers.

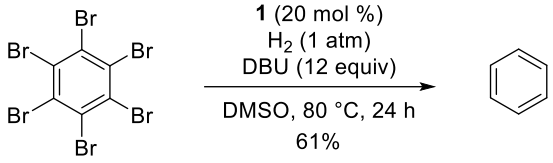

Scheme 3. Hydrodebromination of hexabromobenzene

4-5. Radical clock reaction

As mentioned above, the reluctant reactivity of phenyl triflate in our catalytic system implied that C–X bond cleavage proceeds not via the ionic pathway but via radical pathway.[14] To support this point, a radical clock experiment was performed. The reaction of 1-bromo-2-(but-3-en-1-yl)benzenewas performed in the presence of 2 mol% of **1** and 2 equiv DBU in 4 mL DMSO, and 66% 3-methyl-1*H*-indene was formed as a major product (Scheme 4). This result was a solid evidence of the existence of aryl radicals formed *in situ*. In this case, the formed aryl radical further underwent an intramolecular cyclization and isomerization to afford 3-methyl-1*H*-indene. Such the reaction was also reported in other catalytic reactions.[15]

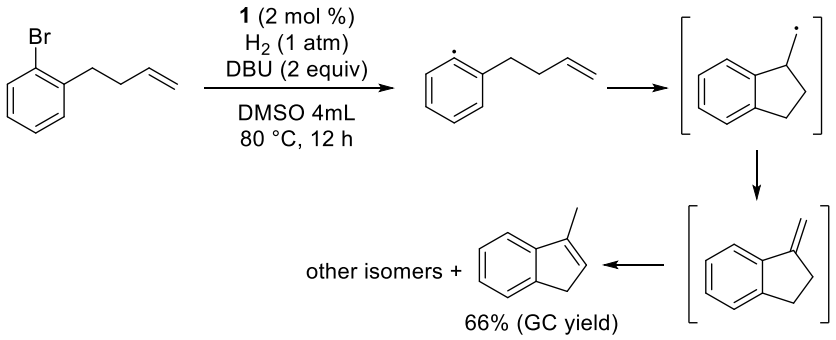

Scheme 4. Catalytic hydrodehalogenation of 1-bromo-2-(but-3-en-1-yl)benzene.

4-6. Kinetic study

In order to shed light on the detail of the catalytic reaction, several kinetic studies were performed. First of all, the examination of hydrodehalogenation of 1-bromo-4-trifluoromethylbenzene was performed in the presence of 2 mol% of **1** and 2 equiv DBU in 4 mL DMSO, and a pseudo-first-order reaction pattern was found (Figure 2). The observed rate constant (k_{obs}) was determined to be 7.71×10^{-5} s^{-1}.

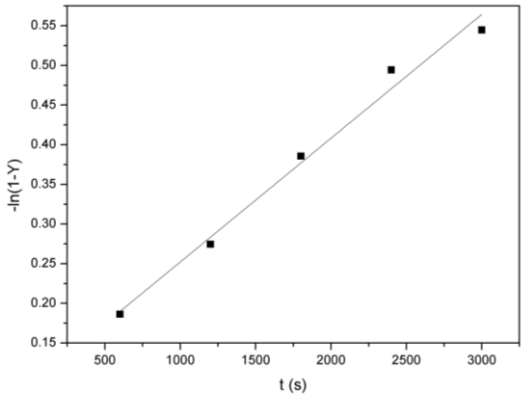

Figure 2. Plots of –ln(1−Y) of 1-catalyzed hydrodehalogenation of 1-bromo-4-trifluoromethylbenzene against time (s). $-\ln(1-Y) = 7.71(0.53)\times10^{-5}\,x + 0.084(0.011)$ ($R^2 = 0.99$). Y = Yield of the hydrogenated product.

Followed by the same protocol, competitive reactions of hydrodehalogenation of various *para*-substitued aryl bromides with 1-bromo-4-trifluoromethylbenzene were also studied, and the rate constants of hydrodehalogenation of each substrate was determined (Chapter 4-8, Table 5). It was revealed that the rate constant increased as the electron-withdrawing ability of the substituent on the aryl halide increased. The kinetic parameter of each substrate ($\log(k_{obs})$) also revealed a good linear correlation with Hammett substituent constant σ (Figure 3). The Hammett reaction constant ρ was calculated to be 0.87.

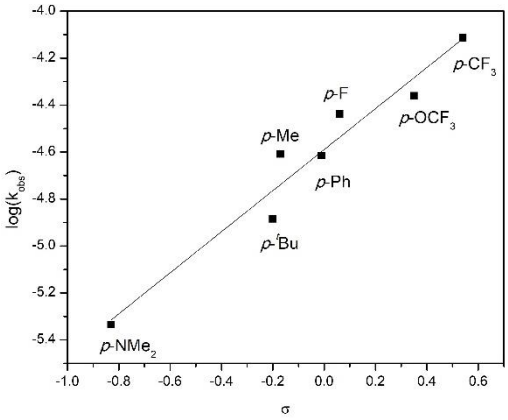

Figure 3**.** Hammett plot for the rate constants (k_{obs}) of **1**-catalyzed hydrodehalogenation against the σ values of para substituents on the Ar groups. $\log(k_{obs}) = [0.87(0.090)]\,\sigma - 4.59\ (0.037)$ ($R^2 = 0.95$).

This result along with the observation in the radical clock experiment suggests that C–X bond cleavage of aryl halides by the PNNP-Co(I) catalyst is accomplished by a radical mechanism. Accordingly, the reaction might start with electron transfer from the Co(I) center to the π* orbital of an aryl halide to generate an aryl halide radical anion. Such behaviors can be also found in various homogeneous catalytic reactions[16] and electrochemical reactions[17]. Moreover, the positive ρ value, 0.87, in the Hammett plot implied the electron-withdrawing substituents could stabilize the substrate with negative charge in the transition state. The determined ρ value is close to the one in the Hammett correlation with the one-electron reduction half-wave potentials of various aryl bromides (ρ = 0.57),[18] which suggested the similarity between these two processes. Hence, one possible transition state is proposed as $[Co(II) + ArX^{\bullet-}]^{\ddagger}$. This result also supports the silent reactivity of phenyl triflate which usually prefers an ionic S_NAr-type oxidative addition mechanism[14].

Further mechanistic insight was surveyed via the Eyring plot from the kinetic study of hydrodehalogenation of 1-bromo-4-trifluoromethylbenzene at different temperature (Figure 4). At 353 K, the activation enthalpy was found as 7.4 kcal/mol, and the activation entropy was a relatively large negative value, –48.4 cal/mol·K. Thus, the activation Gibbs free energy was calculated as 27.5 kcal/mol. It is likely that the rate-determining step of this reaction might involve the incorporation of the substrate into the reaction sphere. The relatively large negative entropy of activation might be due to the influence of steric hindrance of the phenyl groups on the PNNP ligand.

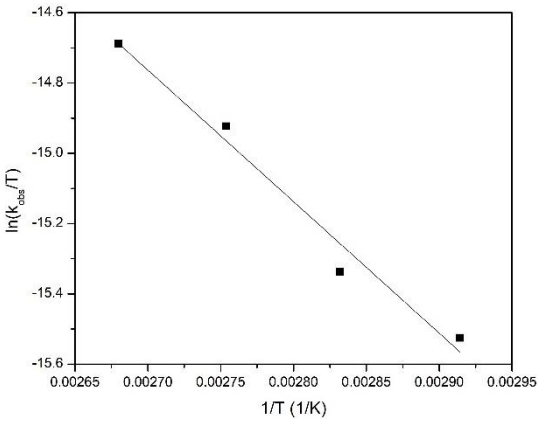

Figure 4. Eyring plot; plots for the rate constants (k_{obs}) of **1**-catalyzed hydrodehalogenation at 343, 353, 363, and 373 K. $\ln(k_{obs}/T) = -3741.7(403)(1/T) - 4.7(1.1)$ ($R^2 = 0.98$).

Further study to shed light on the reaction mechanism was performed. The correlation between $\log(k_{obs})$ and half-peak reduction potential ($E_{p/2}$) of various aryl bromides with different substituents was studied (Figure5),[19] revealing a linear free energy relationship with the slope as

1.99.[20] Although this slope was smaller than expected value of 8.5 based on Marcus's model,[18b, 19] the result suggested the inclusion of the electron transfer process in the rate-determining step.

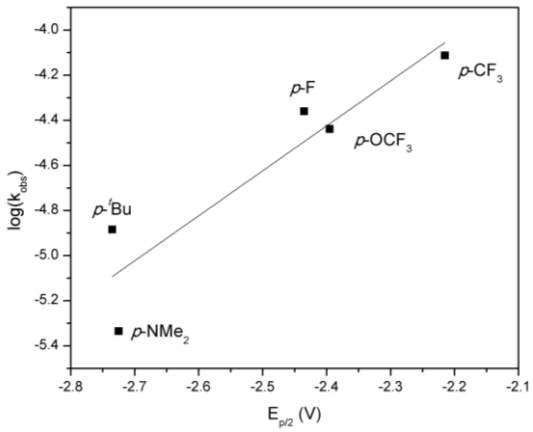

Figure 5. The correlation diagram between $\log(k_{obs})$ and the half peak potential ($E_{p/2}$) of aryl bromides at 80 °C. $\log(k_{obs}) = 1.99(0.47)(E_{p/2}) + 0.36(1.18)$ ($R^2 = 0.86$).

Next, the correlation of the observed rate constant ($\log(k_{obs})$) versus the energy gap of HOMO (**4**) and-LUMO (aryl halides) was examined. To this end, structural optimization of **4** was performed to evaluate HOMO of **4** (Figures 6 and 7) by DFT study.

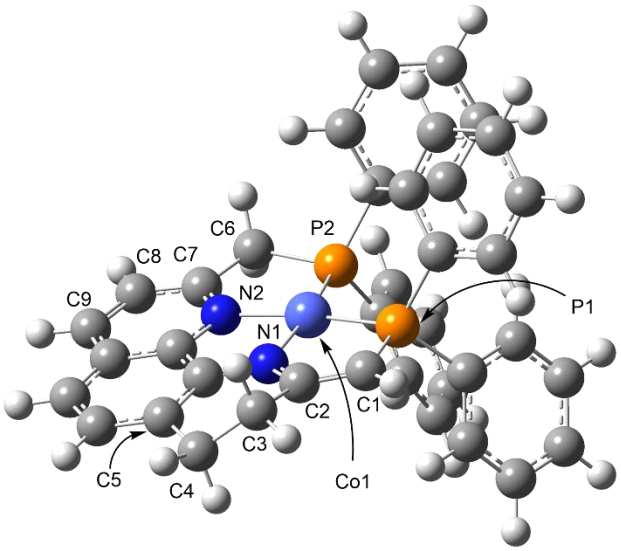

Figure 6. A DFT-optimized structure of **4**. Selected bond distances (Å) and angles (deg): Co1–P1, 2.22; Co1–P2, 2.17; Co1–N1, 1.91; Co1–N2, 1.92; P1–Co1–P2, 107.9; P1–Co1–N1, 83.2; N1–Co1–N2, 83.8; N2–Co1–P2 85.2; C2-C3-C4-C5, –44.9; C6-C7-C8-C9, –179.1.

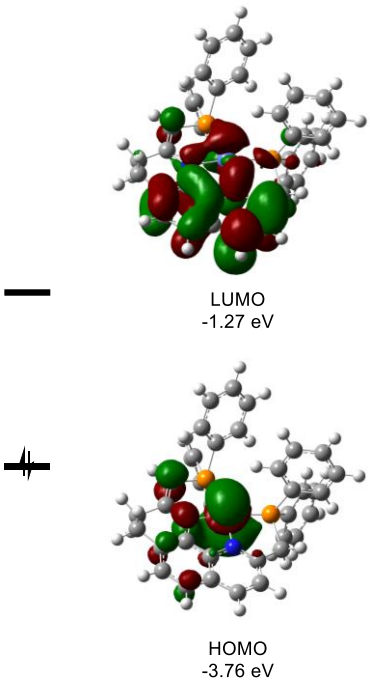

Figure 7. HOMO and LUMO of **4** obtained by DFT calculations.

It was revealed that the HOMO of **4** is mainly composed of d_z^2 orbital on the Co center. The LUMOs of various aryl bromides were similarly evaluated by the DFT study, and the energy difference between the HOMO of **4** and LUMO of aryl halides were estimated. The correlation of the observed rate constant ($\log(k_{obs})$) versus the energy gap of HOMO (4) and-LUMO (aryl halides) was then plotted, showing a similar linear free energy relationship (Figure 8).

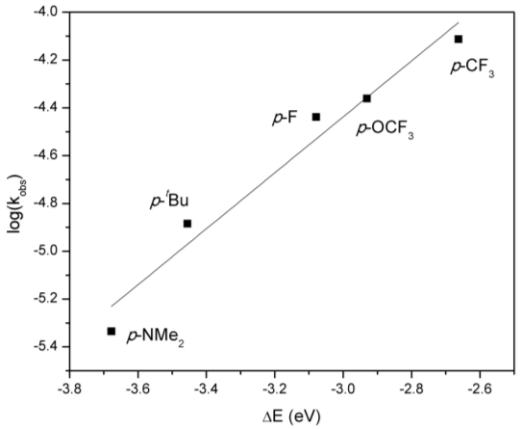

Figure 8. The Plots of $\log(k_{obs})$ against energy difference between HOMO of **4** and LUMO energy level (eV) of aryl bromides. $\log(k_{obs}) = 1.17(0.13)\,\Delta E - 0.93(0.40)$ ($R^2 = 0.98$).

Based on all the results discussed in this section, it is likely that electron transfer from the Co(I) center of **4** to the substrate, which should play an important role in the rate-determining step of the catalytic dehydrohalogenation of aryl halides by **1**.

With the mechanistic studies discussed in this chapter, a probable mechanism for PNNP-Co-catalyzed hydrodehalogenation of aryl halides is proposed (Scheme 5). Complex **1**, which undergoes dissociation to form the cationic $\mathbf{1}^+$ in DMSO, is then deprotonated by DBU to afford **3**. H–H bond cleavage is achieved by **3** to form a Co(I) hydride intermediate, **A**. Probably through homolysis of the benzylic C–H bond and Co–H bond, **A** is transferred into **4**. Finally, a facile C–X cleavage occurs via a radical mechanism, and abstraction of hydrogen then proceeds with the aryl radical formed *in situ* to generate Ar–H and $\mathbf{1}^+$, which is regenerated after rearomatization of the phenanthroline framework and reduction of the Co(II) center.

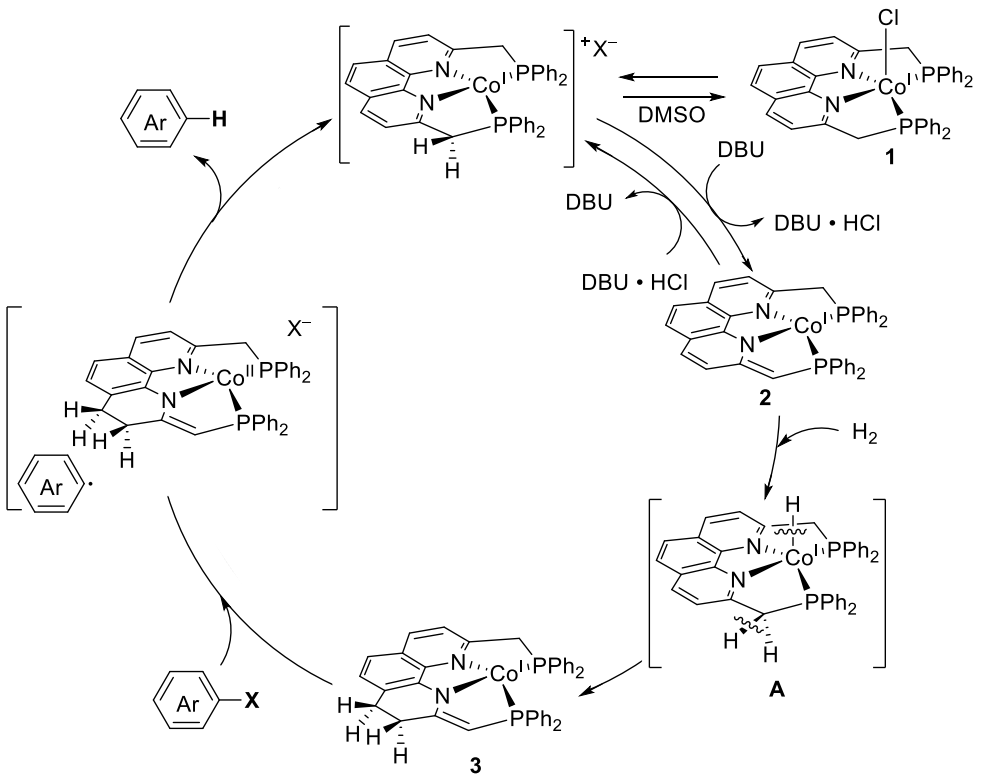

Scheme 5. The proposed mechanism of hydrodehalogenation of aryl halides catalyzed by **1**.

4-7. Conclusion

Radical hydrodehalogenation of aryl halides was achieved via PNNP-Co(I) complexes under 1 atm H_2 through a long-range MLC. The reaction conditions are mild and applicable for various aryl bromides and aryl chlorides. Moreover, degradation of hexabromobenzene, which is a stable fire retardant, was proceeded to afford benzene as the major product. Degradation of deca-BDE

was similarly reduced to tri- and tetrabromodiphenyl ether. Each elementary step in the catalytic cycle was confirmed using alternatively prepared intermediates, establishing one plausible mechanism. The detailed mechanistic study based on the kinetics indicates the radical process during C–X cleavage of aryl halides. As a result, this catalytic system can accomplish radical hydrodehalogenation of aryl halides with H_2 (1 atm). Most importantly, with the application of a long-range MLC via PNNP-Co(I) complexes, a well-controlled radical catalytic system which restrains chaotic radical side reactions to predominately afford the corresponding hydrogenated products from aryl halides. In addition, this system also highlights a base metal catalyst functioned as a hydrogen reservoir through log-range MLC.

4-8. Experimental Details

4-8-1. Identification of the products in hydrodehalogenation of aryl halides

Most of the hydrogenated products were characterized by the comparison with the commercially available products through NMR and GC. Benzene, toluene, and pyridine are reported compounds.[21]

3-Methyl-1H-indene[22]

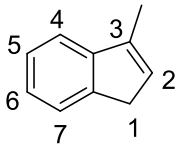

^{1}H NMR ($CDCl_3$, 25 °C) δ 7.46 (d, 1H, Ar-H^4, $^3J_{HH}$ = 7.3 Hz), 7.29-7.35 (m, 2H, Ar-$H^{5,6}$), 7.21 (td, 1H, Ar-H^7, $^3J_{HH}$ = 7.3 Hz, $^4J_{HH}$ = 1.16 Hz), 6.21 (q, 1H, Ar-H^2, $^3J_{HH}$ = 1.6 Hz), 3.32 (t, 2H, Ar-H^1, $^3J_{HH}$ = 2.1 Hz), 2.18 (q, 3H, Ar-CH_3, $^3J_{HH}$ = 2.0 Hz).

4-8-2. Kinetic study

(1) Determination of observed rate constant (k_{obs}) from the reaction of 1-bromo-4-trifluoromethylbenzene with H_2

5 different Schlenk tubes equipped with a Teflon cock were charged with a DMSO solution (4 mL) of 1 (6.7 mg, 0.01 mmol), DBU (152 mg, 1.0 mmol), 1-bromo-4-trifluoromethylbenzene (0.5 mmol), and mesitylene (12.0 mg, 0.1 mmol) in each tube. After Freeze-Pump-Thaw cycles, H_2 gas (1 atm) was introduced into the flask. The reaction solution was kept at 80 °C with stirring. The reaction was terminated after appropriate reaction time. The product yields were determined by GC analysis. A pseudo-first-order reaction with respect to the concentration of 1-bromo-4-trifluoromethylbenzene was confirmed by plotting –ln(1-Y) vs time (Y = product yield in decimals; Figure 2). The rate constants were similarly determined at 70, 90, 100 °C (Table 4). The data was used for Eyring plot.

Table 4. Rate constants k_{obs} for hydrodehalogenation of 1-bromo-4-trifluoromethylbenzene at different temperature

T (°C)	k_{obs} (s^{-1})
70	6.21×10^{-5}
80	7.71×10^{-5}
90	1.20×10^{-4}
100	1.56×10^{-4}

(2) Determination of rate constant k_{obs} for hydrodehalogenation of substrates other than 1-bromo-4-trifluoromethylbenzene

Complex **1** (6.7 mg, 0.01 mmol), DBU (228 mg, 1.5 mmol), 1-bromo-4-trifluoromethylbenzene (113 mg, 0.5 mmol), aryl halide (0.5 mmol), and mesitylene (12.0 mg, 0.1 mmol) as an internal standard were dissolved in 4 mL DMSO and charged in a Schlenk tube equipped with a Teflon valve. After Freeze-Pump-Thaw cycles, H_2 gas (1 atm) was introduced into the flask. The solution was kept at 80 °C for 1 h. The yields of products were determined by GC analysis. Based on the ratio of the product, k_{obs} was determined as shown in Table 5.

Table 5. Rate constants of each substrate at 80 °C

Substrate	k_{obs} (s^{-1})	Substrate	k_{obs} (s^{-1})
1-Bromo-4-trifluoromethylbenzene	7.71×10^{-5}	1-Bromo-4-(trifluoromethoxy)benzene	4.36×10^{-5}
1-Bromo-4-fluorobenzene	3.64×10^{-5}	4-Bromotoluene	2.46×10^{-5}
4-Bromobiphenyl	2.42×10^{-5}	1-Bromo-4-*t*-butylbenzene	1.30×10^{-5}
4-Bromo-*N*,*N*-dimethylaniline	4.62×10^{-6}		

(3) Plot for $\log(k_{obs})$ against HOMO (**4**) – LUMO (substrates) gap

The HOMO energy level of **4** (–3.76 eV) and LUMO energy levels of aryl bromides were estimated by DFT calculation (Table 5). The plot for $\log(k_{obs})$ versus HOMO (3) – LUMO (substrates) gap is shown in Figure 6.

Table 5. The LUMO of mono-substituted 4-substituted-bromobenzenes

substituent	CF_3	OCF_3	F	^{t}Bu	NMe_2

LUMO (eV)	–1.10	–0.83	–0.68	–0.31	–0.083

(4) Plot for log(k_{obs}) against the half peak reduction potential ($E_{p/2}$) of aryl bromides

Cyclic voltammetry was performed with an electrochemical analyzer ECstat-301 by EC Frontier Co., Ltd. The data were collected in DMSO (1 mM) in the presence of [Bu_4N][PF_6] electrolyte (0.1 M), using a glassy carbon working electrode, platinum wire as the counter electrode and the reference electrode equipped with electrochemical outlets, at a scan rate of 100 mV/s at 80 °C. The values were listed in Table 6.

Table 6. $E_{p/2}$ of 4-substituted-bromobenzenes in DMSO (0.1 mM) at 80 °C versus SCE

substituent	CF_3	OCF_3	F	^{t}Bu	NMe_2
$E_{p/2}$ vs SCE (V)	–2.22	–2.44	–2.40	–2.74	–2.73

(5) Plot for activation Gibbs free energy ($\Delta G^{‡}$) against the reaction free energy (ΔG_{80})

The activation Gibbs energy $\Delta G^{‡}$ was calculated based on the following equation:

$$k(T) = \frac{k_B T}{h} e^{-\frac{\Delta G^{‡}}{RT}}$$

(k(T) : rate constant at T (K); the values listed in Tables 5 were used for the calculation, k_B : Boltzmann constant (1.38×10^{-23} J·K^{-1}), h : Planck constant (6.626×10^{-34} Js), R : 8.314 (J·K^{-1}mol^{-1}), $\Delta G^{‡}$: the activation Gibbs free energy)

The free energies ΔG° at 80 °C (353 K) in DMSO of each reaction were determined based on the energy difference between the free energy of the products ([Co(PNNP)]$^{+}$Br^{-} + Aryl-H) and the reactants (**4** + Aryl-Br) estimated by DFT calculation. The calculated values were listed in Table 7.

Table 7. The activation Gibbs free energy ($\Delta G^{‡}$) and the reaction free energy (ΔG°) at 80 °C

Substrate	ΔG_{353} (kcal/mol)	$\Delta G^{‡}_{353}$ (kcal/mol)
1-Bromo-4-trifluoromethylbenzene	–43.0	27.5
1-Bromo-4-(trifluoromethoxy)benzene	–43.2	27.9
4-Bromobiphenyl	–42.1	28.3
1-Bromotoluene	–41.8	28.3
1-Bromo-4-*t*-butylbenzene	–41.7	28.7

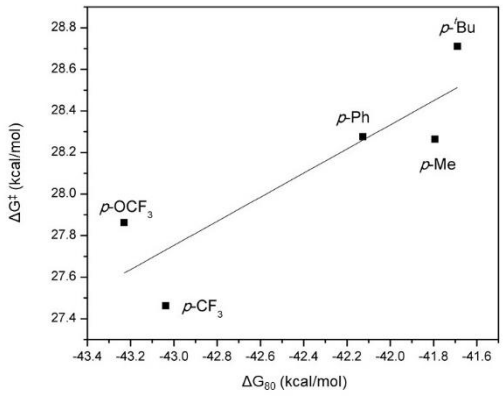

Figure 7. Plot for the activation Gibbs free energy ($\Delta G^{\ddagger}_{353}$) against the reaction free energy (ΔG°_{353}) in DMSO at 80 °C (353 K). $\Delta G^{\ddagger}_{353} = 0.58(0.18)\ \Delta G_{353} + 52.69(7.78)$ ($R^2 = 0.77$).

4-8-3. Details of Theoretical Calculation

All calculations of **3** and substrates were carried out using B3LYP functional[23] with 6-31G for phenyl carbon atoms on the phosphorus atoms and 6-31G(d,p) for other carbon atoms, phosphorus atoms, nitrogen atoms, and bromine atom.[24] Cobalt atom was treated with LANL2DZ pseudopotential and the corresponding basis set.[25] Solvent effects (DMSO) were treated with polarizable continuum model (PCM),[26] and D3 empirical dispersion correction was also applied.[27] It was ascertained that the optimized geometry of $\mathbf{1}^{+}$+Br^{-}, **4**, and aryl bromides exhibited no imaginary frequency. Gaussian 16 suite of programs[28] was used for all calculations.

Table 8. Total energies (Hartrees) of all molecules calculated at B3LYP/LANL2dz-6-31G(d,p) (PCM) level of theory

System	E_{sol} (a. u)	G_{sol} (a. u)
4	–2403.977903	–2403.454672
$\mathbf{1}^{+}$ + Br^{-}	–4975.137154	–4974.639112
1-Bromo-4-trifluoromethylbenzene	–3140.412244	–3140.354362

1-Bromo-4-(trifluoromethoxy)benzene	−3215.631145	−3215.571004
4-Bromobiphenyl	−3034.447657	−3034.313567
1-Bromotoluene	−2842.695970	−2842.611951
1-Bromo-4-tert-butylbenzene	−2960.654142	−2960.488034
Trifluoromethylbenzene	−569.307350	−569.236080
(Trifluoromethoxy)benzene	−644.526579	−644.453035
Biphenyl	-463.341255	-463.193833
Toluene	-271.589103	-271.491704
Tert-butylbenzene	-389.547048	-389.367612

Table 9. Cartesian coordinates of all compounds

4				**1^+**			
Atomic Number	**X**	**Y**	**Z**	**Atomic Number**	**X**	**Y**	**Z**
27	2.266216	4.650996	16.67713	27	6.496003	3.480692	10.56178
15	2.350056	6.780856	16.06522	15	4.468127	3.987924	9.904215
15	3.517097	4.411793	18.43309	15	7.871326	4.21108	9.015022
6	1.206889	6.791248	14.66997	7	5.634297	2.909029	12.17871
6	1.206889	6.791248	14.66997	7	5.634297	2.909029	12.17871
6	-0.1411	5.200386	13.177	6	3.416561	3.284041	11.3005
6	-1.17068	4.074614	13.43314	1	2.62198	3.968973	11.61299
6	-0.55576	2.932702	14.21124	1	2.924953	2.383495	10.91272
6	-0.99284	1.589743	14.18501	6	4.322404	2.910699	12.44815
6	3.541424	2.537048	18.65549	6	3.858229	2.550521	13.73508
6	2.500703	1.939398	17.73711	1	2.791528	2.563794	13.9309
6	2.116603	0.575356	17.77609	6	4.750208	2.181052	14.72775
6	1.162856	0.088459	16.90223	1	4.390321	1.902536	15.71367
6	0.554792	0.955603	15.9528	6	6.141001	2.169683	14.45252
6	-0.45789	0.611335	15.01655	6	7.189329	1.818231	15.37315

6	0.471977	3.277458	15.08975	1	6.916094	1.521092	16.38118
6	1.002788	2.29874	15.97174	6	9.512414	3.480187	9.585868
7	1.012332	4.524193	15.24782	1	9.74932	2.600201	8.977095
7	1.944242	2.77053	16.84906	1	10.3349	4.189552	9.451744
6	3.941696	7.481409	15.46566	6	9.361877	3.066738	11.02922
6	4.087944	8.837595	15.11129	6	10.44819	2.744647	11.8763
6	5.314575	9.31784	14.64038	1	11.45763	2.817482	11.48621
6	6.411833	8.451253	14.52182	6	10.22718	2.340405	13.18214
6	6.276988	7.102417	14.87301	1	11.0632	2.09467	13.82993
6	1.783371	8.045321	17.2757	6	8.900556	2.250425	13.67418
6	0.413571	8.341187	17.4019	6	8.508217	1.85546	15.00078
6	-0.04231	9.177944	18.42852	1	9.283225	1.587032	15.71239
6	0.865491	9.730624	19.34173	6	6.515802	2.548572	13.15322
6	2.232597	9.445203	19.22126	6	7.882753	2.591869	12.76906
6	2.688411	8.607165	18.19862	6	3.715984	3.339805	8.371919
6	5.287581	4.914986	18.46143	6	4.462402	2.426805	7.605376
6	5.686745	6.105289	19.10022	1	5.460206	2.151799	7.927151
6	7.000786	6.573576	18.97907	6	3.931369	1.89344	6.425112
6	7.936032	5.861214	18.21882	1	4.524209	1.20463	5.83334
6	7.548722	4.678388	17.57465	6	2.648576	2.265763	6.00599
6	6.234532	4.212941	17.68927	1	2.23653	1.85669	5.089217
6	2.873668	5.021885	20.04421	6	1.895458	3.172343	6.767499
6	1.698632	5.794718	20.04594	1	0.901599	3.461398	6.441799
6	1.16517	6.274331	21.2492	6	2.425142	3.710159	7.94452
6	1.799741	5.980931	22.46179	1	1.844843	4.423827	8.520635
6	2.970926	5.207597	22.47121	6	4.10039	5.783049	9.89674
6	3.506533	4.73226	21.27016	6	4.133866	6.512264	8.692336
6	5.047901	6.620957	15.34045	1	4.251449	5.994009	7.746569
1	1.009051	7.656099	14.04492	6	4.019567	7.906556	8.706146
1	-0.63415	6.092204	12.77872	1	4.046099	8.456362	7.771081
1	0.566677	4.858325	12.4073	6	3.878264	8.590513	9.920068
1	-1.59059	3.72963	12.48144	1	3.794625	9.672121	9.92933
1	-2.01104	4.488026	14.01231	6	3.848835	7.873317	11.12358
1	-1.78662	1.318252	13.49158	1	3.74028	8.397049	12.06763
1	4.535206	2.147195	18.40692	6	3.961886	6.478527	11.11398
1	3.352727	2.264915	19.69987	1	3.954922	5.940421	12.05696

1	2.581379	-0.07959	18.50625	6	7.703214	3.751891	7.248568
1	0.86753	-0.95685	16.9414	6	7.98276	2.438019	6.82327
1	-0.81875	-0.41202	14.97061	1	8.405362	1.713114	7.511671
1	3.247892	9.517322	15.21685	6	7.698081	2.040148	5.512582
1	5.417657	10.36449	14.37122	1	7.922903	1.026153	5.198657
1	7.364624	8.828438	14.16377	6	7.119735	2.944079	4.611648
1	7.125413	6.429785	14.80097	1	6.8945	2.63237	3.597228
1	-0.2903	7.913711	16.69388	6	6.829263	4.248837	5.027832
1	-1.10186	9.398948	18.5132	1	6.3773	4.953268	4.337302
1	0.511958	10.37733	20.1384	6	7.116804	4.651536	6.336792
1	2.941026	9.869547	19.92595	1	6.883056	5.66418	6.646761
1	3.748004	8.384407	18.12002	6	8.191597	6.015388	9.00401
1	4.973049	6.667347	19.69283	6	7.472345	6.835395	9.892011
1	7.290888	7.492713	19.47818	1	6.727033	6.392113	10.54235
1	8.954088	6.224706	18.12501	6	7.704284	8.216023	9.92707
1	8.265927	4.122329	16.97936	1	7.131608	8.838121	10.60629
1	5.947071	3.310931	17.15744	6	8.658759	8.786619	9.077305
1	1.217418	6.026036	19.10202	1	8.837245	9.856754	9.100622
1	0.266342	6.881727	21.23362	6	9.384189	7.975529	8.191161
1	1.389002	6.352844	23.39507	1	10.12392	8.417069	7.531426
1	3.464691	4.98041	23.41067	6	9.153136	6.597342	8.152835
1	4.421689	4.147839	21.28332	1	9.708162	5.977946	7.455106
1	4.941117	5.581799	15.63142				

4-Bromobenzotrifluoride				**1-Bromo-4-(trifluoromethoxy)benzene**			
Atomic Number	**X**	**Y**	**Z**	**Atomic Number**	**X**	**Y**	**Z**
6	1.0974	0.455278	-0.25004	6	1.113274	0.487906	-0.07144
6	1.640076	-0.77969	0.099833	6	1.65077	-0.77242	0.189527
6	0.782335	-1.80633	0.493398	6	0.787434	-1.84002	0.434808
6	-0.59994	-1.62789	0.542672	6	-0.59807	-1.68008	0.425261
6	-1.13244	-0.38931	0.190654	6	-1.13302	-0.41872	0.164067
6	-0.28528	0.648535	-0.20537	6	-0.26909	0.643716	-0.081
35	1.52075	-3.50602	0.9737	35	1.52405	-3.57264	0.791344
6	-0.86196	1.998324	-0.52685	1	1.753592	1.340129	-0.26663
9	-2.10646	1.906057	-1.04931	1	2.724231	-0.91865	0.200928

9	-0.09899	2.678334	-1.41287	1	-1.25086	-2.52309	0.61771
9	-0.96196	2.777435	0.579336	1	-2.20453	-0.25739	0.148178
1	1.749769	1.262217	-0.564	8	-0.81088	1.901152	-0.40445
1	2.710817	-0.9409	0.064153	6	-1.0378	2.744083	0.633191
1	-1.24879	-2.44034	0.847083	9	0.090847	3.043597	1.307799
1	-2.20533	-0.2357	0.217608	9	-1.90813	2.234141	1.528187
				9	-1.54923	3.872221	0.137028

4-Bromobiphenyl

Atomic Number	X	Y	Z
6	-0.96307	0.952336	-0.80178
6	-0.42173	-0.28962	-0.47468
6	-1.16734	-1.16551	0.311767
6	-2.43687	-0.82179	0.771941
6	-2.96372	0.423453	0.433921
6	-2.24051	1.333208	-0.35639
35	-0.43174	-2.87795	0.769899
1	-0.37094	1.642968	-1.39359
1	0.568111	-0.56674	-0.81872
1	-3.0094	-1.51646	1.375749
1	-3.96254	0.679518	0.772431
6	-2.80943	2.657775	-0.71022
6	-2.59196	3.219359	-1.98053
6	-3.57935	3.381941	0.216744
6	-3.12612	4.464205	-2.31238
1	-2.02115	2.666453	-2.72046
6	-4.1147	4.625992	-0.11607
1	-3.73907	2.978489	1.212101
6	-3.89015	5.172743	-1.38188
1	-2.95254	4.876814	-3.30183
1	-4.70042	5.172372	0.617287
1	-4.30653	6.141579	-1.64066

1-Bromotoluene

Atomic Number	X	Y	Z
6	-0.84875	1.126795	-0.28636
6	-0.30292	-0.11744	0.032079
6	-1.16243	-1.17906	0.306078
6	-2.54569	-1.01765	0.268759
6	-3.06963	0.235366	-0.05199
6	-2.23544	1.325282	-0.33666
35	-0.42575	-2.89755	0.75126
1	-0.17973	1.956576	-0.49724
1	0.771686	-0.25613	0.069608
1	-3.20275	-1.85142	0.489014
1	-4.14825	0.363678	-0.07852
6	-2.81405	2.667406	-0.71441
1	-2.95623	2.738983	-1.79956
1	-3.78966	2.827862	-0.2468
1	-2.15176	3.485806	-0.41808

1-Bromo-4-fluorobenzenebenzene				1-Bromo-4-tert-butylbenzene			
Atomic				Atomic			
Number	X	Y	Z	Number	X	Y	Z
6	-0.83672	1.135046	-0.30117	6	-0.91803	1.157126	0.10046
6	-0.30254	-0.11022	0.031428	6	-0.35396	-0.06462	0.460431
6	-1.16568	-1.16931	0.312308	6	-1.13355	-1.21689	0.377096
6	-2.55102	-1.01279	0.268467	6	-2.45261	-1.15792	-0.05702
6	-3.08644	0.231974	-0.06399	6	-2.99694	0.079556	-0.41295
6	-2.21866	1.281969	-0.34239	6	-2.24819	1.262051	-0.34361
35	-0.43046	-2.88101	0.769623	35	-0.37158	-2.91063	0.870109
1	-0.19636	1.980445	-0.52546	1	-0.2982	2.045244	0.170698
1	0.771231	-0.25059	0.070451	1	0.674275	-0.11877	0.799824
1	-3.20604	-1.84715	0.489778	1	-3.05255	-2.05885	-0.11923
1	-4.15794	0.390159	-0.10776	1	-4.02675	0.098828	-0.7482
9	-2.73655	2.487525	-0.66432	6	-2.81868	2.637226	-0.72793
				6	-1.98071	3.233224	-1.88323
				1	-2.37417	4.215406	-2.16674
				1	-0.93204	3.363351	-1.60059
				1	-2.01533	2.584045	-2.76426
				6	-4.28518	2.553398	-1.18903
				1	-4.93712	2.163278	-0.40073
				1	-4.64397	3.553586	-1.45066
				1	-4.39671	1.919188	-2.07447
				6	-2.74885	3.579402	0.496581
				1	-3.14926	4.565412	0.237084
				1	-3.33735	3.179981	1.32905
				1	-1.72141	3.718199	0.845336

4-Bromo-N,N-dimethylaniline				(Trifluoromethyl)benzene			
Atomic				Atomic			
Number	X	Y	Z	Number	X	Y	Z
6	0.604227	0.512947	0.663945	6	1.097861	0.457939	-0.25054
6	1.260158	-0.6664	1.004352	6	1.633254	-0.7808	0.101919
6	0.808065	-1.8832	0.500059	6	0.788877	-1.82123	0.497904
6	-0.30161	-1.92658	-0.34037	6	-0.59393	-1.62492	0.540485

6	-0.95977	-0.74911	-0.68261	6	-1.13509	-0.38854	0.189011
6	-0.51931	0.508361	-0.19964	6	-0.28604	0.649053	-0.20658
35	1.713662	-3.51236	0.974895	6	-0.86201	1.998485	-0.52713
1	0.976896	1.440398	1.079053	9	-2.10974	1.911103	-1.04542
1	2.118974	-0.63185	1.665761	9	-0.10308	2.680178	-1.41702
1	-0.66003	-2.87439	-0.72694	9	-0.95794	2.781783	0.578273
1	-1.82298	-0.8189	-1.33173	1	1.745552	1.268985	-0.56488
7	-1.15419	1.68152	-0.56176	1	2.707051	-0.93392	0.064472
6	-2.41803	1.618339	-1.28254	1	-1.25069	-2.43393	0.843917
1	-3.19945	1.089679	-0.71706	1	-2.20763	-0.22952	0.213216
1	-2.76692	2.631274	-1.48263	1	1.20786	-2.78498	0.770517
1	-2.29714	1.114025	-2.24779				
6	-0.79679	2.924512	0.107406				
1	0.258563	3.170584	-0.05482				
1	-1.39122	3.738309	-0.3076				
1	-0.97492	2.88555	1.192165				

(Trifluoromethoxy)benzene				**Biphenyl**			
Atomic Number	**X**	**Y**	**Z**	**Atomic Number**	**X**	**Y**	**Z**
6	1.114191	0.490157	-0.0715	6	-0.9614	0.954724	-0.80048
6	1.644047	-0.77488	0.189588	6	-0.42712	-0.29029	-0.46888
6	0.794319	-1.85646	0.437071	6	-1.15945	-1.184	0.316407
6	-0.59162	-1.67725	0.423979	6	-2.43143	-0.82116	0.765989
6	-1.1352	-0.41773	0.164423	6	-2.96626	0.423099	0.432468
6	-0.26856	0.642757	-0.07973	6	-2.2405	1.333135	-0.35609
1	1.74949	1.346256	-0.26733	1	-0.37284	1.650708	-1.39062
1	2.720621	-0.91271	0.198537	1	0.565979	-0.55878	-0.81726
1	-1.25284	-2.5165	0.615163	1	-3.01283	-1.51127	1.370487
1	-2.20595	-0.25011	0.14747	1	-3.96584	0.683975	0.766868
8	-0.81228	1.904613	-0.4038	6	-2.80988	2.658694	-0.71027
6	-1.03869	2.745847	0.631825	6	-2.59534	3.220336	-1.9812
9	0.08884	3.048433	1.308652	6	-3.57789	3.385399	0.216468
9	-1.91038	2.239274	1.528685	6	-3.12919	4.465358	-2.31356
9	-1.55029	3.875372	0.1362	1	-2.02545	2.666584	-2.72126
1	1.21161	-2.83803	0.637839	6	-4.11361	4.629521	-0.11625

1	-3.73654	2.982387	1.212215
6	-3.89135	5.175599	-1.38278
1	-2.95676	4.876821	-3.30383
1	-4.69795	5.176523	0.617922
1	-4.30772	6.144459	-1.64171
1	-0.74329	-2.15296	0.575325

Toluene				**Tert-butylbenzene**			
Atomic				**Atomic**			
Number	**X**	**Y**	**Z**	**Number**	**X**	**Y**	**Z**
6	-0.84832	1.128897	-0.2869	6	-0.91735	1.158065	0.100394
6	-0.31021	-0.11956	0.032381	6	-0.36046	-0.06862	0.458677
6	-1.15465	-1.19724	0.310609	6	-1.12411	-1.23671	0.382965
6	-2.53903	-1.01419	0.267766	6	-2.44506	-1.15499	-0.05472
6	-3.07154	0.236519	-0.05216	6	-2.99811	0.078996	-0.41286
6	-2.23574	1.325825	-0.33688	6	-2.2483	1.261777	-0.34369
1	-0.18398	1.963276	-0.49861	1	-0.30169	2.049971	0.168689
1	0.76778	-0.24952	0.067836	1	0.670944	-0.11222	0.797426
1	-3.20483	-1.8441	0.487255	1	-3.05417	-2.05235	-0.12019
1	-4.15015	0.371298	-0.07999	1	-4.02821	0.103604	-0.74852
6	-2.81475	2.668988	-0.71527	6	-2.81931	2.638008	-0.72827
1	-2.95759	2.743259	-1.80045	6	-1.98222	3.235645	-1.88334
1	-3.79076	2.83056	-0.24802	1	-2.37462	4.218568	-2.16677
1	-2.1532	3.488384	-0.41865	1	-0.93324	3.364028	-1.60109
1	-0.73819	-2.16856	0.562337	1	-2.01754	2.586991	-2.76492
				6	-4.28587	2.556902	-1.19006
				1	-4.93838	2.166231	-0.40244
				1	-4.64415	3.55761	-1.45137
				1	-4.39806	1.922741	-2.07548
				6	-2.75025	3.581568	0.495226
				1	-3.15018	4.568175	0.236163
				1	-3.33934	3.182389	1.327587
				1	-1.72298	3.719323	0.844845
				1	-0.69388	-2.19428	0.661263

Reference

(1) Alonso, F.; Beletskaya, I. P.; Yus, M. *Chem. Rev.* **2002**, *102*, 4009–4091.

(2) (a) Fukuzumi, S. New Perspective of Electron Transfer Chemistry. *Org. Biomol. Chem.* **2003**, *1*, 609–620. (b) Roth, J. P.; Lovell, S.; Mayer, J. M. *J. Am. Chem. Soc.* **2000**, *122*, 5486–5498. (c) Rhile, I. J.; Mayer, J. M. *J. Am. Chem. Soc.* **2004**, *126*, 12718–12719.

(3) (a) Akita, Y.; Inoue, A.; Ishida, K.; Terui, K.; Ohta, A. *Synth. Commun.* **1986**, *16*, 1067–1072. (b) Grushin, V. V.; Alper, H. *Organometallics* **1991**, *10*, 1620–1622. (c) Ferrughelli, D. T.; Horváth, I. T. *J. Chem. Soc. Chem. Commun.* **1992**, 806–807. (d) Cu-cullu, M. E.; Nolan, S. P.; Belderrain, T. R.; Grubbs, R. H. *Organometallics* **1999**, *18*, 1299–1304. (e) Buil, M. L.; Esteruelas, M. A.; Niembro, S.; Oliván, M.; Orzechowski, L.; Pelayo, C.; Vallribera, A. *Organometallics* **2010**, *29*, 4375–4383. (f) Sahoo, B.; Surkus, A.-E.; Pohl, M.-M.; Radnik, J.; Schneider, M.; Bachmann, S.; Scalone, M.; Junge, K.; Beller, M. *Angew. Chem. Int. Ed.* **2017**, *56*, 11242–11247.

(4) Ghosh, I.; Ghosh, T.; Bardagi, J. I.; König, B. *Science* **2014**, *346*, 725–728.

(5) Zhang, J.; Yang, J.-D.; Cheng, J.-P. *Chem. Sci.* **2020**, *11*, 4786–4790. (g) Cowper, N. G. W.; Chernowsky, C. P.; Williams, O. P.; Wickens, Z. K. *J. Am. Chem. Soc.* **2020**, *142*, 2093–2099.

(6) (a) Studer, A.; Curran, D. P. *Angew. Chem. Int. Ed.* **2011**, *50*, 5018 – 5022. (b) Studer, A.; Curran, D. P. *Nat. Chem.* **2014**, *6*, 765–773. (c) Yi, H.; Jutand, A.; Lei, A. *Chem. Commun.* **2015**, *51*, 545–548.

(7) Hokamp, T.; Dewanji, A.; Lübbesmeyer, M.; Mück-Lichtenfeld, C.; Würthwein, E.-U.; Studer, A. *Angew. Chem. Int. Ed.* **2017**, *56*, 13275–13278.

(8) Nozawa-Kumada, K.; Iwakawa, Y.; Onuma, S.; Shigeno, M.; Kondo, Y. *Chem. Commun.* **2020**, *56*, 7773–7776.

(9) *The Merck Index: An Encyclopedia of Chemicals, Drugs, and Biologicals*, 14th ed; O'Neil, M.J., Ed.; RSC.org, 2013.

(10) Speight, J. G. *Lange's Handbook of Chemistry*, 7th ed.; McGraw Hill Education; New York, Chicago, San Francisco, Athens, London, Madrid, Mexico City, Milan, New Delhi, Singapore, Sydney, Toronto, 2017.

(11) Pattenden, G. *Chem. Soc. Rev.* **1988**, *17*, 361–382.

(12) pKa values in H_2O for NEt_3; 10.7, pyrrolidine; 11.3 in H_2O, DBU; 13.5±1.5, MTBD; 15.0±1.0: Tshepelevitsh, S.; Kütt, A.; Lõkov, M.; Kaljurand, I.; Saame, J.; Heering, A.; Plieger, P. G.; Vianello, R.; Leito, I. *Eur. J. Org. Chem.* **2019**, 6735–6748.

(13) pKa value in H_2O for DMAP 9.6: Kaljurand, I.; Kütt, A.; Sooväli, L.; Rodima, T.; Mäemets, V.; Leito, I.; Koppel, I. A. *J. Org. Chem.* **2005**, *70*, 1019–1028.

(14) (a) Jutand, A.; Mosleh, A. *Organometallics* **1995**, *14*, 1810–1817. (b) Jutand, A.; Hii, K. K. M.; Thornton-Pett, M.; Brown, J. M. *Organometallics* **1999**, *18*, 5367–5374. (c) Alcazar-Roman,

L. M.; Hartwig, J. F. *Organometallics* **2002**, *21*, 491–502. (d) Roy, A. H.; Hartwig, J. F. *Organometallics* **2004**, *23*, 194–202.
(15) Isomerization of 1-methylene-2,3-dihydro-1H-indene to 3-methyl-1H-indene was also reported: (a) Léonard, N. G.; Palmer, W. N.; Friedfeld, M. R.; Bezdek, M. J.; Chirik, P. J. *ACS Catal.* **2019**, *9*, 9034–9044. (b) Bhandal, H.; Patel, V. F.; Pattenden, G.; Russell, J. J. *J. Chem. Soc. Perkin Trans. 1* **1990**, 2691–2701.
(16) (a) Studer, A.; Curran, D. P. *Angew. Chemie Int. Ed.* **2016**, *55*, 58–102. (b) Kyne, S. H.; Lefèvre, G.; Ollivier, C.; Petit, M.; Cladera, V.-A. R.; Fensterbank, L. *Chem. Soc. Rev.* **2020**, *49*, 8501–8542.
(17) For example, (a) Nadjo, L.; Savéant, J. M. *J. Electroanal. Chem.* **1971**, *30*, 41–57. (b) Pause, L.; Robert, M.; Savéant, J. M. *J. Am. Chem. Soc.* **1999**, *121*, 7158–7159.
(18) (a) Sease, J. W.; Burton, F. G.; Nickol, S. L. *J. Am. Chem. Soc.* **1968**, *90*, 2595–2598. (b) Tsou, T. T.; Kochi, J. K. *J. Am. Chem. Soc.* **1979**, *101*, 6319–6332.
(19) (a) Marcus, R. A. *J. Chem. Phys.* **1956**, *24*, 966–978. (b) Darcy, J. W.; Koronkiewicz, B.; Parada, G. A.; Mayer, J. M. *Acc. Chem. Res.* **2018**, *51*, 2391–2399.
(20) Here Marcus-Hush theory was also applied, $\Delta G^{\ddagger} = \alpha\Delta G^{\circ}$ + constant, giving $\alpha = 0.58$. See Figure 7.
(21) Fulmer, G. R.; Miller, A. J. M.; Sherden, N. H.; Gottlieb, H. E.; Nudelman, A.; Stoltz, B. M.; Bercaw, J. E.; Goldberg, K. I. *Organometallics* **2010**, *29*, 2176–2179.
(22) Tanaka, S.; Watanabe, K.; Tanaka, Y.; Hattori, T. *Org. Lett.* **2016**, *18*, 2576–2579.
(23) Becke, A. D. *J. Chem. Phys.* **1993**, *98*, 5648–5652.
(24) (a) Ditchfield, R.; Hehre, W. J.; Pople, J. A. *J. Chem. Phys.* **1971**, *54*, 720–723. (b) Hehre, W. J.; Ditchfield, K.; Pople, J. A. *J. Chem. Phys.* **1972**, *56*, 2257–2261. (c) Hariharan, P. C.; Pople, J. A. *Theor. Chim. Acta* **1973**, *28*, 213–222. (d) Francl, M. M.; Pietro, W. J.; Hehre, W. J.; Binkley, J. S.; Gordon, M. S.; DeFrees, D. J.; Pople, J. A. *J. Chem. Phys.* **1982**, *77*, 3654–3665.
(25) (a) Dunning, T. H. Jr.; Hay, P. J. Gaussian Basis Sets for Molecular Calculations. In *Modern Theoretical Chemistry, Volume 3: Methods of Electronic Structure Theory*, Ed. H. F. Schaefer III, Vol. 3; Plenum Publishing Company, New York, 1977; pp 1–28. (b) Hay, P. J.; Wadt, W. R. *J. Chem. Phys.* **1985**, *82*, 270–283. (c) Hay, P. J.; Wadt, W. R. *J. Chem. Phys.* **1985**, *82*, 299–310.
(26) Tomasi, J.; Mennucci, B.; Cammi, R. *Chem. Rev.* **2005**, *105*, 2999–3093.
(27) Grimme, S. *J. Comput. Chem.* **2006**, *27*, 1787–1799.
(28) Frisch, M. J.; Trucks, G. W.; Schlegel, H. B.; Scuseria, G. E.; Robb, M. A.; Cheeseman, J. R.; Scalmani, G.; Barone, V.; Petersson, G. A.; Nakatsuji, H.; Li, X.; Caricato, M.; Marenich, A. V.; Bloino, J.; Janesko, B. G.; Gomperts, R.; Mennucci, B.; Hratchian, H. P.; Ortiz, J. V.; Izmaylov, A. F.; Sonnenberg, J. L.; Williams-Young, D.; Ding, F.; Lipparini, F.; Egidi, F.; Goings, J.; Peng, B.; Petrone, A.; Henderson, T.; Ranasinghe, D.; Zakrzewski, V. G.; Gao, J.; Rega, N.; Zheng, G.;

Liang, W.; Hada, M.; Ehara, M.; Toyota, K.; Fukuda, R.; Hasegawa, J.; Ishida, M.; Nakajima, T.; Honda, Y.; Kitao, O.; Nakai, H.; Vreven, T.; Throssell, K.; Montgomery, J. A., Jr; Peralta, J. E.; Ogliaro, F.; Bearpark, M. J.; Heyd, J. J.; Brothers, E. N.; Kudin, K. N.; Staroverov, V. N.; Keith, T. A.; Kobayashi, R.; Normand, J.; Raghavachari, K.; Rendell, A. P.; Burant, J. C.; Iyengar, S. S.; Tomasi, J.; Cossi, M.; Millam, J. M.; Klene, M.; Adamo, C.; Cammi, R.; Ochterski, J. W.; Martin, R. L.; Morokuma, K.; Farkas, O.; Foresman, J. B.; Fox, D. J. *Gaussian 16* Rev. C.01; Gaussian: Wallingford, CT, 2019.

Chapter 5 Summary

In this thesis, properties of PNNP-Co(I) complexes including their metal-ligand cooperation (MLC) behaviors were revealed. It was also revealed that the PNNP-Co(I) system facilitate H_2 activation via MLC. This is further applied to hydrodehalogenation of aryl halides, achieving degradation of environmentally hazardous fire retardants under 1 atmospheric pressure of H_2. Through mechanistic study, radical process of C–X (X = Cl, Br) cleavage and the following hydrogen atom transfer (HAT) were evidenced in the catalytic reactions. Most importantly, capability of the PNNP-Co(I) system as a H_2 reservoir, which is mediated via MLC, was also demonstrated through this study.

In Chapter 1, importance of cobalt complexes as catalysts is introduced. Reflecting the obstacles of cobalt catalysts, new design and/or modification of ligands is important. In this context, pincer ligands and the concept of MLC and pincer ligands were introduced. Previous reports on Co(I) complexes, which exhibit remarkable reactivity, are also introduced. Furthermore, this chapter finally discuss the importance of the precise design of Co(I) pincer complexes to establish MLC, which is attractive but still a challenging research target in the organometallic field. To this end, the chapter describes the utility of the PNNP ligand, which is a tetradentate ligand with four σ-donating groups and a phenanthroline framework, as a strong-field ligand to stabilize Co(I) center with a low-spin state. It should be also noted that with a delocalized PNNP backbone, the PNNP-Co system could efficiently demonstrate a dearomatization/rearomatization sequence during the MLC processes.

In Chapter 2, properties of PNNP-Co(I) alkyl complexes were studied. Co(I) alkyl complexes are known as key species to achieve remarkable reactivity in various catalytic reactions. It has been previously reported that PNNP-Co alkyl complex [Co(CH_2SiMe_3)PNNP] (**2**) underwent structural transformation upon heating to form **3**, which possesses asymmetric PNNP' ligand with a dearomatized backbone, accompanied by the formation of $SiMe_4$. In this study, [CoMe(PNNP)] (**5**) was newly synthesized and identified by NMR spectroscopy. Synthesis of **2** was re-examined to improve the reaction yield. Reaction of **2** with TEMPO was performed to form TEMPO-alkyl and TEMPO-H. Based on these studies, it was revealed that **2** can afford alkyl radical and H radical. Thus, the possible reaction path for the formation of **3** from **2** was considered to be as follows, (i) **2** undergoes Co–C bond homolysis to generate $(Me_3Si)CH_2^{\bullet}$, and (ii) hydrogen abstraction from the benzylic carbon by $(Me_3Si)CH_2^{\bullet}$ affords $SiMe_4$ (R–H) (Scheme 1).

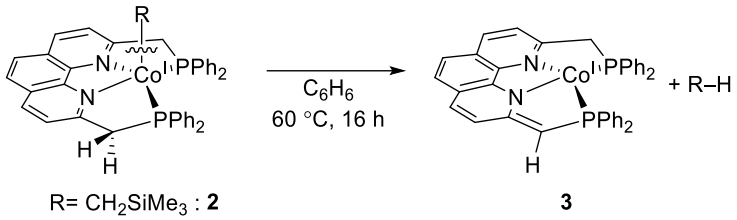

Scheme 1. Structural transformation of **2** into **3**.

In Chapter 3, the mechanism of hydrogenation (H_2) activation by **3** to form **4** bearing a PNNP" ligand with a hydrogenated phenanthroline framework was illustrated (Scheme 2). Based on reaction of **3** with D_2, occurrence of heterolytic H–H bond cleavage via MLC was evidenced (Scheme 2, step i). Moreover, formation of Co(I) hydride intermediate (**A**) was suggested in this process (Scheme 2, step ii). Heating experiment of Co(I) ethyl complex (**7**), which underwent structural transformation to **4**, also supported the formation of **A** (Scheme 2, step iii). Reversibility between **3** and **4** was also supported. Accordingly, a long-range MLC behavior as a H_2 reservoir was demonstrated in the PNNP-Co(I) system.

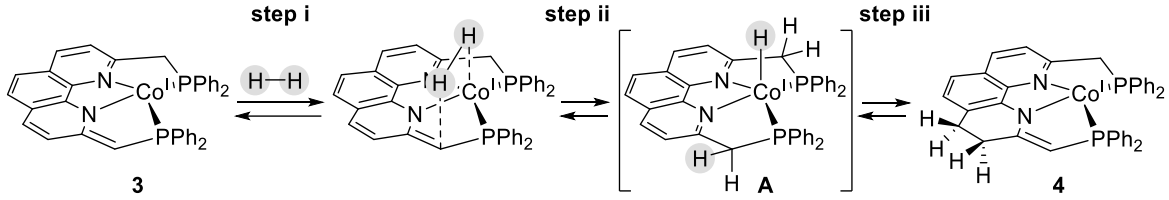

Scheme 2. The proposed mechanism of H_2 activation via **3**.

In Chapter 4, a catalytic hydrodehalogenation of aryl halides is reported (Scheme 3). In this study, a broad substrate scope was achieved (Chapter 4, Tables 2 and 3) under mild reaction conditions (e.g. 1 atm H_2). Moreover, the degradation of fire retardants such as hexabromobenzene and decabromodiphenyl ether (deca-BDE) were accomplished. One possible reaction mechanism was proposed, which was evidenced by detailed mechanistic study sometimes using model systems. Through this study, a radical mechanism for the C–X bond cleavage followed by a hydrogen abstraction from the PNNP" ligand backbone was revealed based on a radical clock experiment as well as kinetic study. Overall, this study demonstrated radical hydrodehalogenation of aryl halides, which is mediated by MLC of the PNNP-Co(I) system. To the best of my knowledge, this is the first example to apply this behavior in catalysis.

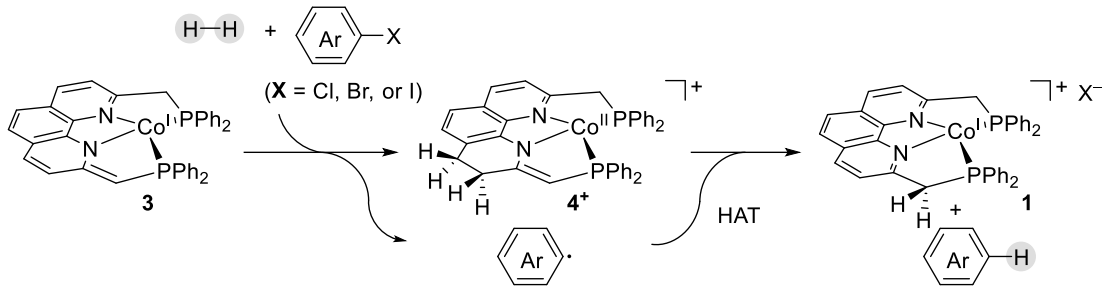

Scheme 3. Hydrodehalogenation of aryl halides via PNNP-Co(I) complexes.

Through this thesis, the PNNP-Co(I) complexes with various characteristic MLC behaviors and their mechanism are disclosed. A unique long-range MLC behavior, which utilizes the phenanthroline framework as a hydrogen reservoir, is manifested. In these reactions, radical properties of PNNP-Co(I) complexes including homolysis of the Co–C bond and the benzylic C–H bonds play a pivotal role. It can also be mentioned that the highly delocalized system synergizing both the PNNP ligand skeleton and the Co center is of importance to accomplish the observed long-range MLC. I believe that with all these studies on PNNP-Co(I) complexes, further application of this system to various catalytic reactions can be expected in the future.

Reference

(1) Khaskin, E.; Diskin-Posner, Y.; Weiner, L.; Leitus, G.; Milstein, D. *Chem. Commun.* **2013**, *49*, 2771–2773.

List of publication

1. Jheng, N.-Y.; Ishizaka, Y.; Naganawa, Y.; Sekiguchi, A.; Nakajima, Y. Co(I) Complexes with a Tetradentate Phenanthroline-Based PNNP Ligand as a Potent New Metal–Ligand Cooperation Platform. *Dalton Trans.* **2020**, *49*, 14592–14597.
2. Nakajima, Y.; Takeshita, T.; Jheng, N.-Y. Metal–Ligand Cooperation Behaviour of Fe and Co Complexes Bearing a Tetradentate Phenanthroline-Based PNNP Ligand. *Dalton Trans.* **2021**, *50*, 7532–7536.
3. Jheng, N.-Y.; Ishizaka, Y.; Naganawa, Y.; Minami, Y.; Sekiguchi, A.; Iizuka, K.; Nakajima, Y. Radical Hydrodehalogenation of Aryl Halides with H_2 Catalyzed by a Phenanthroline-Based PNNP Cobalt(I) Complex. *ACS Catal.* **2022**, *12*, 2320–2329.

Acknowledgements

During the course of this work, firstly and the most importantly, I want to give my supreme tribute to Professor Yumiko Nakajima as my supervisor. The instruction and instillation from her are essential especially on the preparation of research papers and this thesis. Furthermore, her feedback on my research always encourage me to challenge something tougher, and thus this study can achieve a much better status than the original expectation. Meanwhile, I sincerely show my gratitude to Professor Takehiko Kojima as my vice supervisor. Not only in the joint seminar but also in course of research, he always shares specific points of views to highlight the most important issues. Moreover, he often shares the philosophy about how to be a professional scientist, and that is important to shape my attitude on research.

In addition to the two professors, two chemists who are pretty important for me. First of all, I want to express my special appreciation to Professor Akira Sekiguchi. He also always points out some crucial points in my research, and most importantly, encourages me to think deeper and deeper to reveal the insight of each experimental finding even though it is a very tiny phenomenon. Furthermore, his idea about that everyone is equal in front of chemistry is so profound to inspire me to think out of the box to try to reach the truth and break the ceiling. Secondly, I would like to thank Dr. Yuki Naganawa as a vice advisor and supporter in Silicon team at AIST (the National Institute of Advanced Industrial Science and Technology), who always gives me experimental and daily supports directly.

In Silicon team, since significant support are from Dr. Yasunori Minami, especially on experimental support and the discussion for the project of catalytic hydrodehalogenation of aryl halides. I would like to express my appreciation to his help. Similarly, I want to specifically thank Dr. Koya Inomata for discussion, experimental support, and daily support. Furthermore, I would like to express my gratitude to Dr. Shinji Tanaka for the support of lab accessories and technique support of NMR measurements, to Dr. Yoshihiro Shimoyama for discussion and instrumental support, to Dr. Tetsuo Yatabe for the support of experimental works, and Dr. Shiori Fujimori for holding a study group with Dr. Inomata in the lab. In addition, I receive much assistance from technical staff in Silicon team including Mr. Akira Fujita, Mr. Kei Sakamoto, Ms. Atsuko Ogawa, and Mr. Kosuke Iizuka. I also appreciate the cooperation and connection with other group members including Ms. Kazumi Satou, Dr. Haiqing Guo, Ms. Tomoko Sugita, Ms. Nao Matsuyama, Dr. Tomohiro Takeshita, Dr. Siby Mathew, Dr. Monika Gautam, Mr. Takashi Kuragano, etc. Besides, I want to thank the previous group member, Mr. Yusuke Ishizaka, for experimental support.

Furthermore, I want to express my appreciation to all the members in Professor Kojima's lab, specifically to Dr. Hiroaki Kotani for the discussion about electron transfer processes, and

Professor Tomoya Ishizuka for discussion in the joint seminar. In addition, I also want to express many thanks to Professor Taka-aki Ishibashi, Professor Sasamori Takahiro, Professor Junji Ichikawa, and all the staff in the Chemistry Department and Graduate School of Pure and Applied Sciences at University of Tsukuba for the help during my Ph.D. course.

Finally, I have to thank for University of Tsukuba, AIST, and Japan Science and Technology Agency (JST) for research support and financial support. Ultimately, I want to express my sincere gratitude to my family as a backbone to support me to finish my degree.